SYNTHETIC DNA NANOMATERIALS FOR DRUG DELIVERY AND 3D CELL CULTURE

A Dissertation

Presented to the Faculty of the Graduate School

of Cornell University

in Partial Fulfillment of the Requirements for the Degree of

Doctor of Philosophy

by

Pichamon Kiatwuthinon

August 2013

SYNTHETIC DNA NANOMATERIALS FOR DRUG DELIVERY AND 3D CELL CULTURE

Pichamon Kiatwuthinon, Ph. D.

Cornell University 2013

Interest in the use of DNA nanotechnology in biomedical applications has increased tremendously in the last decade due to the uniqueness of DNA properties that allow precise and predictable construction of synthetic DNA building blocks, which later form higher complex DNA structures. Moreover, the synthetic DNA structures can be manipulated by the same molecular toolkits as natural DNA and naturally degraded to metabolite by-products. Thus far, most of the biomedical applications employing DNA nanomaterials are related to gene delivery and detection due to Watson-Crick base pairing rules. For example, the DNA nanostructures have been used in detecting DNA and RNA in biological systems by an innate hybridization property between the DNA nanostructures and target oligonucleotides. Moreover, the DNA nanostructures have been used as a carrier for antisense DNA or siRNA. Here, we present the use of synthetic branched DNA nanomaterials for a co-delivery of Doxorubicin and siRNA and a hydrogel-based scaffold for 3D cell culture. First, we demonstrate the development of the novel DNA-lipid co-delivery nanocarriers called DNAsomes. The DNAsomes can be loaded with both siRNA and hydrophobic drugs that promote synergistic effects. The DNAsomes exhibit lower doses of drugs required for therapy. Furthermore, we propose a novel DNA hydrogel-based scaffold for 3D cell culture. Cells grow, proliferate, and form multicellular spheroids (MCS) inside the DNA hydrogels. The DNA hydrogels are naturally degraded by effects of FBS in the culture media and by-products secreted from the cells. In addition, the DNA hydrogels can be degraded on-demand by a DNase I enzymatic reaction to release cultured MCS without any disruption to the MCS. Also, re-encapsulation of released MCS is possible allowing several

downstream applications of the MCS. Lastly, we demonstrate the potential use of DNA hydrogels for 3D siRNA delivery. The siRNA hybridize to the DNA building blocks forming siRNA hydrogels. The time-specific release of siRNA can occur in the presence of RNase H only degrading RNA/DNA hybrids bridging the DNA hydrogels and siRNA. By adding different amount of RNase H, the siRNA controlled release profiles are different. The siRNA hydrogels can potentially be used to culture and transfect the MCS at the same time.

BIOGRAPHICAL SKETCH

Pichamon Kiatwuthinon received her B.S. degree with first class honors in Biochemistry from Chulalongkorn University, in Thailand in 2005. During her last year of my study, she worked with Professor Napa Siwarangsan and Professor Seeroong Prechanont on a joint project between departments of biochemistry and biochemical engineering. After graduating, she was awarded a scholarship from the Royal Thai Government to pursue a Ph.D. in nanoscience and nanotechnology. In 2006, she started working toward her Ph.D. in the department of Biological and Environmental Engineering at Cornell University under the guidance of Professor Dan Luo. Pichamon will be working as an academic lecturer and researcher in the department of Biochemistry, Kasetsart University, Thailand from August 2013.

TO MY KIATWUTHINON FAMILY AND FRIENDS

ACKNOWLEDGEMENTS

It has been seven years since I first started my Ph. D. at Cornell University. This dissertation has compiled most works throughout my academic experiences here. All works must be credited to my academic committees. First, Prof. Dan Luo, my academic advisor has been giving me good advice. At the same time, I would like to give credits to my other two academic committees, Prof. John March and Prof. Michael Shuler who always support me and shave me to a better scientist. I have learned so much from all of them.

Additionally, I would like to acknowledge another part of my experiences at Cornell as well. My life has completely changed since I first arrived at Ithaca. This beautiful small town has been enchanted me more and more. All those years at Cornell, I learned a lot of things. Most importantly, I learned to be a stronger person as doing Ph. D. is never easy. However, I am grateful to be able to enjoy life along the way of my Ph. D. degree here. A balance of academic and non-academic experiences has greatly contributed to my Ph. D. accomplishment. Moreover, I would never come this far without my family and friends. I would like to give big thanks to my family who never get bored of supporting me. Staying very far away just made me see how important my family is. Mom and Dad are the most amazing persons I have ever seen in the world. Their words always cheered me up when I was disappointed. I thank my brother for taking a care of our parents while I am away from home. I love all of you so much. In addition, I am so thankful that I have good friends that are always standing beside me. First, I thank my best six forever friends (Koi, Orm, Tom, Top, and Yong) who always make me smile and realize what true friends are like. It has been 18 years and counting on since we first knew each other. I would never survive if you all were not there when I needed to talk about everything. My university friends (Ploy, Kwang, Golf, and Duang) are also always there for me. Not only good

old friends, I have bound to new friends at Cornell. My Luo's lab friends who made me feel not too bored along the way of my Ph. D. My Thai friends at Cornell who make me feel like I am home with good food. I will never forget all my seven years at Cornell.

TABLE OF CONTENTS

LIST OF TABLES

LIST OF FIGURES

CHAPTER 1

Introduction

In this dissertation, I focus on developing new platforms utilizing synthetic branched DNA-based nanomaterials for drug delivery and three-dimensional (3D) cell culture. First, I introduce the generic properties of nucleic acids, both DNA and RNA, which rendering a number of advantages for biomedical application. Then, I demonstrate the co-delivery system of small drugs and small interfering RNA molecules (siRNA) by exploiting novel branched DNA-lipid amphiphile building blocks that self-assemble to liposome-like DNAsomes. Next, I purpose a new 3D cell culture hydrogel-based platform using the synthetic DNA hydrogels. The novel DNA hydrogel-based scaffold can be both naturally or on-demand degraded allowing retrieval of encapsulated multicellular spheroids without mechanical and chemical disruption of the spheroids. I then propose another biomedical application by employing the synthetic DNA hydrogels as a siRNA-controlled release reservoir by taking advantages of nucleic acid inherent properties in naturally hybridizing between DNA and siRNA molecules. The siRNA molecules are released and controlled by the presence of RNase H enzymes. Last but not least, I propose the combined two-in-one DNA hydrogel-based scaffold for 3D cell culture and siRNA delivery.

1.1 The fundamental generic properties of nucleic acids

Soon after the discovery the structure of deoxyribonucleic acid (DNA) by Watson and Crick in 1953, further investigations of physical and chemical properties, and organization of nucleic acids at nanoscale levels have been revealed and become useful for nanotechnology (1-3). These extensive studies of the nucleic acid structures include not only DNA structures, but also

ribonucleic acid (RNA) structures that were elucidated a few years after the discovery of the DNA structures.

1.1.1 DNA

The first appearance of the molecular structure of deoxyribonucleic acid (DNA) was revealed by Watson and Crick in 1953 (1), a finding that has catalyzed a growing field of research on DNA.. In total, three main species of DNA consisting of A-, B-, and Z- conformations (4, 5) have been discovered. Each conformation of DNA is reversible and governed by a number of environmental factors. These include for example, pH, which is a degree of hydration, a concentration of metal ions, and the presence of polyamines (6-10). The B-DNA structure is the most common DNA structure found under physiological conditions and widely used in several biomedical applications. Thus, the B-DNA structure will be employed as a DNA structural model and simply referred to as DNA structures throughout this dissertation. The DNA structure consists of two deoxyribonucleotide chains non-covalently held together by two major forces. The first force is a non-covalent hydrogen bond between nucleobases of the two deoxyribonucleotide chains. Second, a van der Waals interaction holds stacking aromatic rings of nucleobases (2, 11). Each of the deoxyribonucleotide chain is comprised of nucleotide subunits where the components include a pentose 2'deoxy pentose sugar ring, phosphate group, and nucleobase. Each of the nucleotide subunit connects to each other by a phosphodiester bond between the 3' hydroxyl groups of one nucleotide and the 5' phosphate groups of an adjacent nucleotide. Specifically, the double-stranded deoxyoligonucleotides form a double helix structure in an anti-parallel direction (5' to 3' direction) generating major and minor grooves alternatively along the double-stranded DNA structures (2). The pentose sugar ring links to the phosphate group at the 5' position and to one of four nucleobases at the 1' position. The four

nucleobases for DNA include adenine (A), guanine (G), cytosine (C), and thymine (T). All four nucleobases have specific interactions and follow Watson-Crick base-pairing rule: A only pairs with T and C only pairs with G by hydrogen bonds. The diameter throughout the DNA structures is about 2 nanometers (nm), rendering a defined geometry for the DNA structures. The length of DNA structures can be varied from a few nm to sub-centimeters (cm) in nature (12). Hence, the DNA molecules are considered to have high aspect ratios (small diameter and long length). As the diameter is constant throughout the structures, the stiffness of any DNA structures are determined by their lengths. The DNA structure of which the length is less than a persistence length (~ 50 nm) behaves as a rigid molecule (3, 13). Longer lengths of DNA structures become more flexible and tend to coil into supercoiling structures. However, the persistence length can be reduced to 1-2 nm in single-stranded DNA in order to add flexibility to the structures (14).

1.1.2 RNA

A structure of RNA is similar to that of DNA such that it also contains a pentose sugar ring, phosphate group, and nucleobases. However, two distinct differences exist between DNA and RNA along the type of pentose sugar rings and regarding one of four nucleobases. The pentose sugar ring at the 2’ position of RNA contains a hydroxyl group while that of DNA is replaced by a hydrogen atom. Besides, a thymidine nucleobase (T) in DNA is replaced by a uridine nucleobase (U) in RNA. Another important distinction between DNA and RNA is that DNA naturally exists in a double-stranded form whereas RNA is usually exists in a single-stranded form. The single-stranded RNA can also form complicated secondary structures due to the extra hydroxyl groups on the sugar ribose rings, thereby increasing the opportunity to form hydrogel bonds. Occasionally, under physiological conditions, RNA appears in double helices in an A-form structure , unlike DNA, due to the presence of an extra 2’ hydroxyl group on the pentose

sugar rings, which prevents the RNA to have a B-form configuration (15). As for the dimensions of RNA, it has been shown that the duplex RNA is stiffer than DNA. Depending on measurement techniques, the persistence length of double-stranded RNA ranges from 60 to70 nm (16, 17).

1.2 Nucleic acid building blocks for nanotechnology

Based on the fundamental properties of the nucleic acids, several of these properties have been utilized in constructing nanostructures and broadly used in many nanotechnology applications (13). First of all, nucleic acid structures are well-characterized in components and molecular organization, which thereby allows one to predict, modify, and tailor physical and chemical properties for specific uses (18). Secondly, the formation of the double helix structures is precisely controlled by the sequences and governed by the Watson and Crick base-pairing rules. Consequently, the precisely designed double-helix nucleic acid structures can form a number of complex and high-ordered nucleic acid nanostructures that can also be manipulated by several molecular toolkits. In addition, the source for obtaining nucleic acids is straight-forward, allowing production to occur in bulk scale (million copies) from both natural and artificial sources. For example, large circular plasmids can be extracted from recombinant bacteria that can produce as high as a milligram scale of DNA in one extraction process. Synthetically, DNA can be produced from solid phase reactions yielding DNA up to a milligram scale as well. More details about obtaining nucleic acids are discussed later in this chapter. In order to thoroughly exploit and manipulate nucleic acids as the building blocks of nanostructures for desired uses,

four key features, which are sources of nucleic acids hybridization, chemical stability and modification, and molecular toolkits—are emphasized in the following section.

1.2.1 Sources of nucleic acids

1.2.1.1 DNA

By taking advantage of the DNA self-replication mechanism of small organisms, a large scale of pre-designed DNA can be produced with high fidelity of corrected inserted sequences based on enzymatic proof-reading properties (19-22). One of the most ground-breaking research used the circular genomic DNA obtained from the virus M13mp18 to self-assemble into complex DNA nanostructures (22). Additionally, DNA can be synthetically generated by chemical and enzymatic reactions. For chemical DNA synthesis, DNA is generated by using solid phase reaction, which allows for an opportunity to freely design the sequences of DNA. However, the solid phase synthesis has limits; such that only short DNA up to about 100 bases can be generated. An enzymatic DNA synthesis, on the other hand, can facilitate DNA production up to several kilobases (kbs). A general technique to enzymatically produce long double-stranded DNA is called polymerase chain reaction (PCR). The PCR reaction mimics the cellular DNA replication machinery and depends on DNA polymerase enzyme activity. Rolling-circle amplification (RCA) reaction was also reported to replicate long single-stranded DNA that thermodynamically folds to form four-armed DNA nanojunctions by stapling with five additional short single-stranded oligonucleotides (23).

1.2.1.2 RNA

A variety of natural RNA carries multiple biological functions (24, 25). These RNA can be classified based on cellular functions such as ribosomal RNA (rRNA), messenger RNA (mRNA),

transfer RNA (tRNA), micro RNA (miRNA), and non-classified RNA. In its natural form, RNA is available in a single strand, transcribed from the antisense DNA strands. As a result, a number of RNA transcripts can interact among bases on their own strands and form secondary structures. In nanotechnology, these RNA sencondary structures can potentially serve as jointing molecules between nucleic acid nanostructures due to the flexibility of the single-stranded forms. However, natural RNA is naturally more prone to degradation than DNA owing to RNA's additional 2' hydroxyl groups, which are sensitive to alkali hydrolysis. Hence, using naturally-occurring RNA as a part of nanostructures can be problematic unless RNA is modified to endure extreme conditions.

Like DNA, RNA can be artificially synthesized with designed sequence specific foled RNA nanostructures. An artificial RNA synthesis can be obtained by either a chemical synthesis or an *in vitro* enzymatic transcriptional approach. The chemically synthesized approach is superior to the enzymatic approach as modified backbones, sugars, and bases that cannot be processed by biological enzymatic reactions can be incorporated to the synthesized RNA stranded. However, current commercial synthesis limits the length of RNA from the chemical synthesis to about 100 nucleotides due to complications in the synthesis process (26). On the contrary, the enzymatic approach, which relies on *in vitro* transcription mechanism of RNA polymerase enzymes, offers the synthetic RNA production up to several kbs. Unfortunately, these long RNA generated from the enzymatic reaction suffers from errors in base proof-reading mechanisms. Also, the modification of RNA in the enzymatic reaction is limited due to the low affinity and efficiency of the RNA polymerases to modified incorporated nucleoside monophosphates (27).

A plethora of sources from which to obtain both DNA and RNA for self-assembling nucleic acid nanostructures exist. Depending on product sizes, purposes, and applications, a suitable

method to obtain nucleic acids can be chosen.

1.2.2 Hybridization

As briefly detailed above, two single-stranded polynucleotides self-associate, or hybridize, via non-covalently hydrogen bonding interactions following Watson-Crick based-paring rules (2). Nucleobases A and G are double-ring pyrine bases (R) while C, T, and U are single-ring pyrimidine bases (Y). According to Watson-Crick base paring rules for nucleic acids, A and G hybridize to T (U) and C, respectively. Watson-Crick base-pairing rules are simple, yet tremendously useful for constructing any nucleic acid-based nanomaterials. The high fidelity and affinity of the base-pairing result in a precise structure formation. Also, hybridization render the benefit of joining two nucleic acid nanostructures by overhang sequences without any physical and chemical reactions. The overhang at the end of the nucleic acid structures hybridize to a pre-designed complementary overhang of the other structures, thereby generating the combined structures. By designing the complementary sequences and thermostability of the overhangs between two nucleic acid structures, higher-ordered structures of nanostructures can be self-assembled in a programmable fashion (18).

1.2.3 Chemical stability and modification of nucleic acids

Two major covalent bonds involved in both DNA and RNA structures are 3'-5' phosphodiester and N-glycosidic bonds linking between two adjacent sugar rings and a sugar ring to a nucleobase, respectively. Both of the covalent bonds are mainly susceptible to hydrolysis and oxidation reactions at different degrees depending on endogenous (primary structures, bases, and sugars) and exogenous parameters such as pH, metal ion, buffer (28). For example, RNA is more susceptible to hydrolysis in alkali environment than DNA because the 2' hydroxyl group

on the ribose sugar is deprotonated leading to a cleavage of the phosphodiester bond (28). On the contrary, the 2'OH group of the RNA renders an inductive effect causing its N-glycosidic bond to be more stable than DNA, which results in enhancing the stability of the phosphodister bond (29). For oxidation, the reactions involve reactive oxygen species (ROS) mainly generated by photolysis and ionizing irradiation of oxygen-containing molecules (30). The ROS are such as hydrogen peroxide, hydroxyl radical and super oxide. In general, the ROS can interact with all components of nucleotides. The most susceptible component is an aromatic ring of nucleobases as they are rich in electron clouds (31, 32). Additionally, the nucleic acid stability comprises a major issue in biomedical fields as nucleic acids undergo fast degradation in the presence of nuclease enzymes that are naturally found *in vivo*. To enhance the stability of nucleic acids, a number of modification methods have been reported and aim at modifying all three nucleic acid components consisting of a phosphate group, a sugar ring, and four nucleobases (27, 33).

To begin with, the phosphate group can be replaced by several chemical groups that are not subject to intracellular nuclease substrates to avoid degradation (33). The short strand of phosphate group-modified oligonucleotides can be conveniently achieved by solid-phase chemical synthesis (27). One of the most conventional phosphate group replacements is to displace a non-bridging oxygen atom with a sulfur atom, thereby creating a phosphothioate group (PS) and making the modified oligonucleotides less susceptible to nucleases by 10- to100-fold (34). The PS oligonucleotides have been widely used in antisense oligonucleotide drug delivery systems (35-37). In addition to the sulfur atom, the oxygen atom can also be replaced by amine or borane groups producing phosphoramidite and boranophosphate oligonucleotides, respectively (38-40). Alternatively, the whole phosphodiester backbone can be replaced by a synthetic peptide backbone rendering a nucleic acid analog called peptide nucleic acid (PNA)

(41). The hybridized structures of PNA to DNA and/or RNA tremendously increase thermal stability and exhibit unique ionic strength properties (42-45).

The pentose sugar ring modification can be achieved by enzymatic reactions utilizing either DNA or RNA polymerases. Limited non-natural nucleoside triphosphates can be incorporated into newly synthesized oligonucleotides based on wild-type polymerase enzyme affinities (27). Some of non-natural 2' deoxynucleoside triphosphates such as 2' *O*-methyl-, 2' amino, and 2' fluoro-nucleoside triphosphates can be processed with low efficiency by T7 RNA polymerases (46-49). Attaining a higher incorporation efficiency of the modified nucleoside triphosphate was achieved by utilizing tyrosine-mutated T7 RNA polymerases (50, 51). These 2' deoxynucleoside triphosphate modifications are widely used in nuclease resistance applications (52-54). In additional to the 2' deoxy-nucleoside modification, 4' C-position has also been modified by a methylene and sulfur group to investigate the effects of polymerase activities to nucleoside analogs (55, 56).

For nucleobases, several positions on purine and pyrimidine bases have been substituted in nucleic acid modifications. Nevertheless, the modification at the positions responsible for hydrogen bond formation can destabilize or demolish a double-helix structure. Thus, general nucleobase modifications are most generally employed for studying contacts between the base-pairing of the nucleic acid structures. Examples of positions involved in the nucleobase modification include7' N-, 3' N-, and 1' N-positions on purine bases (57-59) and 2', 4', and 5' positions on pyrimidine nucleobases (60-62).

1.2.4 Molecular toolkits for engineering nucleic acid nanostructures

Nucleic acid nanostructures can be manipulated by molecular biology techniques such as cutting, rejoining, and degrading through several enzymes (63). For example, numerous restriction enzymes can be used to cut the nucleic acid nanostructures in a specific sequence-dependent manner. The enzymes cut the fragment of nucleic acids into two or more fragments at specific designated sequences on the nucleic acid nanostructures. For instance, Liu and coworkers employed BamHI and EcoRI restriction enzymes to controlled the deformation of DNA hydrogels (64). Also, several sub-classes of ligase enzymes rejoin two fragments of nucleic acids by catalyzing the formation of the phosphodiester bond between 3'-hydroxyl and 5'-phosphate groups of two nucleotides under cofactors such as ATP and NAD (65-68). To demonstrate the use of the ligase enzymes, Luo and coworkers pioneered the construction of higher-ordered DNA nanostructures by ligating Y- and X-shaped DNA building blocks to form dendrimer-like DNA nanostructures and networked DNA hydrogels, respectively (69, 70). Degradation of the nucleic acid can also be achieved by the presence of multiple endo- and exo-nuclease enzymes. Each of the degrading nucleases is unique in digesting different nucleic acid nanostructures. For example, Deoxyribonuclease I (DNase I) cleaves single- and double-stranded DNA at phosphodiester bonds leaving free 3' OH groups. Besides DNase enzymes, ribonuclease enzymes are only specific to RNA molecules. For instance, ribonuclease H (RNase H) only degrades the phosphodiester bond of the RNA hybridizing to DNA in a DNA/RNA hybrid rendering a possibility to control the presence of RNA in the DNA/RNA nanostructures (71). Furthermore, several functional groups can be added on the nucleic acid structures by molecular enzymes. For instance, kinase enzymes can add or remove phosphate groups from the 5' end of the nucleic acid structures. Terminal transferase enzymes catalyze the addition of single deoxynucleotide to

the 3’ end of single- and double-stranded DNA. Further details in using molecular techniques in manipulating nucleic acid structures can be found in the review by Luo (63).

1.3 Self-assembly of nucleic acid structures for biomedical applications

It has been well-demonstrated that nucleic acid-based materials have been used in a variety of applications ranging from mechanical to biological aspects such as charge capacitors, electronic nanodevices, biosensors, bioimaging devices, drug and gene delivery carriers, and in vitro protein production (72-77). In this dissertation, only nucleic acid-based materials that are employed in biomedical applications are included and categorized based on the self-assembled nucleic acid structure. For broader use of nucleic acid structures, several exclusive DNA and RNA nanotechnology reviews can be found elsewhere (15, 18, 78-81)

1.3.1 Self-assembled nucleic acid building blocks

Nucleic acid building blocks are nano-sized subunits self-assembling into high-ordered nucleic acid structures in a controllable fashion. The building blocks, here, are classified into 3 categories including linear, branched, and loop structures. First, a linear building block, which naturally occurs in biological organisms, is used as a short rigid fragment under the persistence lengths. Nonetheless, the short single-stranded nucleic acids, mostly DNA, lack complexity and capacity to assemble into 3D structures. Thus, they are typically found in facilitating the construction of large templates such long single-stranded DNA and RNA molecules into rationally designed 3D structures (20, 82-84). Second, a branched building block is composed of at least three short oligonucleotides complementarily hybridizing to form branched nanostructures such as X-, Y-, and T-shaped nanostructures (18, 70, 85-87). Last but not least, a

loop structure typically founded in RNA occurring through the formation of secondary structures of single-stranded RNA molecules. The complementary sequences between two single-stranded RNA establish a stem leaving non-complementary sequences forming a bulge at the end of the stem. The RNA loops can complementarily interact with the loops nearby and stably form interlocking loop structures such as dimers, trimers, and hexamers (86, 88-90). An important RNA loop building block playing a key role in nucleic acid nanostructures is an aptamer. The aptamers are obtained from a large pool of random single-stranded nucleic acid sequences undergoing *in vitro* selection process called "SELEX" (91, 92). The ultimate nucleic acids with highly conserved sequences create tight and specific binding affinity to a target ligand such as organic molecules, proteins, and living cells, to name but a few (91-97).

1.3.2 Nucleic acid structures for biomedical applications

Exerting nucleic acid nanostructures in biomedical applications have gained tremendously interests due to the following aspects. To begin with, nucleic acid building blocks are rationally designed and precisely controlled in sizes, stiffness, and properties rendering a reduce in side effects and material homogeneousity in both *in vitro and in vivo* (14). Lastly, nucleic acids are biodegradable and biocompatible materials that can be innately metabolized by natural mechanisms and the degraded byproducts are biological metabolites. So far, there are a variety of biomedical systems taking advantages of nucleic acid structures to improve the efficiency of their system.

First, the nucleic acid structures are used to improve the efficiency of biosensing and nucleic acid detection. The nucleic acid structures hold anisotropic properties, thus different functional moieties can be spatially manipulated on such as dyes, small molecules, proteins, and specific sequences (74, 86). For instance, multi-functional dendrimer-like DNA nanostructures so-called

"nanobarcodes" were simultaneously used to detect multiple pathogenic DNA and distinguish each target by exploiting the different color ratios from two fluorescence dyes (69, 74). In addition, DNA tile nanostructures rationally designed to have target probe sequences protruding out from the tiles were introduced to label-free detect RNA by an assistance of atomic force microscope (AFM) (98). The RNA targets were hybridized to probe sequences increasing the tiles' stiffness which can be detected by AFM's cantilevers. Besides nucleic acid detection, DNA tiles demonstrated an ability to detect protein molecules with high specificity and sensitivity (99). In the study, small DNA tiles with modified thrombin-binding aptamers were self-assembled into large DNA nanoarrays with a high local density of the aptamers. An increase in the aptamer's local density facilitates low concentration detection of human thrombin proteins in the solution. Moreover, the short single-stranded DNA building blocks are used in bridging between small molecules and nanoparticles resulting in aggregation and changes in colors, structures, and plasmonic properties, to name a few (100, 101).

For *in vitro* protein production, a cell-free protein producing DNA hydrogels have been addressed to advance the yield of conventional solution-based protein synthesis (72). The genes were tethered inside the DNA hydrogels by rationally designing the complementary sticky ends between the genes and branched DNA building blocks. At least 16 proteins have been successfully reported with fully functional activities after purification. Another benefit of this protein producing gel format is that the genes were entrapped inside the DNA hydrogels protecting the removal of the gene templates during the products' purification steps.

Additionally, nucleic acid nanostructures are widely used as vessels for drug and gene delivery. Numerous types of building blocks self-assemble into a variety of 3D complex nucleic acid nanostructures with empty pockets potentially carrying siRNA, drug, and small molecules

(86, 88, 102-106). In some cases, the drug-carrying nucleic acid nanostructure itself can simultaneously hold therapeutic functionalities. In one example, Tuberfield and co-workers demonstrated that 3D DNA tetrahedral cages could substantially transfect human embryonic kidney (HEK) cells without any transfection reagents (104). Recently, Anderson et al. modified the 3D DNA tetrahedral nanostructures with several cellular-enhancing molecules to carry siRNA up to 6 molecules and delivered the nanostructures into mice for *in vivo* studies (106). Another example was to use cells-targeting aptamers on doxorubicin- encapsulating icosahedra DNA nanostructures to overcome multi-drug resistances in various cancer cells (86, 107). Furthermore, two complementary single-stranded siRNA were used not only to silence targeted genes, but also trigger the formation of polymeric nanoconstructs (105). Similarly, siRNA-carrying RNA microsponges were purposed to carry high copies of siRNA which can be entirely cleaved by Dicer enzymes for potent gene silencing (108). Other RNA building blocks such as X- and Y-shaped nanostructures were also specifically and rationally designed to carry different siRNA molecules giving highly accurate siRNA ratios for multimeric gene silencing in one shot of treatments (85, 109-111). In addition to drug and gene delivery, nucleic acid nanomaterials also shade some light on tissue engineering and regenerative medicine applications. The synthetic DNA hydrogels were previously purposed to simultaneously encapsulated cells under physiological conditions (70). Preliminary results from Chinese Hamster Ovary (CHO) cell-encapsulating DNA hydrogels showed no sign of cellular toxicity both *in vitro* and *in vivo*.

1.4 Challenges and future perspective

To date, the utilization of synthetic nucleic acids as nanomaterials has been rapidly gaining interests in biomedical applications. It is because the precisely controlled physical and chemical

properties of nucleic acids. Also, the synthetic nucleic acids can identically exert molecular biology techniques as the same as the natural nucleic acids. With these great advantages, a number of biomedical applications embrace nucleic acid nanotechnology to alleviate critical issues in the fields such as degradability and biocompatibility of materials. Along with fortunate natural-like properties, synthetic nucleic acid nanomaterials are unpleasantly sensitive to several factors under physiological conditions. The current straight forward solution is to modify nucleic acid structure components including phosphate groups, sugar rings, and nucleobases. Chemical and enzymatical syntheses are the current methods to generate modified nucleic acids. Unfortunately, the length, cost, degree of modification, and yield of the synthetic nucleic acid production are still bottlenecks in freely manipulating modified nucleic acids for biomedical applications. Momentarily, several emerging advanced technologies producing efficient modified nucleic acids are of interest to conquer those limitations (112, 113). Nevertheless, with synthetic nucleic acids, some biological properties have been diminished or inactive owing to the non-natural changes in the chemical structures. Thus, one must take a compromise between advantages of modification and damages of biological activity of the nucleic acid nanomaterials. Another important challenge of utilizing nucleic acid materials in biomedical applications is when the materials are operated *in vivo*. In general, the half-lives of natural nucleic acids in fetal bovine serum (FBS) are in the ranges of several minutes. The modification and self-assembly of synthetic branched nucleic acids prolong the half-lives from minutes to hours. In addition to prolonging the half-lives, the nucleic acid materials also need to be delivered to targeted cells and to be non-fouling to circumvent non-targeted side effects and minimize the adsorption of proteins, respectively (114). Consequently, solitary modified nucleic acid nanomaterials might not fulfill these requirements for *in vivo* treatments. Hence, the impetus in incorporating

supplemental molecules to achieve all essential needs resulting in complicated systems that are needed to be carefully evaluated before performing *in vivo*.

All in all, the nucleic acid nanomaterials have demonstrated attractive properties that are very beneficial to biomedical fields. While widely used in several applications, a number of pitfalls in exerting the nucleic acid nanomaterials are still challenges and waiting to be improved. As a consequence, there is a plenty of room to improve the use of nucleic acid nanomaterials for an efficient biomedical applications.

1.5 Significance of this dissertation

Since the concept of DNA nanotechnology has established by Seeman *et al.*, a plethora of biomedical applications employing nucleic acid structures has been purposed. The synthetic nucleic acid structures render accurately controlled structures reducing the degree of material's dispersity, hence, diminishing heterogeneous drug loading per the nucleic acid structure. Another advantage of using nucleic acid nanomaterials in biomedical application is that synthetic and natural nucleic acid components are identical allowing identically natural molecular biology techniques to manipulate complicated synthetic nucleic acid structures. The degraded byproducts, in addition, are naturally non-toxic under physiological conditions. Hence, the works discussed in this dissertation specifically focus on employing nucleic acid nanomaterials for the co-delivery of drug and delivery and for 3D cell culture system. Firstly, I used novel DNA-lipid amphiphiles self-assembling into liposome-like structures named DNAsomes. The DNAsomes employed multifunctional properties. To begin with, the DNAsomes naturally carries siRNA molecules and cancer drugs by hybridizing and intercalating, respectively, enabling an efficient co-delivery

system. Furthermore, the DNAsomes can spatially conjugate with fluorescent dyes and track the delivery routes inside cells. The co-delivering DNAsomes improve efficiency and enhance synergistic of the delivery which ultimately reduce the dose of drugs required. Secondly, I will purpose the use of synthetic DNA hydrogels as a novel hydrogel-based scaffold for 3D cell culture. The synthetic DNA hydrogels, as earlier discussed, can undergo the same biological reactions as natural DNA. As a result, the synthetic DNA hydrogels can be either naturally degraded in the presence of nuclease-containing cell culture media or harvested on-demand by the enzymatic reactions. Thus, the synthetic DNA hydrogel-based scaffold can see its application in 3D cell culture as it will allow cellular mechanisms to naturally process the materials over time once they are implanted *in vivo*. Lastly, I will present the novel siRNA-DNA chimera hydrogels for *in situ* siRNA encapsulation and controlled releases. The synthetic DNA hydrogels are used to tether small siRNA molecules. The releases of siRNA are only governed by RNase H enzymatic reaction. I will also demonstrate a potential in employing the siRNA-DNA chimera hydrogels for a two-in-one siRNA delivery and 3D cell culture platform platform which can be useful for siRNA delivery of 3D cell spheroids.

CHAPTER 2

Synthetic branched DNA structures for a co-delivery of therapeutic drugs and siRNA

2.1 Introduction

In drug delivery systems, a plethora of synthetic nanocarriers have been demonstrated to efficiently deliver therapeutic molecules into living cells due to their controllability in physical and chemical properties (115). The synthetic nanocarriers play several important roles in increasing drug delivery efficiency. To begin with, tunable synthetic materials were tailored to increase drug solubility and encapsulate drugs, thereby providing an efficient way to shuttle drugs across cellular membrane (116). Moreover, the delivery by nanocarriers, in addition to increasing drug uptake, demonstrated bypassing drug-efflux pumps which are known to be one of the mechanisms causing multidrug resistance (MDR) (117-120). Additionally, the size ranges of nanocarriers are able to escape from the renal clearances resulting in an increase in drugs' half-life in circulating systems (114). Thus far, a number of materials have been implicated as potential nanocarriers such as lipid-based vesicles (micelles and liposomes), vesicle-like polymers (polysomes), and inorganic nanoparticles (114, 116, 121, 122). One of the most traditional drug nanocarriers is lipid- based vesicles comprised of both natural and synthetic lipid molecules, which self-assemble by re-hydrating dried lipid films in aqueous solution into vesicles with hollow cores.

Several forms of therapeutic agents have been accepted as they demonstrated potent therapeutic effects such as DNA, siRNA, antibodies, and peptides (123, 124). Through medical advancement, emerging nanocarriers carrying multiple therapeutic agents on the same carriers have been proposed to elevate poor therapeutic efficiency of individual drugs especially in cancer treatments (119, 122). The co-delivery of therapeutic agent combinations has been

confirmed the combined and synergistic effects compared to individual multi-drug treatments (119, 125-127). For instance, the co-delivery of Bcl-2 siRNA or antisense molecules and Doxurubin (Dox) exhibited enhanced chemotherapic efficiency in lung cancer models (119, 128). The Bcl-2 siRNA molecules are responsible for Bcl-2 anti-apoptosis protein inhibition and, thus, enhancing apoptotic pathways in cancer cells (129). Along with the Bcl-2 gene inhibition, Dox inhibits DNA replication by intercalating nucleobases which prevent a DNA unwinding process and induce cell death. These combined actions accelerated the toxicity level to investigated lung cancer cells.

Physical entrapment and chemical conjugation are the two main mechanisms that are responsible for therapeutic agent loading. First, the therapeutic agents are embedded inside self-assembling vesicles and nanoparticles inside the hollow-core structures. Second, several chemical conjugations are found to immobilize the therapeutic agents onto nanocarriers' surface.

Even though several co-delivery platforms have been reported in the past decades, issues regarding the synthesis of materials, such as difficulty in obtaining high therapeutic agent loading pose persistent challenges (115, 121). For example, in lipidic-based platforms, the resulting lipid-based carriers are inconsistent in size and therefore drug-loading efficiency. In polymer-based platforms, most of polymersomes are synthesized under harsh conditions which are deadly toxic to living cells. The polymer materials are also non-degradable by natural metabolisms. Inorganic-based materials, similar to polymersomes, cannot be metabolized and possibly accumulate after the delivery which can cause cellular toxicity. Additionally, formulating various therapeutic agents into one nanocarrier is more challenging especially when different types of therapeutic agents are encapsulated and precise multiple drug ratios of are required for the co-delivering systems (127).

In contrast to the aforementioned mentioned synthetic nanocarriers, synthetic self-assembled DNA nanomaterials are biodegradable, spatially controlled, and monodisperse materials. The biodegradable synthetic DNA materials are naturally degraded in the presence of nucleases which conveniently metabolize the DNA into nucleotides. Also, the precise controls are due to their well-defined sequences, which self-assemble by complementarily specific base-paring,such as X-, Y-, T- DNA building blocks and higher ordered structures including tetrahedron and cubic structures. Previously, branched synthetic DNA nanomaterials have demonstrated several properties and characteristics such as multivalency, monodispersity, anisotropicity, spatial controllability and a number of functional group modifications (130). Here, we further investigate DNA's base-pairing and its intercalating properties for an inherent siRNA and small drug carrier. By combining vesicle-like self-assembling properties of lipids, we are able to create a novel lipid-DNA core-shell-like structure called DNAsome in which its size, siRNA, and drug loading capacity can be precisely and spatially controlled.

2.2 Design and Synthesis of multivalent and anisotropic branched DNA-lipid amphiphile building blocks

The building blocks for self-assembling DNAsomes consist of Y-shaped DNA conjugated to lipid molecules. The Y-shaped DNA structures were comprised of three single-stranded oligonucleotides designed to have half of the sequences of one strand complementarily hybridize to that of adjacent strands. The 5' end of each oligonucleotide was designed to orthogonally react with various functional groups. For this specific multifunctional delivery application, each of the 5' end of the three oligonucleotides was rationally modified with primary amine groups ($-NH_2$)

for lipid conjugation, tracer fluorescent dyes for *in situ* cellular tracking, and 21 nucleotide complementary sequences of an antisense siRNA molecules as shown in figure 2.1. The equal moles of three functionalized oligonucleotides self-annealed to Y-shaped DNA building blocks by increasing and slowly decreasing the temperature from 95 °C to 4 °C. The multivalent Y-shaped DNA building blocks were then covalently conjugated to N-glutaryl phosphatidylethanolamine (NGPE) lipid molecules by reacting between active ester groups on NGPE and primary amine on the 5' end of the Y-shaped DNA building blocks (Figure 2.2a). The conjugation between the Y-shaped DNA building blocks and NGPE molecules generated a new covalent amide bond rendering amphiphilic properties to the DNA-lipid amphiphile building blocks. In addition to amphiphilic properties, the DNA-lipid amphiphile building blocks inherently contain nucleic acid properties where functional nucleic acids including siRNAs, aptamers, and antisense oligonucleotides can naturally hybridize to the structures without further modification. In order to confirm the formation of the new amide bonds, high performance liquid chromatography (HPLC) was used to characterize the amide bond formation. The results from HPLC indicated an extra peak, thereby confirming the new amide bond formation in the DNA-lipid amphiphile building blocks (Figure 2.2b). Non-reacted lipid molecules, Y-shaped DNAs, and DNA-lipid amphiphile building blocks were labeled as A, B, and C, respectively and purified from the DNA-lipid amphiphile building blocks. Moreover, we characterized the HPLC products by 3% agrose gel electrophoresis to confirm the formation of the lipid-DNA building blocks as the smear band presented in lane 2 (Figure 2.2c). Additionally, fourier transform infrared (FT-IR) spectroscopy revealed transmission bands from the amide bonds (N-H bending vibration) at around 1660 cm^{-1} and 1590 cm^{-1} (black line) compared with negative bands on branched NH_2- modified DNA (red line) and DNA structure controls (blue line) (Figure 2.2d).

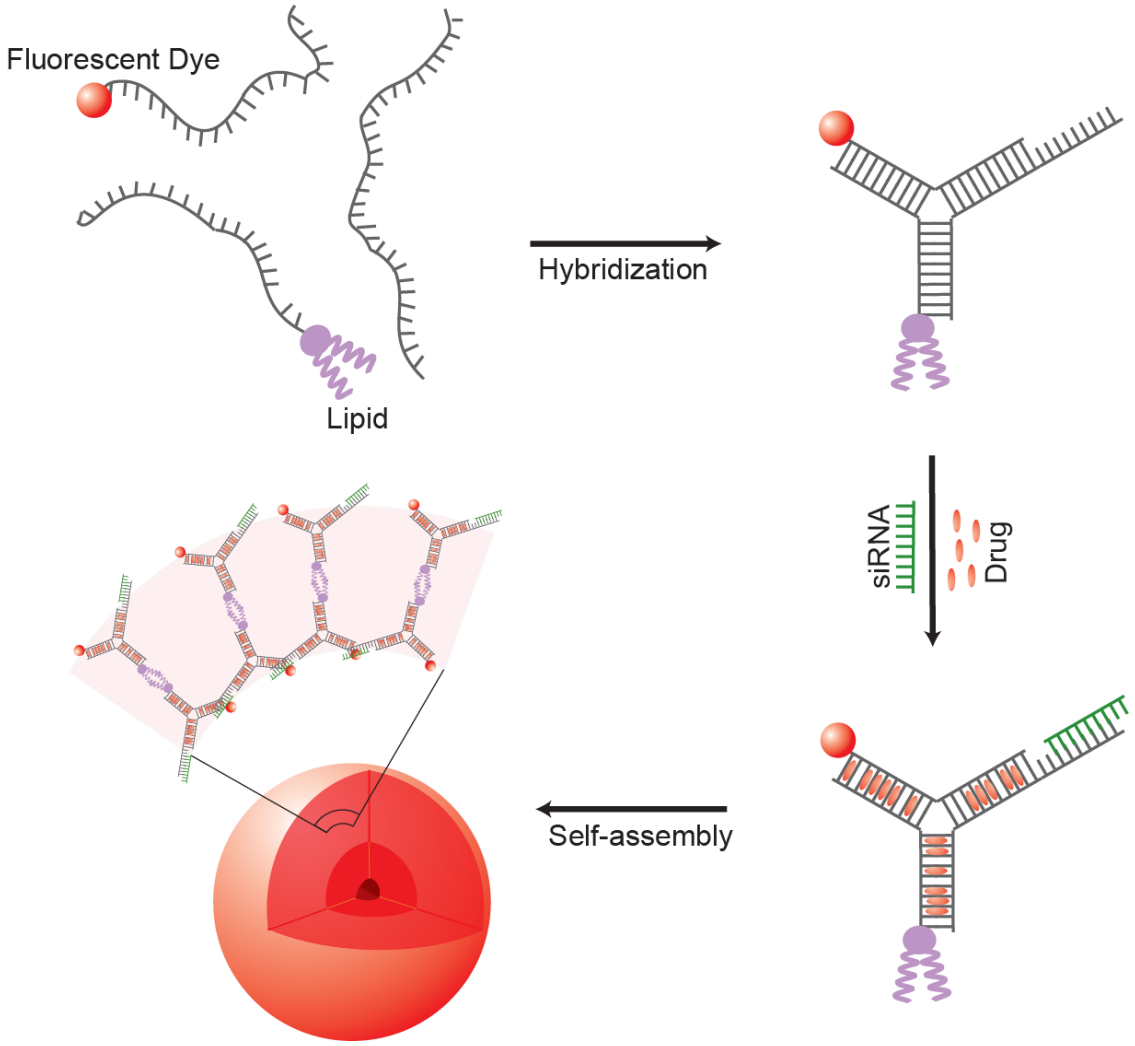

Figure 2.1. Schematic illustration of the construction of DNAsome for the delivery of RNAi agents. DNAsomes and functional groups are not drawn to scale. The resultant DNAsome possesses not only the capability and capacity to store drugs and siRNA, but also molecular probe ability.

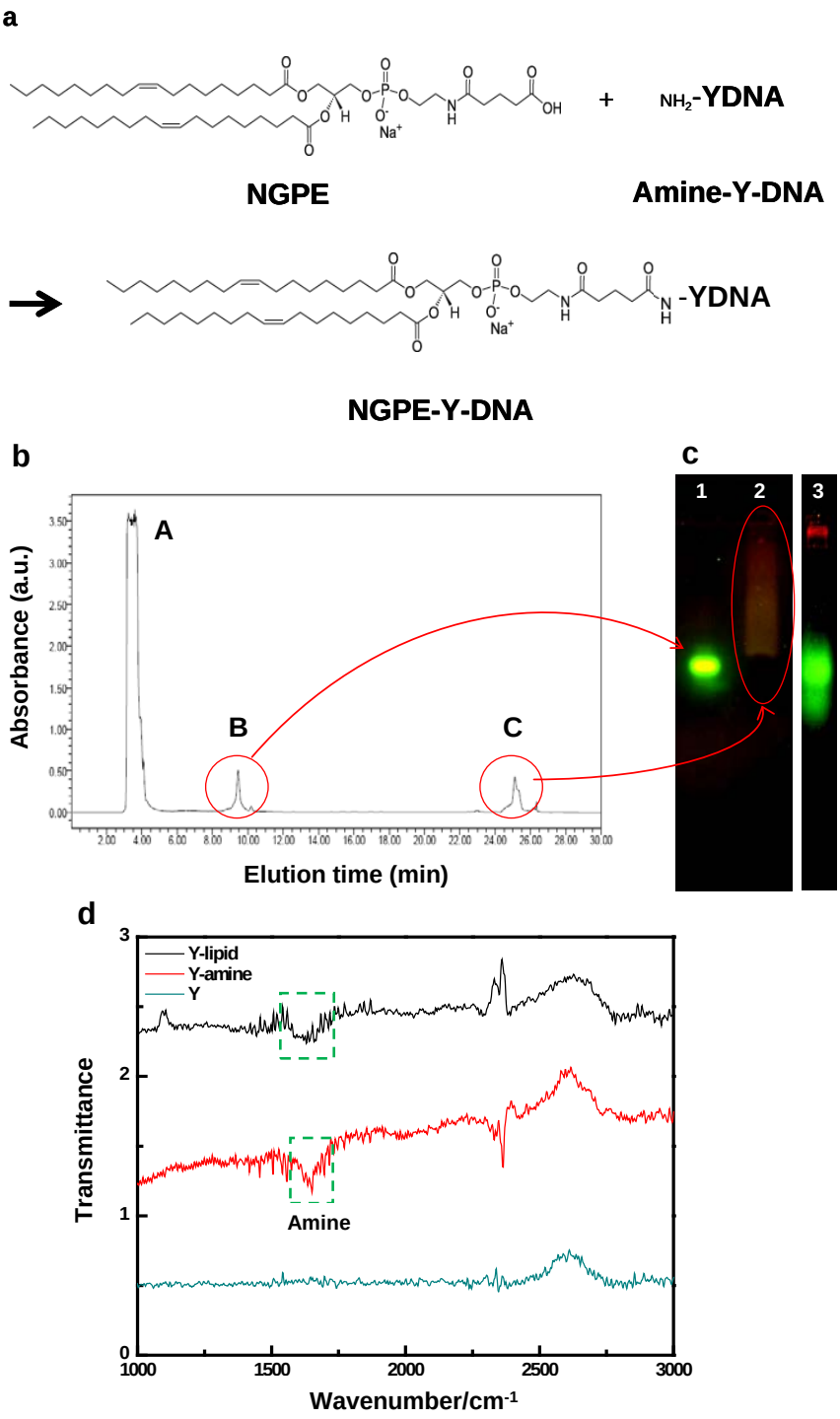

Figure 2.2. Preparation and characterization of Y-DNA-lipid amphiphiles. a. Synthesis of Y-DNA-lipid amphiphiles. The Y-DNA-lipid conjugates were achieved through reactions between the amine modified groups of Y-DNA and the activated ester groups of the lipid molecules.

Figure 2.2. Preparation and characterization of Y-DNA-lipid amphiphiles (continued). The final products were obtained by performing HPLC purification to ensure removal of unreacted reagents as well as impurities. **b.** HPLC chromatogram of products formed in the reaction of Y-DNA and lipid. The separation of unreacted lipid (A), NH_2-Y-DNA (B), and Y-DNA-lipid conjugate (C) were achieved by a gradient elution. The elution time (min) is on the x-axis; the ultraviolet absorbance at 260 nm (mV) is on the y-axis. **c.** Mobility shift of Y-DNA and lipid conjugates. Gel electrophoresis of HPLC fractions was conducted at a constant voltage of 90 volts for 60 min. (3 % agarose gel) Lanes 1 2 and 3 indicate NH_2-Y-DNA, Y-DNA-lipid conjugate and Y-DNA + lipid mixture, respectively. **d.** FT-IR spectroscopy. FT-IR spectrum of Y-DNA-lipid conjugates revealed transmission bands from an amide bond. The IR spectrums of lipid conjugated Y-DNA confirm the presence of amide I band (C=O stretching vibration) and amide II band (N-H bending vibration) at around 1660 cm^{-1} and 1590 cm^{-1} (black line). These results show carboxylated lipid and amine modified Y-DNA formed amide bonding through reaction between a carboxylic group and amine group. However, amine modified Y-DNA shows only N-H bending vibration at around 1630 cm^{-1} (red line) and Y-DNA do not show any band (blue line).

2.3 Formation and Characterization of DNAsomes

To self-assemble DNAsomes, purified DNA-lipid amphiphile building blocks were dialyzed against water in a cellulose membrane bag to form liposome-like DNAsomes. Consequently, the liposome-like DNAsomes were freeze-dried and collected as dried products for later drug and siRNA loading. After dialysis, several techniques were utilized to characterize the morphology and properties of DNAsome. We first began to investigate the minimal concentration of DNA-lipid amphiphile building blocks required to assemble liposome- like DNAsome structures by determining critical micelle concentration (CMC) (Figure 2.3a). We used pyrene, a tetracyclic hydrophobic molecule, as its the fluorescence intensity is highly sensitive to the solvent polarity. The pyrene fluorescence probes are poorly solubilized in aqueous phase but strongly partition in hydrophobic environment, in this case DNAsome structures. The DNA-lipid amphiphile building block was varied from 0.01 to 2190 nM. At 17 nM concentration, the fluorescence intensity ratio dramatically increased, thereby demonstrating the formation of DNAsomes.

Moreover, we used förster resonance energy transfer (FRET) to obtain the internal packing information between each DNA- lipid amphiphile building block inside the DNAsomes (Figure 2.3b). The two fluorescence FRET pairs, Cy5 (red) and green Cy3 (green), were individually labeled to the DNA-lipid amphiphile building blocks. The fluorescence intensity (I) between Cy5 (I_R) and Cy3 (I_G) was used as the intensity ratio (I_R/I_G) to determine the distance between the DNA-lipid amphiphile building blocks organized inside the DNAsomes. In the FRET experiments, a simple mixture of Cy3-, Cy5- DNA building blocks, and unlabeled free lipid molecules were used as a control. Two species of Cy3- and Cy5- labeled DNAsomes were mixed and assembled as a sample. The I_R/I_G was 3.2 times higher for the DNAsome than for the control. This result suggests that the internal structure of DNAsomes consisted of the DNA-lipid

amphiphile building blocks that are closely-packed within FRET distance (< 10 nm). We further explored the structure packing and the core components by employing an electron energy loss spectroscopy (EELS) (Figure 2.3c). A phosphorous compound signal was detected, thereby confirming the presence of DNA phosphate groups at the dense core of the DNAsome structure. Dynamic light scattering (DLS) was employed to investigate the effects of the DNA-lipid amphiphile concentrations on sizes and charges (Figure 2.3d). The sizes of DNAsomes increased linearly from 110.7 ± 12.9 to 1102.5 ± 91.2 nm as the DNA- lipid amphiphile building block concentration increased from 0.5-11 μM. Within the same range of the concentration, the zeta potentials also showed a linear relationship from -10.77 ± 0.81 mV to -35.60 ± 1.27 mV. It is notable that as the concentration of DNA amphiphile increases, both the surface area per particle and the volume per particle increase more rapidly than the zeta potential. Thus, the charge per unit area (and per unit volume) decreases with increasing DNA- lipid amphiphile building block concentration, and consequently the DNAsomes become less repulsive to the building blocks. These results suggest that, unlike conventional liposomes, the size of our DNAsomes can be precisely controlled over a wide range simply by adjusting the concentration of Y-DNA amphiphiles. Last but not least, we investigated the morphology of the DNAsomes. The morphology was observed by a confocal microscopy technique (Figure 2.4a). The fluorescent dyes were covalently attached to the 5’ end of the DNA-lipid amphiphile building blocks as previously described. The DNAsomes were observed as spherical core-shell structures with a dense core and hollow region in the center surrounded by a low-density shell. Similarly, the core-shell structures with dense core morphologies were also observed with scanning transmission electron microscope (STEM) (Figure 2.4b).

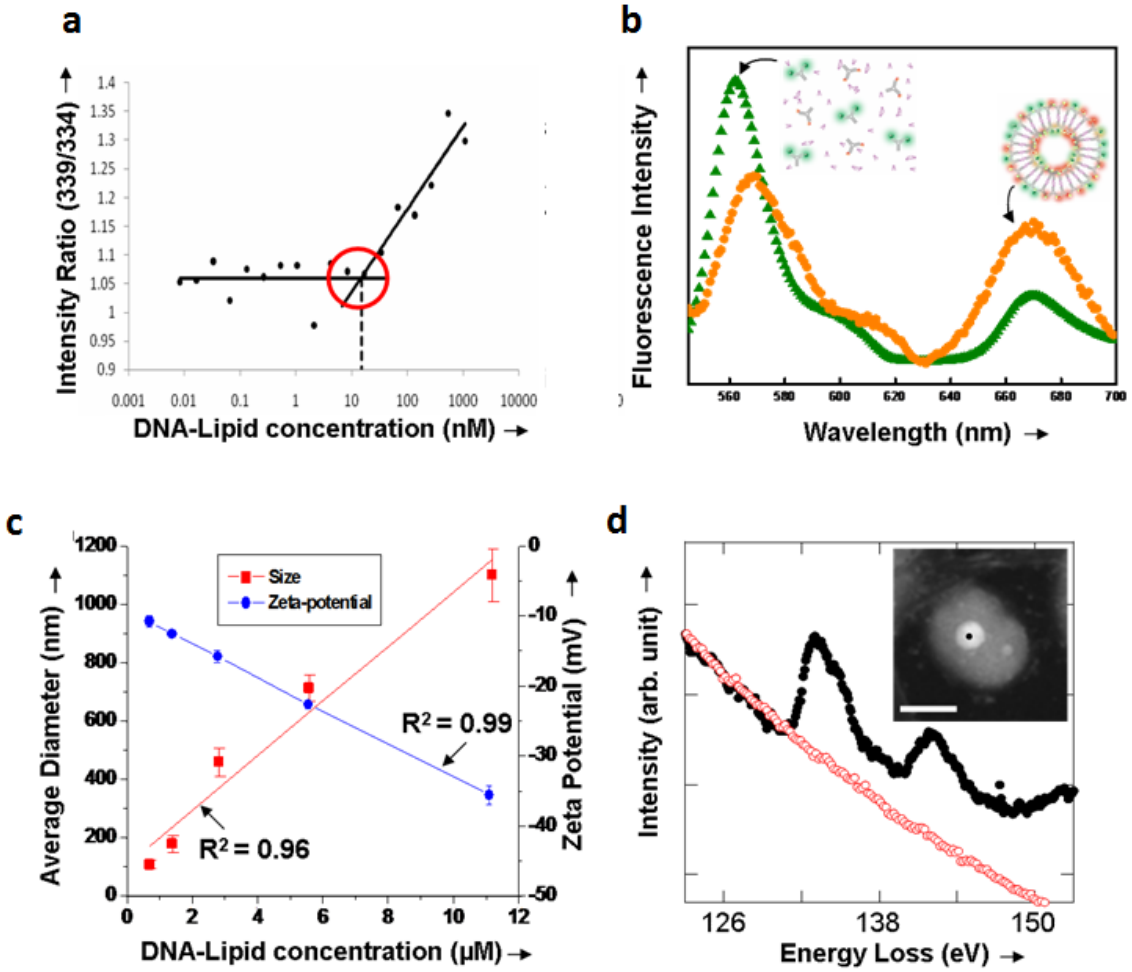

Figure 2.3. Characterization of DNAsomes. a. Critical Micelle Concentration (CMC) The concentration of Y-DNA amphiphile was varied from 0.01 nM to 2190 nM. Here, pyrene was used as a fluorescent probe (no other fluorescent dyes were used in these experiments to prevent interference). b. Fluorescence intensity of free lipids and Y-DNA mixture (green), and DNAsomes made by Y-DNA amphiphile (orange) was compared by Fluorescence resonance energy transfer (FRET). c. Phosphorus EELS spectra of DNAsomes. Phosphorus signal is detected in the core of DNAsomes. Raw EELS spectra from DNAsomes (inset) are shown where the black spectrum is taken from the core. The spectra are scaled so that the pre-edge intensity is the same. The scale bar is 500 nm. d. Zeta potential and size distribution of DNAsomes as a function of Y-DNA amphiphile concentrations.

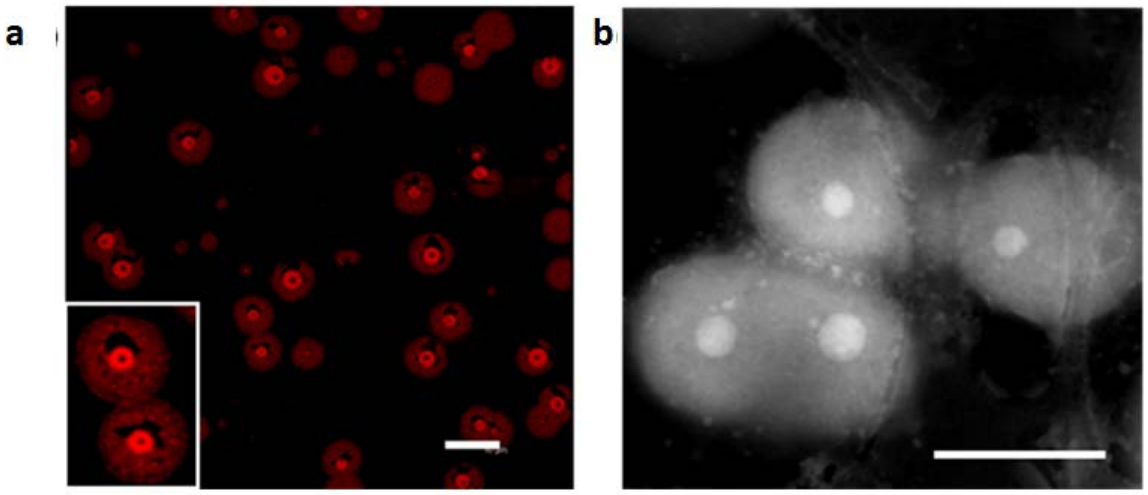

Figure 2.4. Morphology characteristic of DNAsomes. a. Confocal microscopy image of self-assembled DNAsome. The scale bar is 5 μm. b. ADF-STEM image of DNAsomes. The ADF-STEM image shows the spherical shape of the DNAsomes that contain a dense core. The scale bar is 500 nm.

2.4 DNAsomes as a co-delivery nanocarrier

Due to the unique characteristics of DNAsomes, both DNA and RNA can be inherently attached by complementary base-paring to spatially designed sequences on the DNAsomes' structure rendering DNAsomes as an inherent gene carrier. Prior to performing *in vitro* siRNA transfection, we first evaluated the cellular toxicity of DNAsomes and compared with that of commercial transfection reagents including Lipofectamin2000 (L2K) and DOTAP by MTT (3-(4, 5-dimethylthiazolyl-2)-2, 5-diphenyltetrazolium bromide). Chinese Hamster Ovarian (CHO) cells were used as model studies through the experiments. Nearly 100% cell viability of CHO cells was obtained after incubating with DNAsomes for 24 hours while L2K and DOTAP reduced cell viability to about 80% and 40%, respectively (Figure 2.5). Next, we compared the siRNA transfection efficiency of DNAsomes to that of L2K and DOTAP at each reagent's optimum conditions. A house-keeping GAPDH gene was used as a model mRNA target. GAPDH siRNA-loaded DNAsomes were prepared by re-dissolving dehydrated DNAsome products with equal molar of single-stranded GAPDH siRNA in PBS buffer overnight. L2K and DOTAP were prepared by suggested manufacturing protocols. At optimal conditions, DNAsomes demonstrated about 46% siRNA transfection efficiency (Figure 2.6a) which is comparable to L2K (Figure 2.6b) and DOTAP (Figure 2.6c) but remained significantly higher cell viability than the other two reagents. This result might be attributable to the fact that DNAsomes are entirely made of negatively charged DNA and neutral lipid exhibiting overall negatively charged while typical transfection reagents are made of cationic polymers exhibiting positively-charged which are well-known to be highly toxic to the cells.

2.5 Intracellular uptake and mechanism studies of DNAsomes

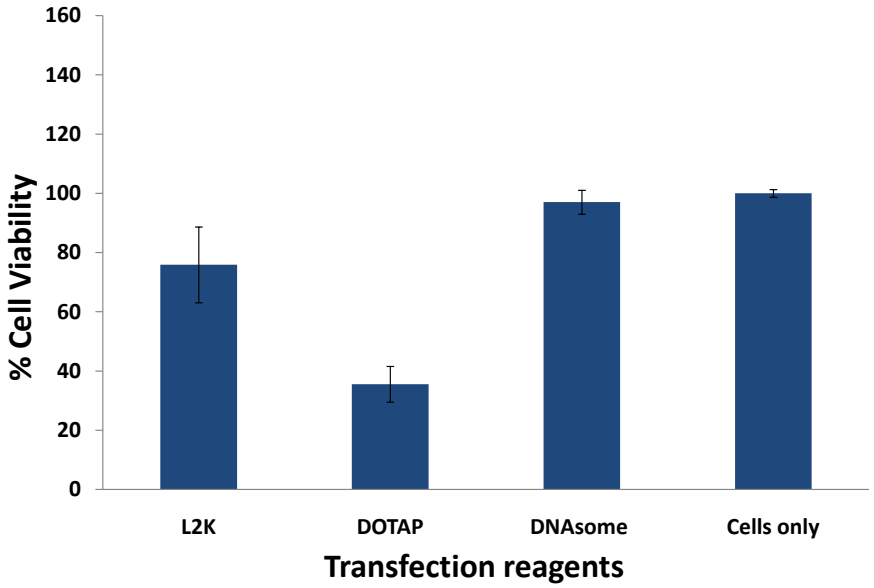

Figure 2.5. Cell viability of transfection reagents. Viability of CHO cells after incubation with the various transfection reagents (Lipofectamin2000 (L2K), DOTAP, and DNAsome) as measured by by the MTT assay.

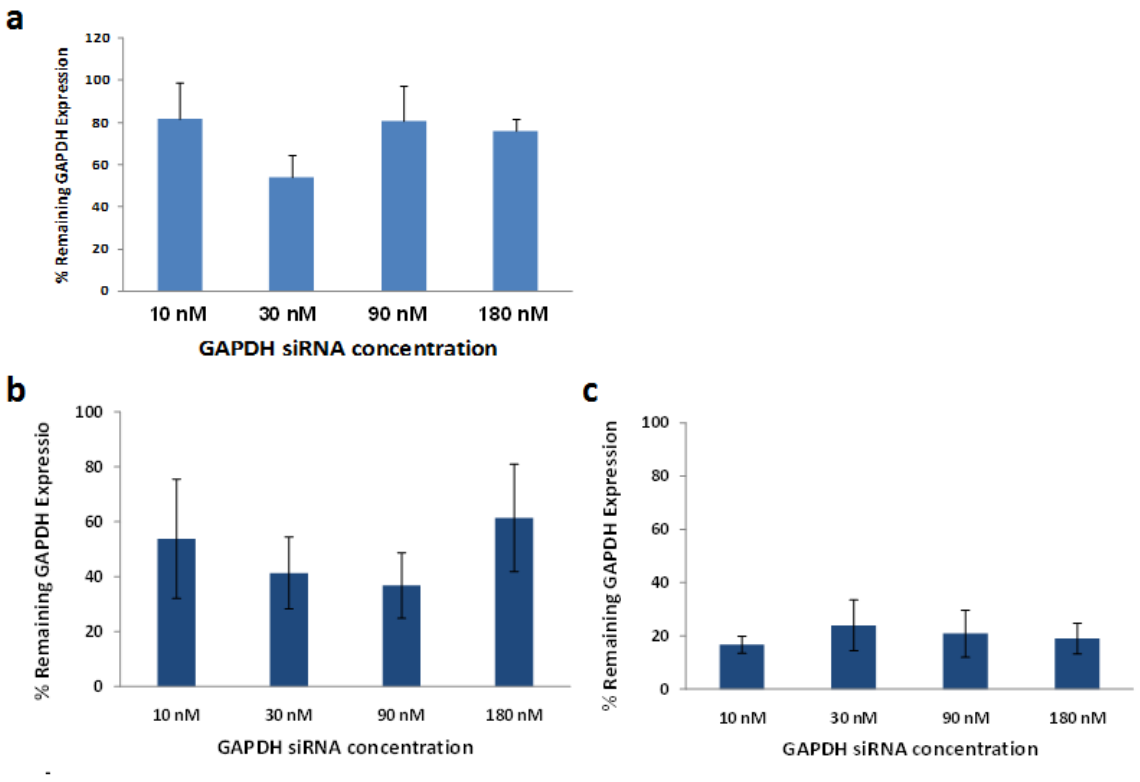

Figure 2.6. Transfection efficiency of siRNA-based transfection reagents. a. % Remaining GAPDH expression after the cells were transfected with DNAsomes from CHO cells. b. % Remaining GAPDH expression, finding with L2K and c. % Remaining GAPDH expression, finding with DOTAP.

To determine a cellular uptake pathway of DNAsomes, fluorescence-labeled DNAsomes were incubated with CHO cells at 4 and 37 °C to primarily determine if the uptake mechanism depends on endocytotic mechanisms. Z-directional sliced images observed by a confocal microscope presented fluorescence signals inside the cells only at 37 °C, thereby confirming the characteristic of endocytosis (Figure 2.7). Sub-endosomal uptake mechanisms were also studied by pre-treating various endocytotic inhibitors before transfecting the cells with GAPDH siRNA-loaded DNAsomes (Figure 2.8). Three major endocytotic pathways comprising caveolae-mediated, actin-mediated, and microtubules- dependent pathways were suppressed by filipin complex, cytochalasin B, and nocodazole, respectively. The condition that cells were transfected with GAPDH siRNA-loaded DNAsomes was used as a non-inhibiting control. The caveolae-mediated endocytosis was predominantly responsible for a main uptake pathway for DNAsomes because, in fact, the filipin complex totally avert the GAPDH protein activity inhibition. Also, DNAsomes can alternately enter the cells via the actin-mediated pathway and microtubules-facilitated pathway as partial GAPDH protein activity inhibition was found when cytochalasin B and nocodazole were presented in the transfection. Notably, the z-directional sliced confocal images also showed the fluorescence-labeled siRNA localized in both cytoplasm and nuclease of the cells, thereby demonstrating a potential in deliverying siRNA or drugs throughout the entire cells.

2.6 Drug loading and Characterization of drug-loaded DNAsomes

To further study the potential of co-delivering small drugs and siRNA molecules, a cancer intercalating drug, doxorubicin (Dox), was used in the model study. Dox is a widely-used hydrophobic drug in several cancer treatments. Its planar structure plays an important role in

inhibiting growth of cancer cells by impeding the DNA replication (Figure 2.9c). Thus, in addition to being embedded in hydrophobic lipid layers of the DNAsomes, Dox can be loaded in DNAsomes by interacting in the groves of the DNA doubled helix. The loading mechanism was simply obtained by mixing the dehydrated DNAsome with Dox at room temperature by slow shaking overnight. The resulting Dox-loaded DNAsomes were then centrifuged to remove non-encapsulated Dox (Figure 2.9d). Also, we compared the change in sizes after Dox loading by DLS techniques and found that narrow size distributions were obtained with an average size of 254 nm and 322 nm for before and after Dox loaded DNAsomes, respectively (Figure 2.9a, b). After Dox and siRNA loading, we first characterized the controlled release profiles of Dox and siRNA in PBS buffer (Figure 2.9e). Both Dox and siRNA continuously released from DNAsomes with distinct releasing properties. This could due to the fact that Dox and siRNA have different binding affinities to DNAsomes which are intercalation and hybridization, respectively.

2.7 A co-delivery of DNAsomes for synergistic effects

Co-delivery of several drug combinations has been demonstrated to increase the efficiency in treating a number of cancers (116, 119, 127). To demonstrate the use of DNAsomes as a co-delivering nanocarrier, we chose Dox and Bcl-2 siRNA that have been reported to exhibit combined effects as our model drug combination study (119). *In vitro* co-delivery studies of DNAsomes were determined by quantifying cell viability after treating with Dox-siRNA- loaded DNAsomes. The concentration that causes 50% cell toxicity (IC_{50}) was used to determine the efficiency of co-delivering measured by (3-(4,5-dimethylthiazol-2-yl)-2,5-diphenyltetrazolium bromide) (MTT) assay (Figure 2.10). In control experiments, we individually treated CHO cells

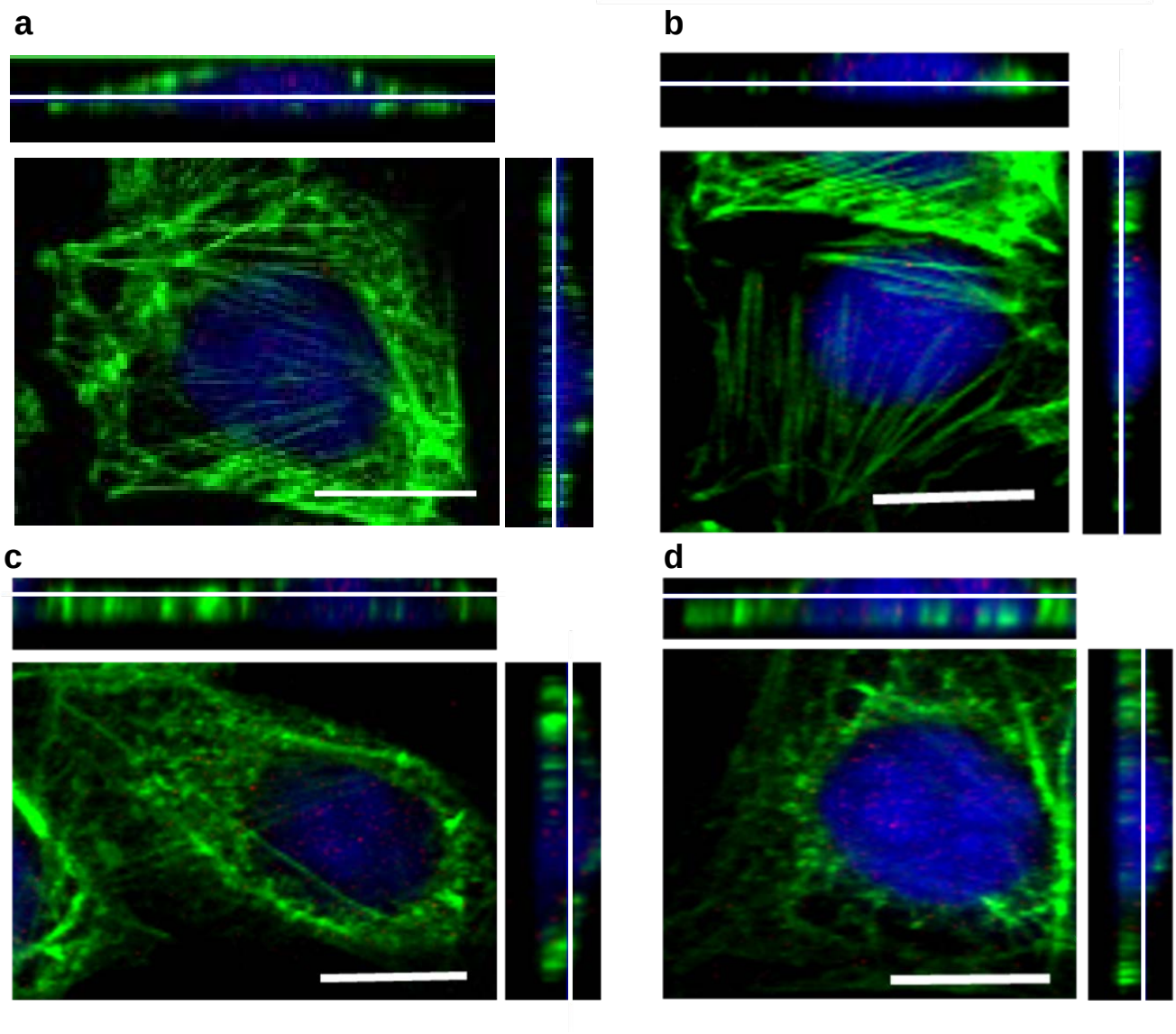

Figure 2.7. Confocal microscopy images of DNAsomes delivered to CHO cells. a-d. DNAsomes were hybridized with fluorescence-labeled siRNA (red) and transfected into CHO cells (blue, nuclei; green, actin) at 37 ºC overnight. Confocal images were used to project side views (Z-directional slices) of CHO cells, thereby exhibiting the intracellular delivery of siRNA-labeled DNAsomes. The scale bar is 10 μm.

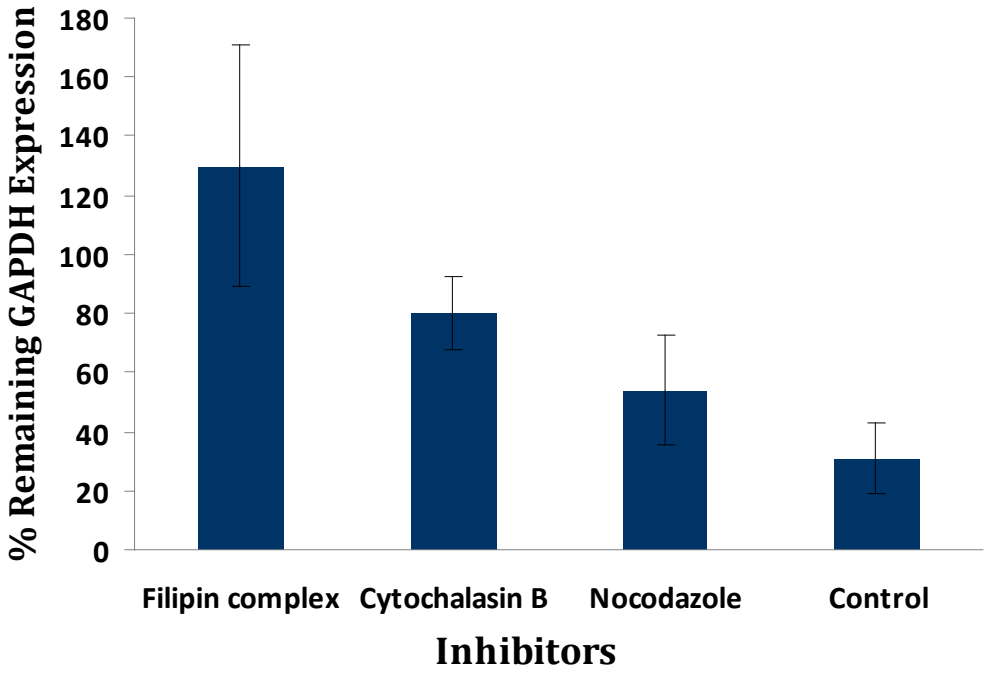

Figure 2.8. Investigation of the endocytosis mechanism for DNAsomes. The cellular endocytosis mechanism of our DNAsome was investigated by endocytosis inhibition studies. Cells were incubated with filipin complex to inhibit caveolae-mediated endocytosis.Cytochalasin B and nocodazole were also used to disrupt actin-mediated and microtubules-dependent endocytosis pathways, respectively. The control contained no inhibitors

with free Dox, free Dox with siRNA, and Dox-loaded DNAsomes. As expected, the IC_{50} of free Dox and free Dox with siRNA at 59 μM was dramatically reduced to 5 μM when Dox-loaded DNAsomes were used in the study. Once both Dox and siRNA were encapsulated in DNAsomes, the IC_{50} was much reduced from 5 μM to about 2 μM when Dox and siRNA- loaded DNAsomes were employed, thereby supporting the synergistic co-delivering approach by the DNAsome nanocarrier.

2.8 Conclusion

In sum, we have proposed a novel multivalent and anisotropic liposome-like core-shell structure nanocarrier called DNAsomes. The DNAsomes are obtained from the self-assembly of DNA-lipid amphiphile building blocks. Each 5' end of Y- shaped DNA structures are spatially conjugated to three functionalities including siRNA, lipid molecules and fluorescent dyes. The sizes and surface charges of the DNAsomes can be finely tuned by altering building block concentrations. Additionally, the DNAsomes can carry a siRNA through inherently complementary base-pairing properties. Similar to siRNA, other therapeutic nucleic acids such as an antisense oligonucleotide, functional gene, and aptamer, can be naturally loaded in the DNAsomes by employing the same concept of inherent hybridization. To the best of our knowledge, this is the first report to utilize the multivalent and anisotropic DNA- lipid amphiphile building blocks for co-delivering drugs. We expect to achieve multiple drug delivery by altering the branched DNA structures in the building blocks for future drug delivery applications.

2.9 Materials and methods

2.9.1 Synthesis of Y-DNA building blocks

All chemicals utilized in this study were obtained from Sigma-Aldrich (St. Louis, Missouri) unless otherwise mentioned. The Y-DNA building blocks were designed and synthesized according to the previous papers published by our group. All oligonucleotides including fluorescent labeled oligonucleotide strands were commercially synthesized with standard desalting (Integrated DNA Technologies, Coralville, Iowa). Table 2.1 and 2.2 show oligonucleotide sequences utilized in this experiment. Briefly, oligonucleotides were dissolved in annealing buffer (10 mM Tris, pH = 8.0, 1 mM EDTA and 50 mM NaCl) with a final concentration of 0.2 mM. Y-DNA was synthesized by mixing the same molar amount of corresponding oligonucleotide strands. The nomenclature is as follows: Y_{01}, Y_{02}, and Y_{03} are the three corresponding single oligonucleotide chains that form a Y-DNA. Hybridizations were performed according to the following procedures: (1) Denaturation at 95 °C for 2 min. (2) Cooling at 65 °C and incubation for 2 min. (3) Annealing at 60 °C for 5 min. (4) Further annealing at 60 °C for 0.5 min with a continuous temperature decrease at a rate of 1 °C per min. The annealing steps were repeated a total of 40 times. The final annealed products were stored at 4 °C.

2.9.2 Construction of the DNA-lipid amphiphiles and DNAsome

Succinyl NGPE (0.3 mg), 0.5 ml of 0.016 M octylglucoside in MES buffer (pH 5.5), EDC (2 mM) and NHS (5 mM) were then reacted with shaking for 10 min and centrifuged at 2.5 kG for 60 sec, followed by 20 µl of 0.1 M NaOH (pH 8.0) with repeated shaking and centrifugation. Mixtures were then added to the prepared Y-DNA products, and incubated for 4 hours at room

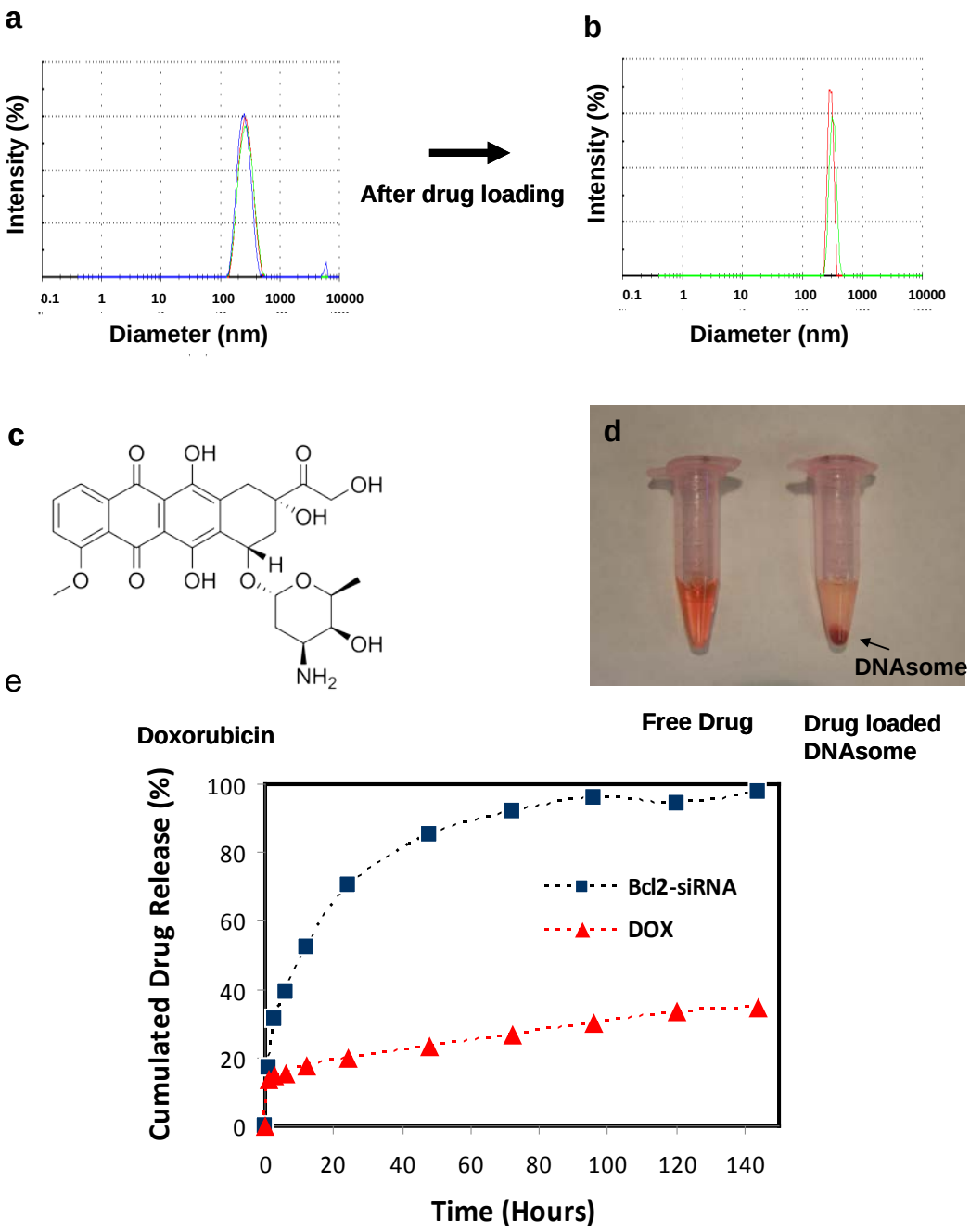

Figure 2.9. Drug loading and drug release profile of DNAsomes a. The average size of DNAsome before drug loading is 254nm. b. The average size of DNAsome after drug loading is 322nm. c. The chemical structure of Dox d. Photograph of tubes containing Dox solution and Dox-loaded DNAsomes. e. Drug release profiles from Bcl2-siRNA (■), Dox- loaded DNAsomes (▲).

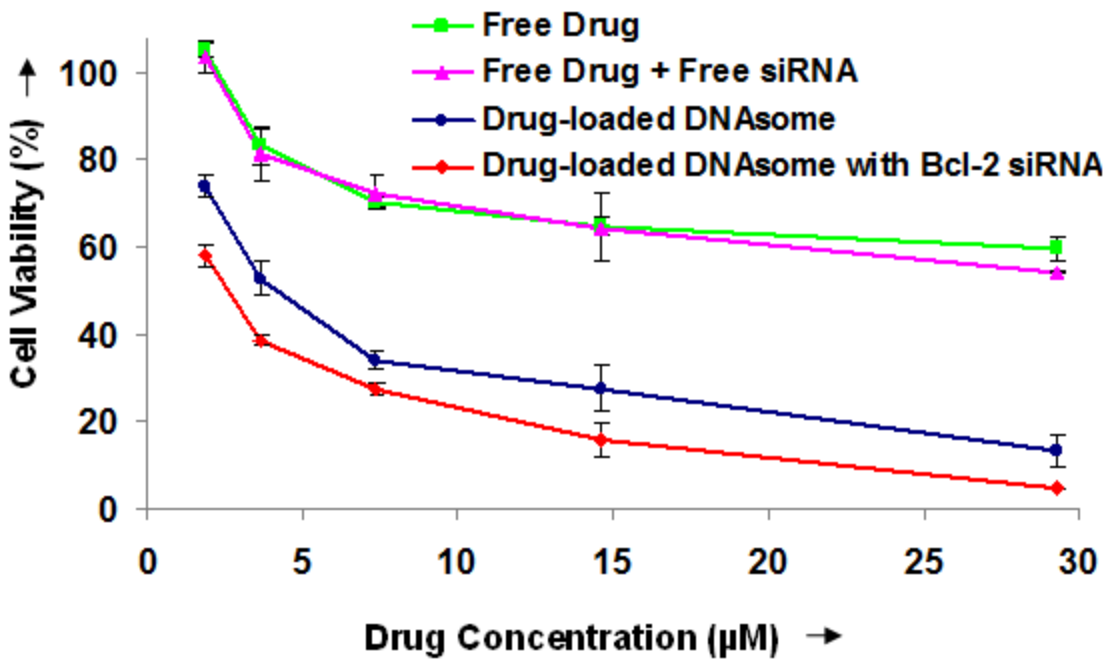

Figure 2.10. Co-delivery of Bcl-2 siRNA and Dox. Viability of CHO cells measured by MTT assay after incubation with free Dox, free Dox and free siRNA, Dox-loaded DNAsome, and Dox-loaded DNAsome hybridized with Bcl-2 siRNA, respectively.

temperature. High performance liquid chromatography (HPLC) was performed to remove non-reacted products and the impurities. The running conditions were as follows: XBridge C18 column equipped with a photo-diode array detector (Waters Corp, Milford, Massachusetts). The gradient used was 0–50% acetonitrile in 0.1 M triethylammonium acetate (TEAA, pH 7.0) as the mobile phase within 30 min at a flow rate of 1.0 mL/min with UV detection (260 nm). The functionalized Y-DNA-lipid amphiphiles was further dialyzed to prepare DNAsomes against 100 ml of aqueous solution for 48 hrs using a cellulose membrane bag. After dialysis, DNAsomes were collected and frozen using a freeze-dryer system (Labconco Corp, Kansas City, Missouri) to achieve final products.

2.9.3 Characterization of DNAsomes

Fourier transform infrared spectroscopy (FT-IR)

To characterize the conjugation of lipid and Y-DNA, FT-IR microspectra were used with Galaxy series FT-IR 5000 (GL5020, Mattson, Arizona). The spectra were scanned in the transmission mode from 4000 to 500 cm^{-1} with 100 scans per point and resolution of 4 cm^{-1}. Each sample of 100 µl was squeezed between two BaF_2 windows.

Morphological study

For the STEM imaging experiment, samples were prepared as follows: approximately 1 µl of DNAsomes was mixed with 100 µl of Tris (30 mM, pH 8.0) before 2.5 µl of 5 % 2, 4, 6 Tri(dimethylaminomethyl phenol) (DMP) 30 was added to the mixture. A drop of the mixture (50 µl) was placed onto a sheet of parafilm and covered with a petri dish for 7 minutes at room temperature. The DNA molecules were then picked up by touching the drop with a carbon-coated TEM grid (Electron Microscopy Sciences, Fort Washington, Pennsylvania), and were left covered with a petridish for another 3 minutes. The sample was then stained with 2 % uranyl

acetate (negative staining reagent) for 1 minute. The grid was then blotted with a filter paper and allowed to dry in air. The grids were visualized at a voltage of 100 kV using a FEI Philips TECNAI 12, after rotary coated with Pt/Pd.

Critical micelle concentration measurement (CMC)

The CMC of Y-DNA-lipid amphiphile in buffer/solvent was analyzed by fluorescence spectroscopy using pyrene as a hydrophobic fluorescence probe. Aliquots of pyrene solutions in acetone (20 μL of 30 μM pyrene) were added to empty tubes, and the acetone was allowed to evaporate overnight. Then, 90 μL of aqueous Y-DNA-lipid amphiphile solution with concentrations ranging from 0.01 nM to 2190 nM was added to the tubes. The solutions were equilibrated for 24 hours at room temperature. When Y-DNA-lipid amphiphile concentrations reach above the CMC, pyrene preferentially partitioned into the hydrophobic part of the assembled core/shell structures. As pyrene moved from hydrophilic to hydrophobic environment, its excitation and emission spectra both exhibited a shift. The fluorescent spectra of the samples were recorded with an SLM 8000c Spectrofluorimeter (SLM) at room temperature (20^{o}C). The excitation spectra were recorded from 280 to 360 nm with an emission wavelength of 395 nm. The CMC of Y-DNA-lipid amphiphile was determined by plotting the intensity (peak height) ratio of the 339 nm peak to the 334 nm peak from the emission spectra versus the logarithm of polymer concentration. The CMC value was taken from the intersection of the tangent to the curve at the inflection with the horizontal tangent through points at low concentrations.

Förster resonance energy transfer (FRET)

To confirm the formation of DNAsome, Cy3 (donor) and Cy5 (acceptor) were chosen for fluorescence resonance energy transfer (FRET) experiments because of the large spectral overlap between emission spectrum of Cy3 and excitation spectrum of Cy5. Two Cy3 or Cy5 were

labeled on a single Y-DNA. With 540 nm laser light, FRET tests were performed by checking fluorescence intensity changes before conjugation of lipid and fluorescence dye labeled Y-DNA and after conjugation of lipid on Y-DNA upon emission at 565 nm and 665 nm.

2.9.4 Cell culture, fluorescence, and transfection studies

Cell maintenance

CHO cells were cultured at 37 °C with 5% CO_2 in Ham's F-12K Nutrient Mixture, Kaighn's Mod, F-12K (Mediatech, Manassas, Virginia) supplemented with L-Glutamine, 10% fetal bovine serum (FBS, Mediatech, Manassas, Virginia), and 1% penicillin/streptomycin (P/S, Mediatech, Manassas, Virginia).

Fluorescence labeling and imaging of cell

CHO Cells (2×10^4 cells) were cultured in a 25 cm^3 flask and plated on the day of experiments by reverse transfection method. CHO cells in suspension media were then transfected and added to the well just before adding the 30 nM fluorescently labeled GAPDH siRNA-hybridized DNAsome in the presence of serum-free media (OPTi-MEM I, Invitrogen, Carlsbad, California) in each well on Lab-Tek chamber slides (8 wells, Permanox slide, Nunc) for 24 hours at 37°C. Then cells were washed three times with PBS and fixed with 4% paraformaldehyde. The method of staining cells by two fluorescent dyes were mentioned previously our papers (73). Briefly, actin filaments and nuclei were stained with Alexa Fluor488 phalloidin (Invitrogen, Carlsbad, California) and DAPI (40,6-diamidino-2-phenylindole) with an antifade reagent (Invitrogen, Carlsbad, California) according to the supplier's protocol. Fluorescence images of the cells were achieved by Zeiss LSM 510 Meta confocal microscope.

Transfection studies

The antisense siRNA strand of Glyceralhehyde-3-Phosphate Dehydrogenase (GAPDH) and

non-complementary sequence of siRNA were obtained (Ambion, Inc., Austin, Texas) and synthesized as a single-stranded siRNA from IDT (Coralville, Iowa). The sequences are (5' - rArArA rGrUrU rGrUrC rArUrG rGrArU rGrArC rCrUrU - 3') for GAPDH siRNA and (5'- rCrCrG rUrArU rCrGrU rArArG rCrArG rUrArC rUrUrU -3') for non-complementary siRNA respectively. The single-stranded siRNA was hybridized to the DNAsome at the sticky end of the Y-DNA as described above. After hybridization, the siRNA-DNAsome complex was diluted in serum-free media (OPTi-MEM I, Invitrogen, Carlsbad, California) to 5 µL final volumes for each amount of siRNA. The amounts of GAPDH siRNA were varied at 10, 30, 90, and 180 nM. The molar ratio of DNAsomes and single-stranded siRNAs was 1:1. After CHO cells (1×10^4 cells in 95 µL P/S –free media) were plated in each well of a 96-well plate, 5µL of prepared samples at different siRNA amounts were added and then mixed gently. The cells were incubated in the controlled-temperature at 37 °C with 5% CO_2 incubator for 4 hours before all complex media were replaced by 200 µL of fresh serum-contained F-12K media. The plate was further incubated until 48 hours and was measured remaining GAPDH protein level by using KDalert^{TM} GAPDH Assay Kit (Ambion, Inc., Austin, Texas) as per the kit's protocol. Briefly, the supernatant was removed and washed three times with 1 x PBS buffer. 200 µL KDalert lysis buffer was added to each sample well. The plate was then kept at 4 °C for 20 minutes. After the cells were lysed, 10 µL of each sample was transferred to a clean 96-well plate. Next, 90 µL of KDalert Mix was quickly added and the fluorescence emitted was immediately measured every one minute by the real-time kinetic mode from a Synergy 4 Hybrid multi-mode microplate reader (Biotek Instrument, Inc., Winooski, Vermont) using a 560 nm excitation and a 590 nm emission filter. The kinetic reaction was run for 4 minutes.

Investigation of endocytosis mechanism of DNAsomes uptake

To investigate the cellular endocytosis mechanism of DNAsomes, CHO cells (1x 10^4 cells) were trypsinized and plated in each well of a 96-well plate. Then, cells were pre-incubated with three endocytosis inhibitors for one hour at 37 ºC with 5 µg/mL of filipin complex, 5 µg/mL of cytochalasin B, and 10 µg/mL of Nocodazole, and 10% of DMSO only as a positive control. Cells were cultured with GAPDH and negative siRNA (30 nM) conjugated DNAsomes respectively for 4 hours. The new media was replaced and additionally incubated for 44 hours (total of 48 hours). An inhibition of endocytosis was determined by Ambion KDalert GAPDH assay (Austin, TX).

Cell cytotoxicity evaluation (MTT)

The cytotoxicity of the DNAsome and siRNA-hybridized DNAsome was determined by MTT (3-(4, 5-dimethylthiazolyl-2)-2, 5-diphenyltetrazolium bromide) cell viability assay (ATCC, Manassas, Virginia). CHO cells were plated in 96-well plate at 8,000 cells per well. Next, the DNAsome and siRNA-loaded DNAsome at different concentrations was added and incubated for 24 hours. Then, the supernatant was replaced by 120 µL of fresh full media and incubated for an additional 24 hours. After 48 hours incubation, 12 µL MTT reagent was added and cells were incubated for 2 hours and purple precipitate was observed. 100 µL of detergent reagent was then added and incubated in the dark at room temperature for another 2 hours. Absorbance was measured with a specific monochrome filter at 570 nm by the Synergy 4 Hybrid multi-mode microplate reader (Biotek Instrument, Inc., Winooski, Vermont). The cytotoxicity (%) of each sample was compared to control cells in full media.

Drug loading and In vitro drug release measurements

Two drug candidates (Bcl-2 siRNA and DOX) were selected to evaluate in vitro drug release profiles. To load model drugs, Cy5 labeled siRNA solution (60 µM, IDT, Coralville, Iowa) and a

doxorubicin (DOX) solution (20 ng/µL), which intercalates DNA, was prepared and incubated with DNAsome in 300 µL of distilled water for 48 hrs at room temperature under gentle shaking to allow both drugs to be encapsulated into DNAsome. After the loading process, each reaction solution was centrifuged at 14000 rpm for 20 min and the supernatant was removed to separate the unloaded drug from DNAsome. The DNAsome was then re-dispersed into 300 µL of PBS solution (pH 7.4) with gentle and continuous shaking (100 rpm) at 37 °C. The amount of DOX or siRNA released from the DNAsome was measured by fluorescence intensity (Doxorubicin excitation 480 nm, emission 550 nm and Cy5-siRNA excitation 650 nm, emission 670 nm). Cumulative drug release profiles were calculated based on the equation below

$$\text{Cumulative Drug Release [\%]} = (Mt / Mo) \times 100$$

where Mt is the amount of accumulated drug released from the DNAsome at time t, and M_0 is the amount of drug loaded into the DNAsome. Here, M_0 was calculated by subtracting the amount of unloaded drug from initial drug fed.

Table 2.1. Oligonucleotide sequences of the Y-DNA building blocks with fluorescent dyes for DNAsome synthesis

Strand		Sequence
Y - DNA (FRET)	**Y_{01}**	5' - /NH_2/ CTT ACG GCG AAT GTC ATG CGG ATC CA - 3'
	Y_{02}	5' - Cys 3 🟢 - GGT CAT CCA TGA CAA CTT TAG GCT GAT TCG GTC ATT CGC CGT AAG - 3'
	Y_{03}	5' - Cys 3 🟢 - TGG ATC CGC ATG AAC CGA ATC AGC CT – 3'
Y - DNA (FRET)	**Y_{01}**	5' - /NH_2/ CTT ACG GCG AAT GTC ATG CGG ATC CA - 3'
	Y_{02}	5' - Cys 5 🔴 - AG GCT GAT TCG GTC ATT CGC CGT AAG -3'
	Y_{03}	5' - Cys 5 🔴 -TGG ATC CGC ATG AAC CGA ATC AGC CT - 3'
Y - DNA (Confocal)	**Y_{01}**	5' - /NH_2/ CTT ACG GCG AAT GTC ATG CGG ATC CA - 3'
	Y_{02}	5' - AG GCT GAT TCG GTC ATT CGC CGT AAG -3'
	Y_{03}	5' – BODIPY 630/650 🔴 - TGG ATC CGC ATG AAC CGA ATC AGC CT - 3'
Y - DNA (Control)	**Y_{01}**	5' - /NH_2/ CTT ACG GCG AAT GTC ATG CGG ATC CA - 3'
	Y_{02}	5' - AG GCT GAT TCG GTC ATT CGC CGT AAG -3'
	Y_{03}	5' - TGG ATC CGC ATG AAC CGA ATC AGC CT - 3'

Note that the labeled fluorescent dye is represented by a dot with the same color.

The same colored sequences represent complementary pairs.

Table 2.2. Oligonucleotide sequences of the siRNA and Y-DNA building blocks for siRNA delivery

Strand		Sequence
GAPDH siRNA		5' - **rArArA rGrUrU rGrUrC rArUrG rGrArU rGrArC rCrUrU** - 3'
GAPDH siRNA (Confocal microscopy)		5' - Cys 5 ● - **rArArA rGrUrU rGrUrC rArUrG rGrArU rGrArC rCrUrU** - 3'
Bcl-2 siRNA		5' - **rCrArC rArUrC rUrCrC rCrArC rArUrC rCrCrA rCrUrC rGrUrA rGrCrC rUrU** - 3'
Negative siRNA		5' - **rCrCrG rUrArU rCrGrU rArArG rCrArG rUrArC rUrUrU** - 3'
Y - DNA (GAPDH)	**Y_{01}**	5' - /NH_2/ CTT ACG GCG AAT GTC ATG CGG ATC CA - 3'
	Y_{02}	5' - **GGT CAT CCA TGA CAA CTT T**AG GCT GAT TCG GTC ATT CGC CGT AAG - 3'
	Y_{03}	5' - TGG ATC CGC ATG AAC CGA ATC AGC CT - 3'
Y - DNA (Bcl-2)	**Y_{01}**	5' - /NH_2/ CTT ACG GCG AAT GTC ATG CGG ATC CA - 3'
	Y_{02}	5' - **CTA CGA GTG GGA TGT GGG AGA TGT G**AG GCT GAT TCG GTC ATT CGC CGT AAG - 3'
	Y_{03}	5'- TGG ATC CGC ATG AAC CGA ATC AGC CT - 3'
Y - DNA (Negative)	**Y_{01}**	5'- /NH_2/ CTT ACG GCG AAT GTC ATG CGG ATC CA – 3'
	Y_{02}	5'- **AGT ACT GCT TAC GAT ACG G**AG GCT GAT TCG GTC ATT CGC CGT AAG - 3'
	Y_{03}	5'- TGG ATC CGC ATG AAC CGA ATC AGC CT - 3'

Note that the labeled fluorescent dye is represented by a dot with the same color.

The bold sequences represent complementary pairs.

CHPTER 3

Synthetic networked DNA structures for 3D cell culture

3. 1 Introduction

In general, *in vitro* cell cultures conventionally refer to cells growing on a two-dimensional (2D) surface, a format that inhibits a number of key cellular functions (131-134). This cellular function impairment occurs because 2D cell culture eliminates *in vivo* conditions, including tightly bound cellular junctions between cells and their neighbors. In addition, the traditional 2D culture completely abolishes the interaction between cells and surrounding biological cues such as extracellular matrices (ECM) and growth factors (135). To date, *in vitro* 3D cell culture forming multicellular spheroids (MCS) have been widely demonstrated and applied to various applications ranging from fundamental cell and cancer biology to tissue engineering and regenerative medicine (136-140). An example of using *in vitro* 3D cell culture for fundamental studies includes the recapturing of gene expression profiles from cells that only express in 3D culture environments (141). Another example includes forming 3D multicellular tumor spheroids for *ex vivo* avascular solid tumor models. The avascular tumor spheroids from 3D cell culture simulate heterogeneity of drug diffusion gradient, intracellular adhesion junction barrier, and cell proliferation that could not be obtained by 2D cell culture (142, 143). In regenerative medicine, 3D cell cultures help promote cell differentiation of several types of stem cells. For instance, embryonic stem cells successfully differentiated into hepatocyte-like ultrastructures when cultured inside 3D collagen scaffolds, whereas the structures cannot be obtained in 2D cell culture (144).

To generate multicellular spheroids from *in vitro* 3D cell cultures, a number of techniques have been developed, including a hanging drop method, rotary orbital motion, liquid-overlay culture, 3D porous- and hydrogel-based scaffold (134, 145-150). One of the most widely used 3D formation methods is the hydrogel-based scaffold. Owing to high water content (> 98%), the hydrogel-based method provides encapsulated cells a similar environment to physiological conditions. The hydrogels can mimic characteristics such as limited gas exchange, nutrient and metabolic byproduct diffusion (140, 151, 152). Most conventional hydrogel-based scaffolds for 3D culture were originally from natural products such as extracellular matrix (ECM) derivatives from animals and alginate derivatives from plants (153). Specifically, ECM is a mixture consisting of proteoglycans, proteins, and soluble factors that are essential for tissue formation and cellular maintenance *in vivo*. One of the most well-known ECM derivatives for 3D cell culture, referred to as a gold standard natural scaffold, is Matrigel^{TM}, consisting of a mixture of laminins, type IV collagens, and heparin sulfate proteoglycans. These components render cell attachment to surrounding tissues (154). Additionally, plant derivatives such as alginate derivatives, extracted from seaweed composed of α-L-guluronic acid and β-D-mannuronic acid building blocks alternately connected forming linear copolymers, have been also reported as a scaffold alternative (155). In spite of excellent physiology-mimicking conditions for 3D cell culture, these natural materials adversely hinder the use in clinical studies due to several reasons. To begin with, natural derivative hydrogels are likely to cause immunostimulatory effects to animal acceptors since they are originally from different species (140). Additionaly, each batch of these natural derivatives varies in their components. As a result, both the biophysical and biochemical properties are extremely varied and uncontrolled, thereby resulting in poor reproducible results and therapeutic evaluation (140, 156).

As a consequence, the obstacles stemming from utilizing natural derivatives have inspired the development of synthetic materials as novel scaffolds for 3D cell culture. The synthesis of artificial materials should not only eliminate inconsistent and ill-defined biochemical and biophysical properties, but also support essential cellular behavior such as cell interaction, proliferation, and differentiation (149, 157). In fact, key requirements need to be achieved before new synthetic materials can be employed as scaffolds for 3D cell culture. First, the new synthetic materials have to allow adequate nutrient, gas, and waste product exchange with surrounding culture media for optimal cellular proliferation and function. Second, the new synthetic materials have to be susceptible to and degradable by cell-secreting molecules at similar rates of cell proliferation, migration, and reorganization to form mature multicellular structures (150, 158, 159). Lastly, resulting byproducts emitted from the new synthetic material degradation must not be toxic to encapsulated cells (153).

Thus far, a great number of synthetic materials have been developed with better controlled mechanical properties, chemical properties, and cell biocompatibility compared to the natural materials (140, 160). For instance, photocrosslinkable poly (ethylene glycol) (PEG) hydrogels are synthetic materials widely used as a hydrogel-based scaffold for 3D cell culture due to their cytocompatibility, non-immunogenicity, and antifouling property (161-163). However, chemical modification is required in the preparation steps of the formation of PEG hydrogels to allow crosslinking between PEG molecules, which is highly time-consuming (164, 165). The most commonly used functional groups for PEG crosslinking is an acrylate group which allows hydrogel formation through photopolymerization (165). After photo initiation, the PEG hydrogels can form with *in situ* cell encapsulation of cells, eliminating the need for post cell-seeding steps (160, 166). The photo- initiated reaction of PEG-based hydrogels has effectively

demonstrated cell encapsulation without cellular toxicity (164, 165, 167). Although they show successful cell encapsulation, PEG is neither biodegradable nor bioadhesive to cells unlike typical extracellular matrices. As a result, embedded cells fail to maturely proliferate and arrest death owing to biologically inert and non-adhesive properties of the PEG-based hydrogels (149, 168, 169). Consequently, incorporation of natural ECM has been utilized to recapture natural biochemical properties in the synthetic hydrogels (138, 160, 170, 171). In the case of PEG, in addition to cross-linking modifications, PEG has to be modified with cell adhesion moieties and emzymatically sensitive signals to regain biofunctional and degradable properties (160). For example, fibrinogen was cross-linked on acrylate-modified PEG side chains resulting in hybrid PEG-based hydrogels that recapitulated cell adhesion for endothelial and smooth muscle cells (172). Similarly, hyaluronic-modified PEG hydrogels were also used in cartilage tissue engineering that aimed for enhancing cell-hydrogel interaction and enzymatically-responsive hydrogel degradation (173). As for synthetic peptides, several short peptide-mimicking fibronectin cell adhesion motifs including GRGDSP, IKVAV, and KQAGDV were commonly utilized to conjugate to the PEG-based hydrogels (174-182). Other functional synthetic short peptides such as GPQGIAGQ, GGLGPAGGK, GPQGIWGQ, and AAAAAAAAAK have been also employed as enzyme-sensitive degradation motifs in the PEG-based hydrogels (133, 149, 150, 167, 180, 182-184).

Alternatively, purely synthetic extracellular matrix-mimicking peptide hydrogels called PuraMatrix^{TM} were proposed by imitating nano and micro structures of natural ECM components (170, 185-187). Driven by ionic interactions between charged synthetic short peptides and ions in the culture media, self-assembly of fibrillar PuraMatrix^{TM} hydrogels occurs simultaneously with *in situ* cell-encapsulation (170). The 3D cell culture by PuraMatrix^{TM} allows encapsulated

cells to interact with synthetic extracellular matrix environments promoting proliferation and differentiation of a number of cell lines, for example neural cells, chondrocytes, and liver progenitor cells (188-190). Even though PuraMatrix^{TM} has been successfully developed in culturing cells with synthetic extracellular matrix conditions, its degradation process is still problematic as the peptide sequences of PuraMatrix^{TM} cannot be naturally degraded by available enzymes *in vivo*.

In addition to the hydrogel-based scaffolds, biodegradable and biocompatible polyester porous structures have been also extensively used to support 3D cell culture such as poly lactic acids (PLA), poly glycolic acids (PGA), and poly lactic- *co*-glycolic acids (PLGA) (191-193). PLGA, the most popular FDA-approved polyesters, which is composed of copolymerizing of different ratios of PLA and PGA, can be simply degraded by hydrolysis which yields cellular metabolites as byproducts (191, 193, 194). Moreover, the rate of PLGA degradation can be tuned by controlling hydrophilic ratios between PLA and PGA (194, 195). While numerous advantages have been demonstrated upon using PLGA as a 3D scaffold, some concerns have also been raised and subsequently addressed. A major concern is the production of porous PLGA scaffolds which involve several chemicals and porogens resulting in harsh conditions for *in situ* cell encapsulation. Hence, a post-cell seeding method is required and causes problems in limited cell accessibility resulting in large void volume inside the 3D scaffold (196). Another controversial concern is the accumulation of metabolite byproducts that might possibly cause adverse effects on cell proliferation in both *in vitro* and *in vivo* (191).

Recently, our group has pioneered the development of self-assembled enzymatic-catalyzed DNA hydrogels purely made of synthetic branched DNA building blocks (70). In the report, we showed that the DNA hydrogels encapsulate Chinese ovary hamster (CHO) cells with cell

viability and active metabolic function after cell encapsulation. Additionally, the DNA hydrogels that were injected into B57L mice for *in vivo* studies did not exhibit toxicity when compared with PBS control. The DNA hydrogels are also easily manipulated by different endo- and exo-nucleases (64, 70, 72). We employed the synthetic DNA hydrogels as a biocompatible and biodegradable scaffold for an *in vitro* 3D cell culture. In the study, we demonstrated that (1) the formation of synthetic DNA hydrogels occurred under physiological conditions and simultaneously encapsulate cells with high cell viability; (2) the encapsulated cells proliferated as a spheroidal structure inside the synthetic DNA hydrogels at least 9 days before the DNA hydrogel naturally degraded; (3) the flexibility of the DNA hydrogels respond to essential physiological cues; (4) last but not least, we demonstrated on-demand retrieval of multicellular spheroids (MCS) without mechanical disruption to MCS by utilizing DNase I enzymatic reactions.

3.2 Optimization of DNA hydrogel formation for 3D cell culture

The DNA hydrogels are synthetic materials that can be manipulated by a number of molecular toolkits. In addition, they are non-toxic to immobilized cells for a period of time throughout the *in vivo* study (64, 70). Branched X-DNA building blocks were prepared as reported previously (70). The scheme of X-DNA building blocks self-assembly and oligonucleotide sequences are shown in Figure 3.1 and Table 3.1, respectively. For a 3D cell culture, we first optimized the condition of DNA hydrogel formation to obtain the highest cell viability for *in situ* cell encapsulation. The DNA hydrogels, formed under two different ligation buffers, were incubated with HeLa S3 cells in the presence of 1x serum-free Optimem-I media for 6 hours. The ligation

conditions and their components in the optimization experiments are shown in Figure 3.2 a and b. Note that NEBuffer 1 buffer was supplemented with 1mM ATP throughout experiments as a required co-factor for a complete ligation. After incubation, cell viability was determined by alamarBlue reagents. The cell viability dropped dramatically to 35% and 85% after incubating with T4 ligase buffers and NEBuffer 1, respectively ($P < 0.05$). We hypothesized that high cellular toxicity was caused by a high concentration of dithiothreitol (DTT) supplemented in the T4 ligase reaction buffers. The DTT can passively diffuse through cell membrane, affecting the stability of disulfide bond of proteins located inside endoplasmic reticulum (ER), cell proliferation, and cell-cell interaction, to name a few (197, 198). We thus further investigated the effects of DTT concentration on cell viability by incubating cells with different concentrations of DTT containing serum-free media (Figure 3.2c). The results confirmed the severe cellular toxicity of high levels of DTT in the culture media as 10, 1, and 0.1 mM of DTT result in 29%, 49%, and 94% cell viability, respectively (Figure 3.2c). Interestingly, compared at the same DTT concentrations, the cellular toxicity from ATP-containing buffers was significant lower than that from DTT solution alone. These results correlated with previous works that showd that after receiving DTT, unfolded proteins can reversibly fold back to their native structures in ATP-supplemented conditions (198, 199). To avoid the deleterious effects of DTT to cellular functions, we chose NEBuffer 1 containing 1mM DTT concentration as a ligation buffer to form cell-encapsulating DNA hydrogels throughout the experiments.

3.3 Characterization of new condition of DNA hydrogels for 3D cell culture

The newly adapted condition for the formation of cell-encapsulating DNA hydrogels consisted of

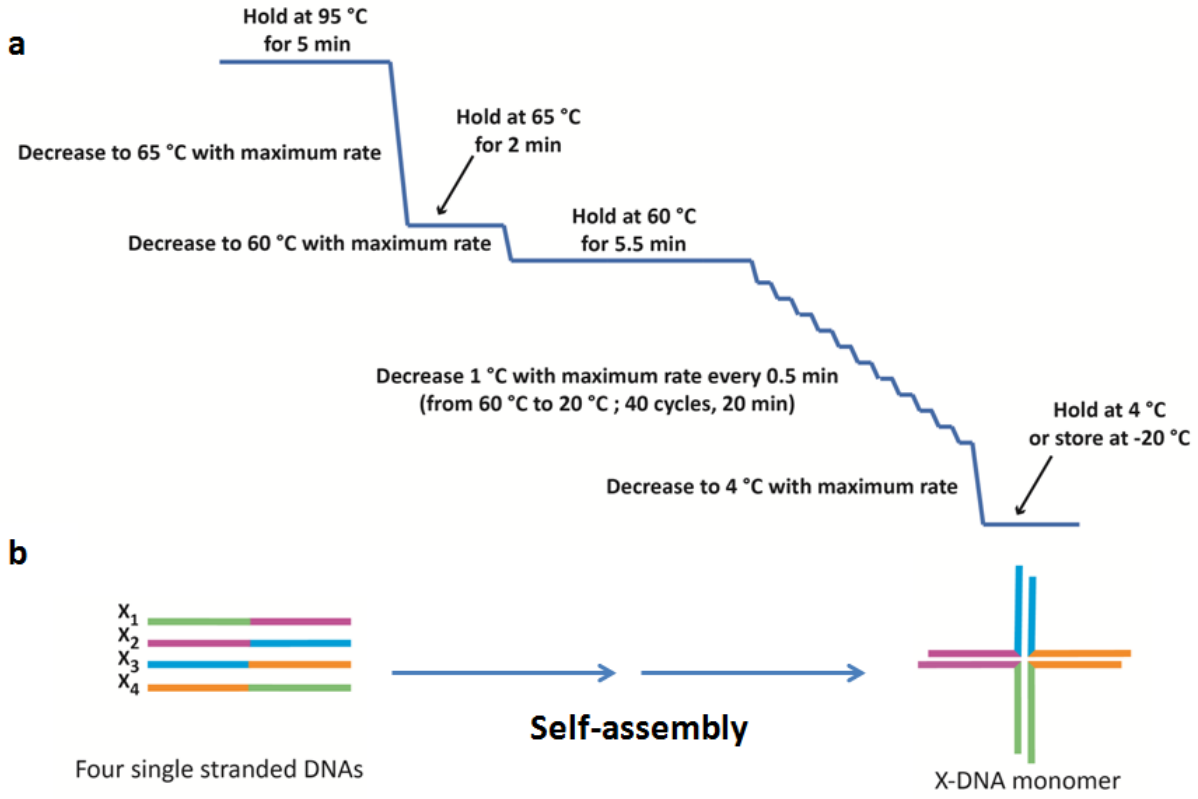

Figure 3.1. a. Schematic illustration of temperature gradient for X-shaped DNA self-assembly. b. Iimage demonstrating the self-assembly of the X-DNA building block in which half of each oligonucleotide is complementary to adjacent oligonucleotides forming X-shaped DNA.

a

Components	Concentration (mM)
Tris-HCl	50
$MgCl_2$	10
ATP	1
Dithiothreitol	10
pH at 25 °C	7.5

b

Components	Concentration (mM)
Bis-tris-propane-HCl	50
$MgCl_2$	10
Dithiothreitol	1
pH at 25 °C	7.0

c

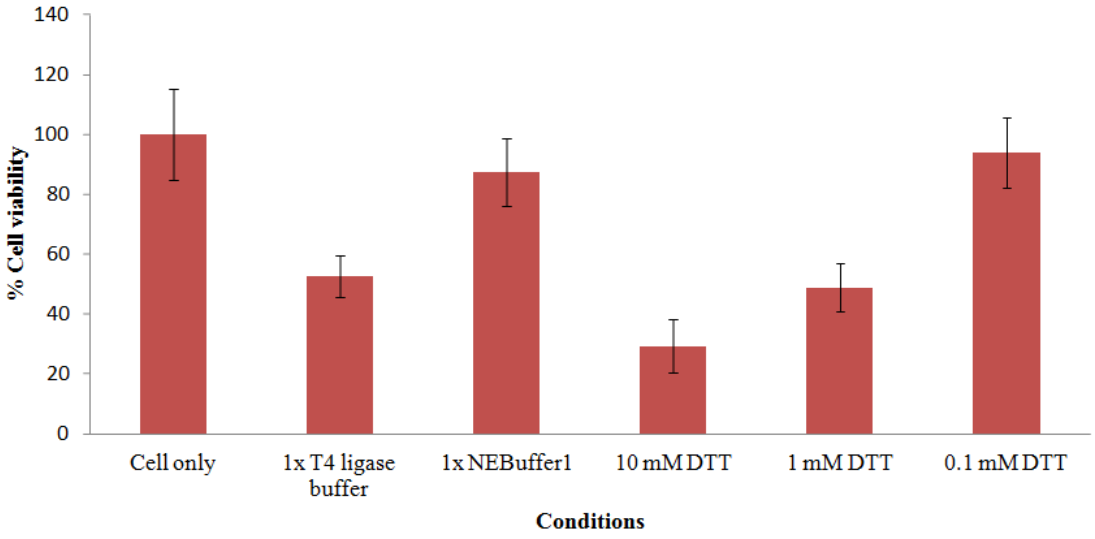

Figure 3.2. The components of two ligation buffers and cell viability in different buffer conditions. a. The components of T4 ligase buffer provided with the T4 ligase enzyme kit and used to form regular DNA hydrogels in the previous publication. b. The components of NEBuffer 1 which is an alternative buffer for DNA ligation. c. The cell viability of HeLa cells in various conditions after 6 hour of incubation. Note that all conditions were prepared in 1x serum-free media.

1 mM ATP-supplemented NEBuffer1 and 1x serum-free cell culture media. Next, we characterized major physical properties to compare with the original reported DNA hydrogels (70, 200). To begin with, we compared the ligation efficiency between both DNA hydrogels formed from both T4 ligase and NEBuffer1 buffer conditions. As the DNA T4 ligase enzymes have been shown to reduce their enzyme activity in the presence of NaCl higher than 150 mM, we investigated the activity of the DNA T4 ligase enzyme activity in the presence of typical culture media in the reaction (201, 202). The efficiency of X-DNA building block incorporation into the DNA hydrogel is used to indicate the active T4 ligase enzymes in the reaction. It was shown that the efficiency of X-DNA building block incorporation for T4 ligase and NEBuffer1 buffers are 70% and 75%, respectively (Figure 3.3a). Thus, changes in ligation buffers and the presence of monovalent cations from the cell culture media did not inhibit the DNA T4 ligase enzyme activity when compared with the regular DNA hydrogels. Next, the DNA hydrogel swelling ratios between the two DNA hydrogel conditions were determined by weight differences between swollen and dried states of the DNA hydrogels (Figure 3.3b). The DNA hydrogels, formed according to Materials and Methods Section 3.7.1, were equilibrated with PBS buffer at room temperature for 24 hours. Then, excess supernatant was carefully removed and the weights of the swollen state of the DNA hydrogels were measured. The results demonstrated that the DNA hydrogels adapted from NEBuffer1 supplemented with serum-free cell culture media and that from the DNA T4 ligase buffers swelled 27.9-fold and 71.7-fold compared to their dried states, respectively. This difference in the swelling ratio is likely due to the fact that the presence of cationic ions such as Na^+, Ca^{2+}, and K^+ is known to stabilize repulsive forces between negatively-charged phosphate groups on DNA backbones (10, 203, 204). Hence, a 2.5-fold decrease in the swelling ratio of the NEBuffer1-adapted DNA hydrogels

compared to the regular DNA T4 ligase buffer hydrogels likely results from a higher concentration of mono- and multi-valent ions in the culture media presented in the DNA hydrogel formation. The electrostatic repulsion of the DNA hydrogel structures from the adapted condition was greatly reduced leading to less swelling and less hydration of the DNA hydrogels. As a result, we anticipated to observe smaller pore sizes from the adapted DNA hydrogels than those from the regular DNA hydrogels. We further investigated morphologies of the DNA hydrogels under a scanning electron microscope (SEM) and found that both of the DNA hydrogels displayed distinct porous structures (Figure 3.3c). Larger porous DNA hydrogel structures were obtained from the regular DNA hydrogels while smaller porous and more densely-packed structures were obtained from the newly-adapted DNA hydrogels. As a result, the decreases in the swelling ratio corresponded to changes in the DNA hydrogel microstructure, confirming the effects of additional mono- and multi-valent ions from serum-free media incorporated into the DNA hydrogels.

3.4 Characterization of cell-encapsulating DNAhydrogels

After optimizing the condition for forming *in situ* cell-encapsulating DNA hydrogels, various adherent and suspension cell lines were embedded in the DNA hydrogel to demonstrate versatile uses of the DNA hydrogel as a novel hydrogel-based scaffold for 3D cell culture.

3.4.1 Proliferation of cells encapsulated inside DNA hydrogels

In our model study, we investigated the proliferation curve of suspension HeLa S3 cell lines after their encapsulation inside the DNA hydrogels. The HeLa S3 cell lines, suspension cells that were

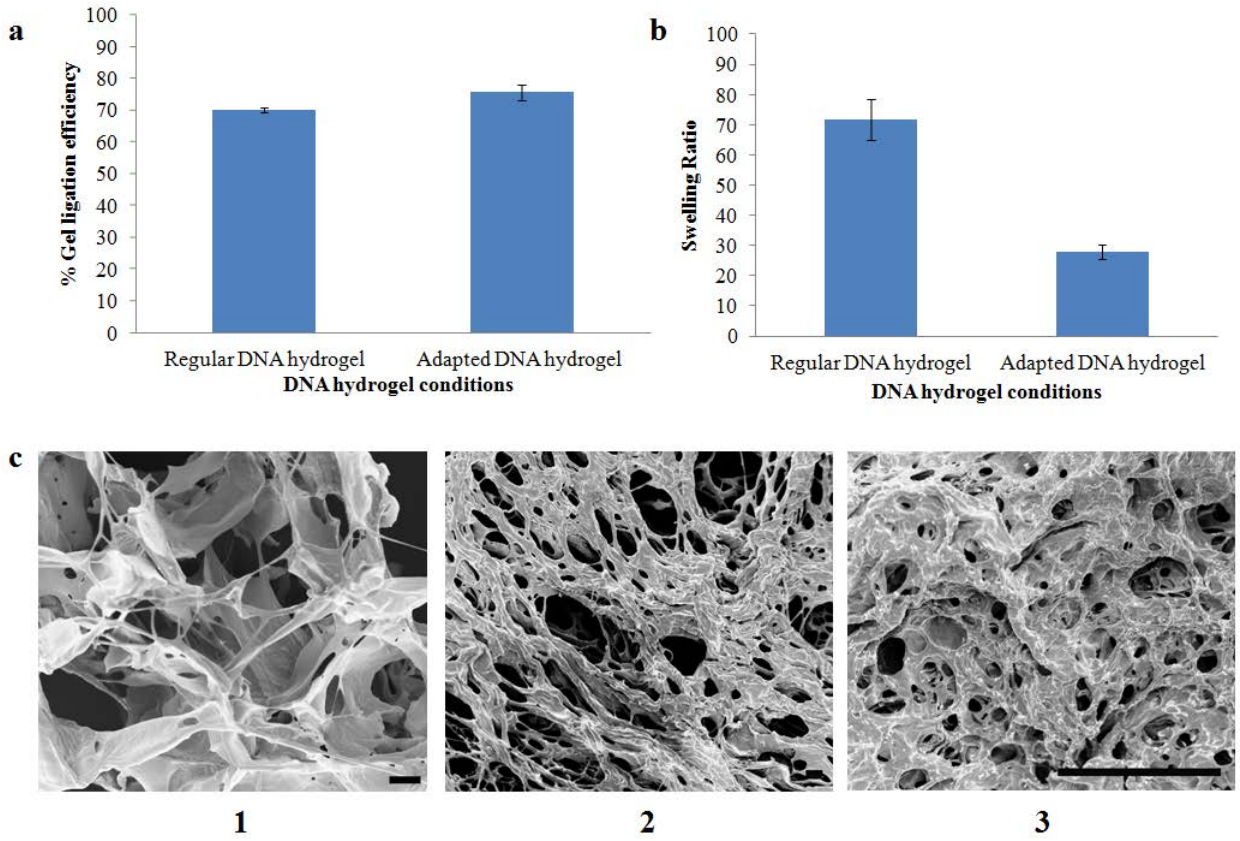

Figure 3.3 Characterization of regular and adapted DNA hydrogels. a. Gel ligation efficiency of regular and adapted DNA hydrogels. b. Swelling ratio measured by weight differences between wet and dry states of regular and adapted DNA hydrogels. c. Morphological studies of freeze-dried 0.1 mM DNA hydrogels by SEM. From left to right, (1) regular DNA hydrlgels, (2) adapted DNA hydrogels without serum-free cell culture media, and the adapted NEBuffer1 DNA hydrogels with serum-free cell culture media (working condition). (Scale bars are 20 μm)

mutated from anchoring-dependent HeLa cell lines, were used to represent characteristics of cancer cells. The HeLa S3 cells were encapsulated and evenly distributed inside the DNA hydrogels with high cell viability after the first hour of *in situ* cell encapsulation indicated by Calcein AM, a fluorescent dye that stains live cells (Figure 3.4a). On the fourth day of culture, the cells proliferated and formed loose MCS (Figure 3.4b). The proliferation rate of the HeLa S3 cells was monitored by a dye exclusion method and total cell numbers. For the proliferation curve, the total cell numbers were plotted on the y-axis against culture times on the x-axis (Figure 3.4c). After observed for 9 days, HeLa S3 cells encapsulated inside the DNA hydrogels followed a typical proliferation curve, indicating normal cell functionality of the cells inside the DNA hydrogels. The growth of HeLa cells started reaching a plateau at day 7 with MCS formation. On day 9 of culture, the DNA hydrogels were completely degraded leaving all MCS precipitating at the bottom of the culture dishes. It is worth noting that 59% of DNA hydrogels remained in 10% FBS containing media (cell culture condition) after 9 days of incubation in the absence of cells (Figure 3.5). Therefore, the DNA hydrogel degradation was likely dependent on an additional presence of embedded cells that affected the surrounding environment of the DNA hydrogels. Subsequently, the natural degradation phenomenon of DNA hydrogels is caused by not only nuclease-containing serum in the cell culture media, but also the presence of the cells and molecules secreted from the cells encapsulated inside the hydrogels. This is very beneficial for extracting MCS from the DNA hydrogels for downstream applications, as MCS can be retrieved without any physical or chemical treatments minimizing disruption of the encapsulated cells.

3.4.2 Morphology of multicellular spheroids forming inside DNA hydrogels

We further investigated cell morphology after MCS were formed inside the DNA hydrogels. In the previous 3D proliferation study, HeLa S3 cells formed loose MCS with no spread-out morphology. Also, we found that the average MCS sizes enlarged as incubation times increased (Figure 3.6a). In addition to the HeLa S3 cell line, we also encapsulated anchorage-dependent cell lines including HeLa and CHO-K1 inside the DNA hydrogels and monitored their proliferation and morphology. Both HeLa and CHO-K1 grew and formed MCS with unique morphological characteristics. After six days of 3D cell encapsulation, HeLa cells formed tight and smooth-edged MCS while CHO-K1 cells formed grape-like MCS (Figure 3.6b and c), respectively.

3.4.3 Surface functionalization of cellular recognizing signals on DNA hydrogels

One of the most important cell behaviors when cells are cultured in synthetic materials is the formation of focal adhesion and their response to the surrounding environment (181, 205). In this study, we demonstrated the flexibility of a chemical conjugation between DNA materials and short peptides, which are synthetic cellular signals. For a model study, we chose to conjugate the 3’ end of the X-DNA building blocks to a short synthetic cell-attaching signal arginine (R), glycine (G), and asparatate (D) (RGD) peptide. The short synthetic RGD peptide artificially simulates interactions between cells and extracellular matrices, thereby triggering the release of several intracellular signals, such as signals for cell adhesion, cell migration, and cell proliferation (174, 181, 206). Hence, we incorporated the synthetic RGD peptides to one of four branches of the X-DNA building blocks. Specifically, we designed the system such that one 5’ end of the DNA oligonucleotides reacted with a decanoic acid diester linker resulting in a reactive *N*-Hydroxysuccinimide (NHS)-conjugated oligonucleotides. These NHS-functionalized

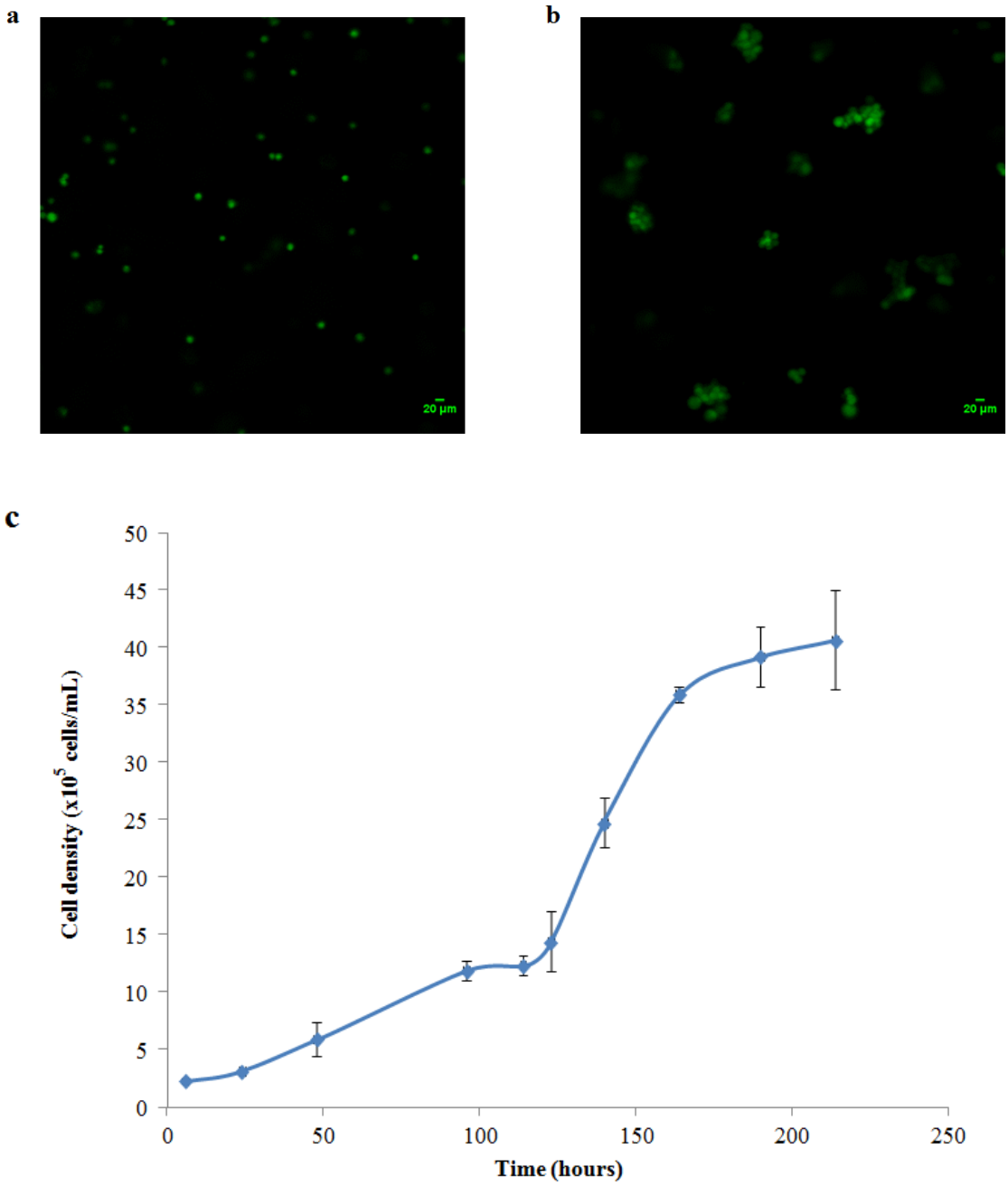

Figure 3.4. Cell viability and proliferation of HeLa S3 cells-encapsulated DNA hydrogels. a. Cell viability of HeLa S3 cells, determined by Calcein AM live staining dyes, after 6 hour and 96 hour encapsulation. b. Proliferation curve of HeLa S3 cells cultured inside the DNA hydrogels for 9 days until the DNA hydrogels completely degraded.

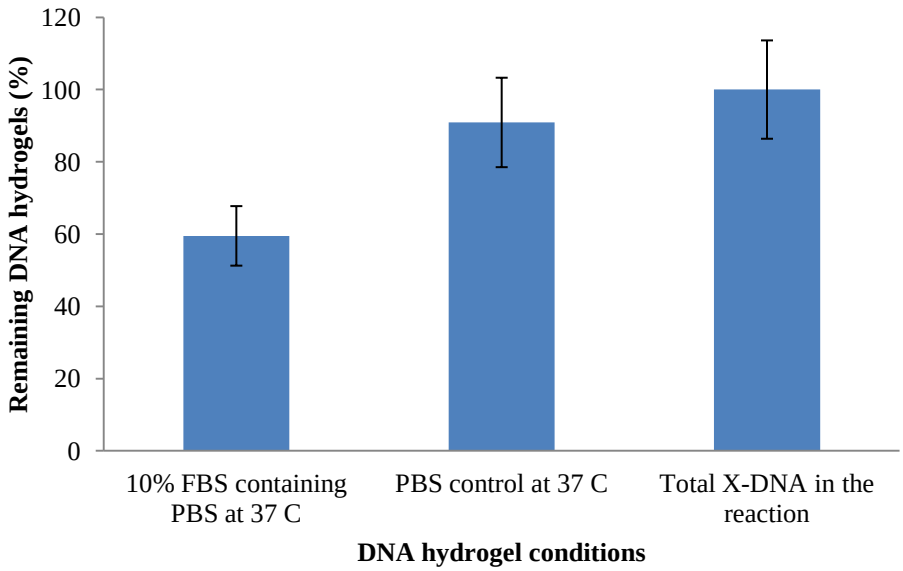

Figure 3.5. Effects of 10 % fetal bovine serum (FBS) on the degradation of the DNA hydrogels without cells encapsulated. The remaining DNA hydrogels were investigated after 9 days by quantifying the total nucleotides of the DNA hydrogels left in the reactions. From left to right, the DNA hydrogels were incubated in 10% FBS in PBS and PBS only at 37 °C compared with the total X-DNA building blocks used in the hydrogel formation.

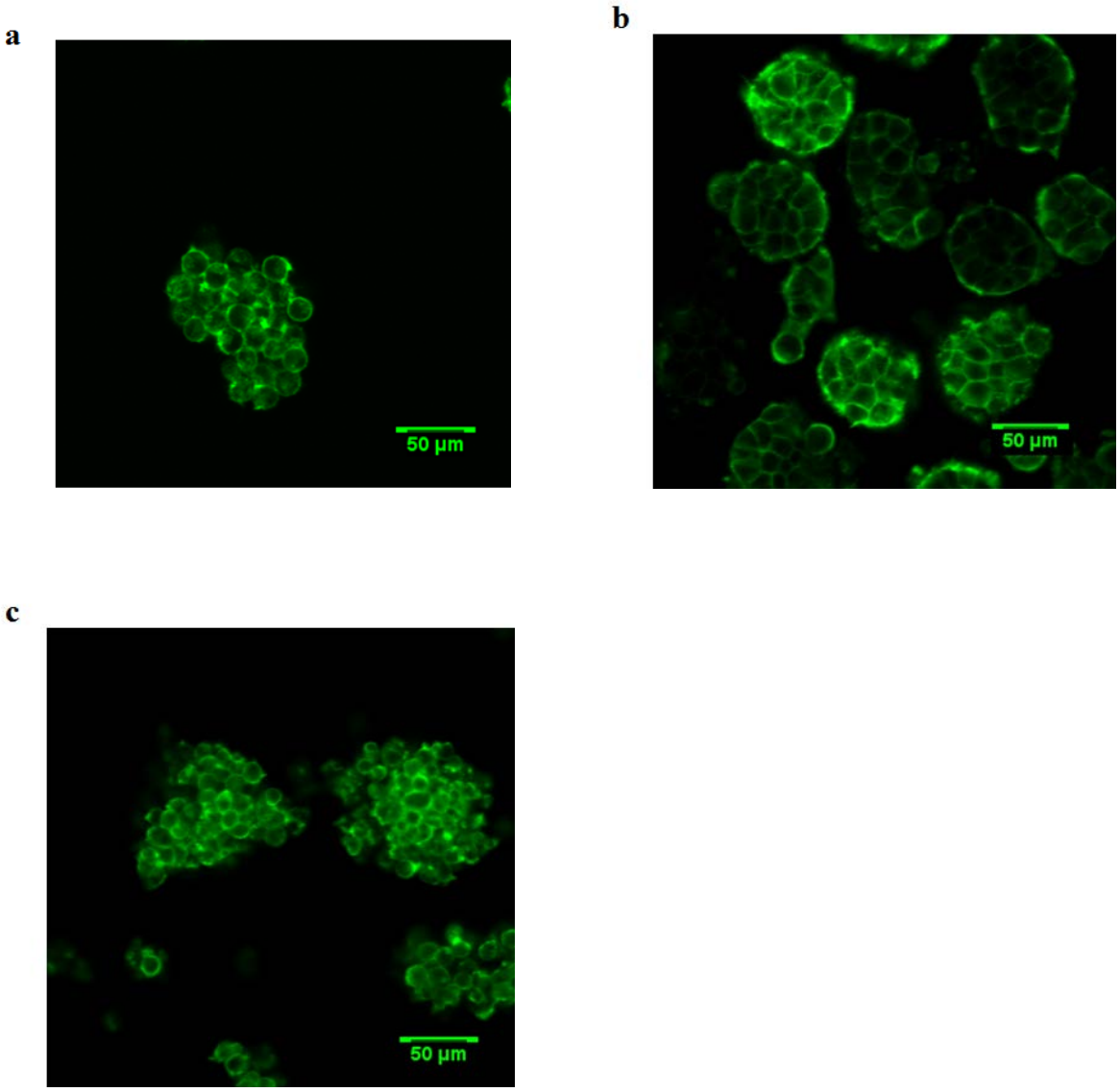

Figure 3.6. Mophological study of MCS cultured inside the DNA hydrogels after 6 days of the 3D cell culture. The images were taken by confocal microscope. Three cell lines were used in the encapsulation experiments including HeLa S3 (a), HeLa (b), and CHO-K1 (c). F-actin filaments were stained with Alexa 488-conjugated phalloidin.

DNA oligonucleotides effectively formed a stable amide bond via the primary amines of the lysine amino acid (K) side chain of the RGD peptides. The N- and C- terminals of the RGD peptide were also capped with acetyl and primary amide groups, respectively, to protect non-specific reactions. The conjugation reaction occurred on the oligonucleotide-supported resins with an excess of free synthetic RGD peptides. The NHS groups reacted with the primary amine groups on lysine amino acids covalently generating the RGD-conjugated DNA oligonucleotides linked by amide bonds. The RGD- modified and non-modified oligonucleotides were characterized and purified by denaturing polyacrylamide gel electrophoresis (PAGE) (Figure 3.7a). The RGD conjugation efficiency was calculated to be approximately 60% employing Image J quantification. The self-assembly of the RGD-modified X-DNA building blocks was successfully achieved without an interference from the synthetic RGD peptides (Figure 3.7b). To form the RGD-modified DNA hydrogels, the RGD-modified X-DNA building blocks were mixed with non-modified X-DNA building blocks in different ratios and followed the protocol of non-modified DNA hydrogel formation. HeLa cells were encapsulated inside the RGD-modified DNA hydrogels with fixed concentration of the non-modified X-DNA building blocks and various concentrations of the RGD-modified X-DNA building blocks. The concentrations of the non-modified X-DNA building blocks were fixed at 120 μM and the RGD-modified X-DNA building blocks were 0.4 and 6.8 μM resulting in the ratios of 300:1 and 20:1, respectively. For both RGD-modified DNA hydrogels, HeLa cells were embedded and cultured for 4 days and observed under a confocal microscope (Figure 3.8a). The same tight, smooth-edged MCS that was previously found in the purely non-modified DNA hydrogels was also observed in the RGD-modified DNA hydrogels. For comparison, we encapsulated HeLa cells in PuraMatrix^{TM}, extracellular matrix-mimicking synthetic peptide hydrogels typically used to study cell-

extracellular matrix interactions (151, 170, 188-190). In the experiments, a brief PuraMatrix™ optimization was performed and 0.15% w/v concentration was chosen to use as a model comparison. HeLa cells encapsulated inside PuraMatrix™ showed a spread-out morphology with lamellipodia and filapodial extension (Figure 3.8b). Also, the cells formed multi-layer structures instead of MCS, indicating a stronger interaction between cells and surrounding synthetic peptide hydrogels than the interaction between cells and surrounding cells that was observed in the DNA hydrogels. These morphological differences could be due to a number of factors. As previously reported, in addition to RGD densities, the changes in cellular morphology are also dependent on other factors including stiffness of the synthetic materials, affinity and spacer length between RGD signals, and cellular binding receptors (181, 207). Hence, further optimization is required to acquire a better understanding of the morphological changes and other cell-extracellular matrix interactions in the synthetic DNA hydrogels. Despite producing no differences on the morphological changes, the HeLa MCS exhibited higher cell growth in the presence of the RGD peptides at 300:1 molar ratio. Average sizes of 55.3 (± 7.80) and 70.2 (± 11.90) μm were reported for the HeLa spheroids embedded in non-modified and RGD-modified DNA hydrogels, respectively. Thus, the incorporation of functional synthetic RGD peptides to the synthetic DNA hydrogels was seen to enhance the cell proliferation. With these results, we have demonstrated the potential in conjugating several short synthetic peptides to the synthetic DNA hydrogels for cellular response and surface functionalization.

3.5 On-demand recovery of MCS by DNAse I enzymatic reaction

As indicated in section 3.4.1., the cell proliferation of the MCS inside the synthetic DNA hydrogels naturally accelerated the gel degradation, thereby leading to the release of the MCS without mechanical and chemical disruption to the MCS structures. Additionally, we also demonstrated that the MCS in the synthetic DNA hydrogels can be harvested on-demand by using one of the molecular toolkits associated with DNA: DNase I enzymes. HeLa cells encapsulated in the DNA hydrogels were cultured for 4 days and the MCS were released by adding DNAse I-containing culture media and incubating at 37 °C for one hour (Figure 3.9a). The released MCS were still intact and conserved their spheroidal shapes (Figure 3.9b). Then, the released MCS were simply collected by centrifuging at 100 rcf for 1 minute. The collected MCS were re-encapsulated inside newly prepared DNA hydrogels without causing any damages to the MCS structures that were observed under a confocal microscope after 24 hours of re-encapsulation (Figure 3.9c). Moreover, the viable encapsulated MCS were fluorescently stained by Calcein AM (Figure 3.9d). The DNase I enzymes accelerated the degradation rates of the DNA hydrogel, giving the advantage of effectively releasing MCS at all stages of the 3D cell culture.

3.6 Summary

In conclusion, we have successfully demonstrated the use of the synthetic DNA hydrogels as a novel DNA hydrogel-based scaffold for 3D cell culture. The formation of the synthetic DNA hydrogels occurred at physiological conditions, which mean that cells can be encapsulated during gel formation and thereby eliminating multiple steps of cell loading. Moreover, the DNA hydrogels swelled approximately 28 times, forming highly porous structures in which cells are

able to reside and proliferate. At the same time, the porous DNA hydrogel structures are loose enough for nutrients and waste byproducts to be exchanged with surrounding culture media resulting in a typical growth curve of encapsulated cells. Additionally, the MCS grew inside both non-modified and RGD-modified DNA hydrogels as tight, smooth-edged MCS while the cells grew inside PuraMatrix^{TM} as multi-layers in spread-out morphology. Furthermore, we confirmed that the functional synthetic RGD peptide conjugation led to a significant increase in the MCS sizes, thereby indicating higher rates of cell growth. Also, the synthetic DNA hydrogels are naturally and gradually degraded in a response to nuclease-containing culture media and growing encapsulated cells. Alternatively, the DNA hydrogels could also undergo on-demand MCS retrieval utilizing DNAse I enzymes. The retrieved MCS were conveniently purified and re-encapsulated in newly formed DNA hydrogels for downstream processes with full cell function and high cell viability.

3.7 Materials and Methods

3.7.1 Synthesis and Preparation of DNA hydrogels

Synthesis of DNA hydrogel building blocks

All DNA sequences were reported in Table 4.1. All standard DNA oligonucleotides were commercially synthesized from Integrated DNA Technologies, Inc (Coralville, Iowa) with desalting purification. An activated carboxylic acid N-hydroxysuccinimide (NHS) ester-conjugated DNA oligonucleotides attached on supporting beads were purchased from TriLink BioTechnologies, Inc. (San Diego, CA). All the standard DNA oligonucleotides were dissolved

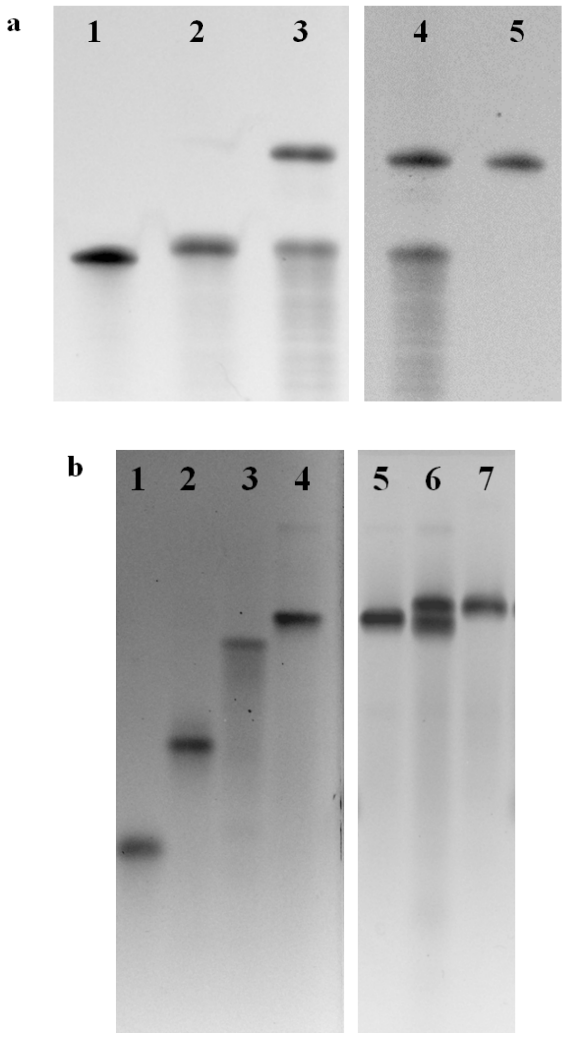

Figure 3.7. Characterization and purification of RGD-modified X-DNA building blocks. a. 15% denaturing PAGE of RGD-conjugated oligonucleotides. Lane1: oligonucleotide controls, Lane2: NHS-conjugated oligonucleotide controls, Lane3 and 4: RGD-conjugated oligonucleotides, and Lane5: purified RGD-modified oligonucleotides. b. 3% Nusieve agarose gel electrophoresis of the annealing RGD-modified X-DNA building blocks. Lane1: one oligonucleotides, Lane2: two oligonucleotides, Lane3: three oligonucleotides, Lane4 and 5: four oligonucleotides (X-DNA building blocks), Lane6: RGD-modified X-DNA building blocks without purification, and Lane7: RGD-modified X-DNA building blocks after the purification of conjugated oligonucleotides.

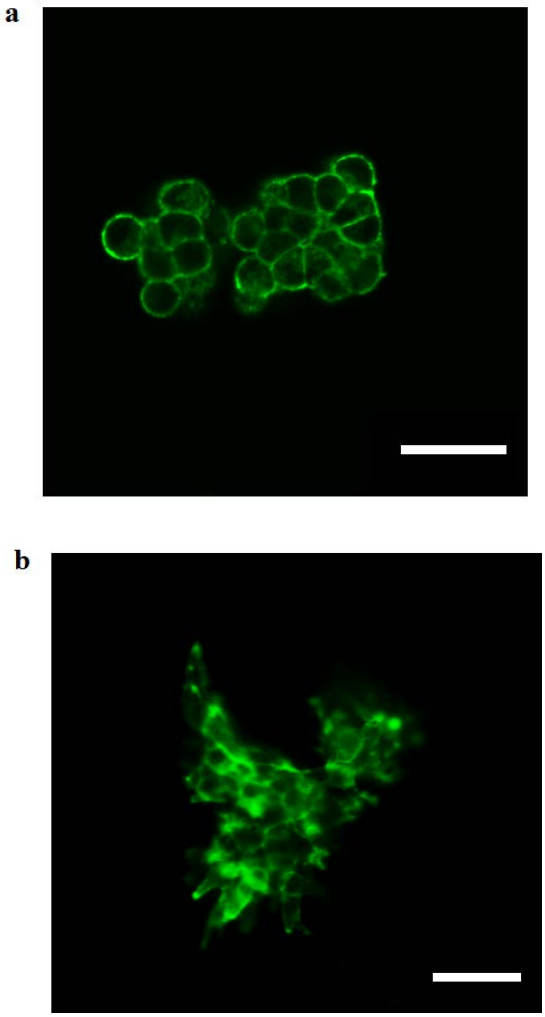

Figure 3.8. MCS morphology of HeLa cells after 4 days of 3D cell culture by a confocal microscope. a. HeLa MCS encapsulated inside RGD-modified DNA hydrogels demonstrating a tight, smooth-edged MCS. b.HeLa cell-encapsulating PuraMatrix^{TM} demonstrating a spread-out morphology with lamellipodia and filapodial extension. The scale bar is 50 µm.

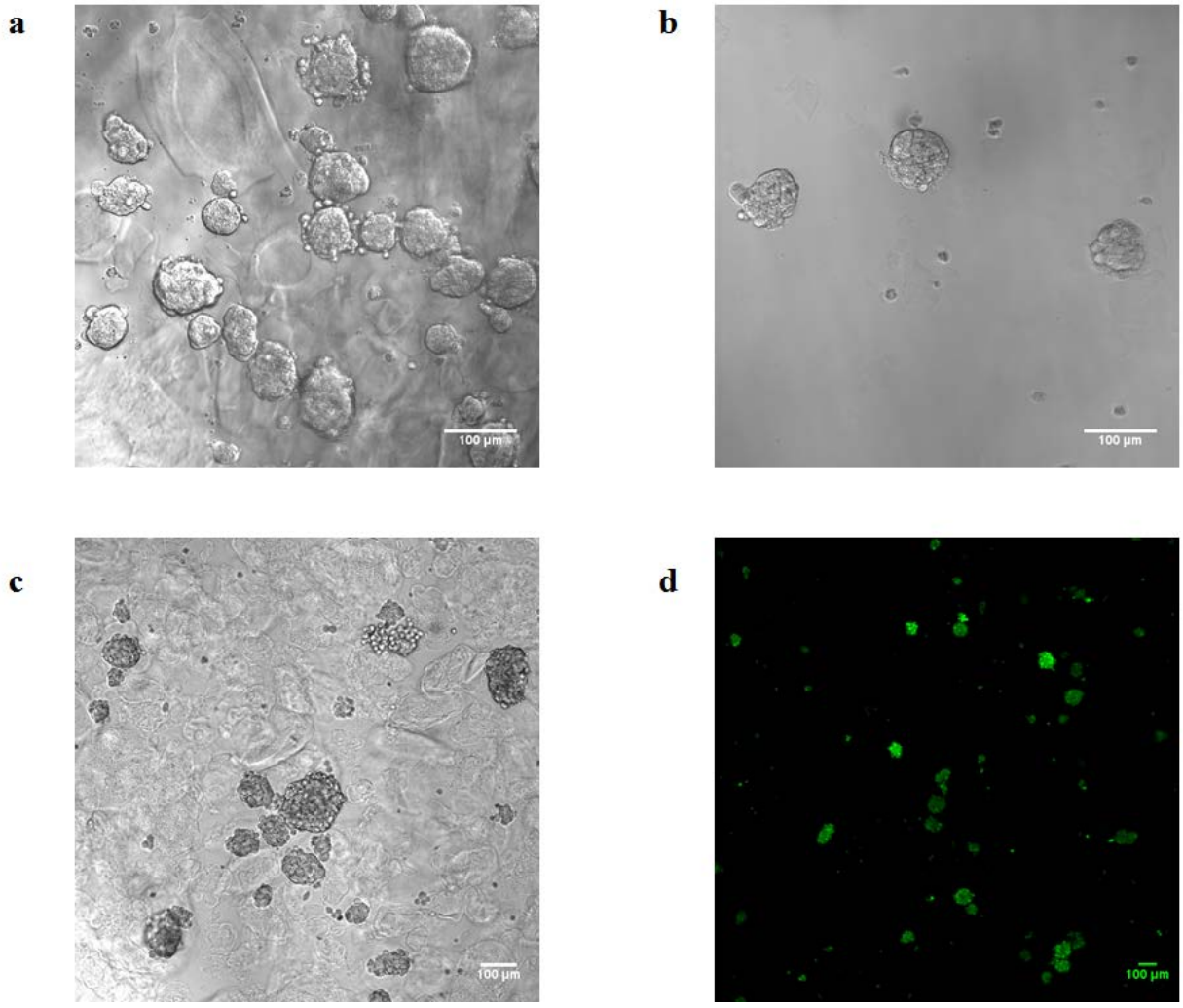

Figure 3.9. On-demand release of MCS from DNA hydrogels. a. HeLa cells were encapsulated inside DNA hydrogels for 4 days. b. HeLa MCS were released from the DNA hydrogels by adding DNAse I enzymes for one hour. c. The released HeLa MCS were re-encapsulated inside the DNA hydrogels again (The image was taken after 24 hour re-encapsulation). d. The re-encapsulated HeLa MCS were stained with Calcein AM and imaged by a confocal microscope.

in 10 mM Tris (pH = 8.0) in 1 mM ethylenediaminetetraacetic acid (EDTA) solution at 1 mM concentration. For an annealing procedure for the X-DNA building blocks, an equivalent molar of all 4 DNA oligonucleotides were mixed at 200 μM final concentration. The X-DNA building blocks were formed according to following procedures: (i) Denaturing at 95 °C for 2 min. (ii) Cooling at 65 °C and incubation for 5 min. (iii) Annealing at 60 °C for 2 min. (iv) Further annealing at 60 °C for 0.5 min with a continuous temperature decrease at a rate of 1 °C per min for a total of 56 cycles. The final annealed X-DNA building blocks were kept at -20°C until used.

Design and formation of DNA hydrogels

The standard DNA hydrogel formation protocol was reported previously (70). For the cell-encapsulating DNA hydrogels, the standard protocol was adjusted for the cell compatibility as follows: Briefly, the X-DNA building blocks were mixed with NEBuffer 1, supplemented with 1mM ATP, and DNA T4 ligase from NEB (Madison, WI) at 1x serum-free media final concentration. The reaction was incubated at room temperature in a sterile condition for 6 hours for complete enzymatic reaction. Then, the X-DNA hydrogels were washed with serum-free media and used for the characterization experiments of DNA hydrogels for 3D cell culture purpose.

Preparation of synthetic RGD peptide and RGD-modified DNA oligonucleotide conjugates

The synthetic short RGD peptide, Peptite 2000 was purchased from AdvancedBioMatrix, Inc (San Diego, CA). The lyophilized peptides were dissolved in DMSO and used immediately after dissolving. The NHS-conjugated oligonucleotides on supporting beads were added to RGD solution in DMSO and the reaction was done on a vigorous shaker at room temperature overnight. After the reaction, the supporting beads were pelleted, DMSO supernatant was taken

out, and the RGD-conjugated DNA oligonucleotides were cleaved from the supporting beads by adding anhydrous ammonium hydroxide at room temperature. After cleaving, the ammonium hydroxide was evaporated and the DNA oligonucleotides were re-dissovled in water. The agarose gel electrophoresis was used to characterize and purify the RGD-modifid DNA oligonucleotides.

3.7.2 Characterization of DNA hydrogels

Swelling ratio

The effects of the presence of cell culture media to the DNA hydrogel's properties were investigated by determining a swelling ratio of the DNA hydrogels. The DNA hydrogels were formed in the presence of 1x cell culture media final concentration as previously described in the DNA hydrogel formation section. Briefly, a fifty-micro liter reaction of the DNA hydrogels was formed in a microcentrifuge tube and incubated for 6 hours in a sterile condition. Two hundred micro liters of PBS buffer were added to the gel to equilibrate the gels for 24 hours at room temperature. After equilibrated, the supernatant was removed from the DNA hydrogels by pipetting and the leftover liquid was dabbed by blotting paper on top of the gels. The DNA hydrogels were then weighted and lyophilized overnight with Freezone freeze dryer from Labconco, Inc. (Kansas City, MO) The dried DNA hydrogels were re-weighed on a scale and subtracted by media only dried in the tubes as a control. The experiments were done in triplicate.

DNA hydrogel ligation efficiency

To determine the efficiency of X-DNA building blocks incorporating into the DNA hydrogels, 200 μM of the DNA hydrogels were formed and incubated in 200 μL PBS buffer at 60 °C for 24 hours in a thermocycler with 105 °C lid temperature to protect the evaporation

throughout the reaction. The supernatant was taken out and digested by a combination nuclease enzyme including DNase I, Exo I, and Exo III at 37 °C overnight to nucleotide products. The concentration of nucleotides was measured by Nanodrop 1000 and compared with the digested X-DNA building block amounts used to form the DNA hydrogels. The ligation efficiency was calculated as following,

$$\text{The ligation efficiency} = \frac{(\text{The total amount of X-DNA} - \text{The amount of DNA in supernatant})}{\text{The total amount of X-DNA}} \times 100\,\%$$

DNA hydrogel degradation

The DNA hydrogels made according to section 3.7.1 were incubated with 10% serum-containing cell culture media for 9 days at 37 °C. After incubated, the DNA hydrogels were washed with PBS buffer and digested to nucleotides by a combination solution of DNAse I, Exo I, and Exo III enzymes overnight at 37 °C. The concentration was measured by nanodrop and compared to initial digested total X-DNA building blocks used to form the DNA hydrogels.

3.7.3 Cell culture and *in situ* cell encapsulation inside DNA hydrogels

Cell maintenance

All cell lines were purchased from ATCC (Manassas, VA). All culture media and supplements were purchased from Mediatech, Inc. (Manassas, VA). Human cervical adenocarcinoma S3 cells (HeLa S3) were maintained in Kaighn's Modification of Ham's F-12 Medium (F-12K) supplemented with 10% FBS, 100 IU/mL penicillin, and 100 µg/mL streptomycin. HeLa cells were cultured in Dulbecco’s Modified Eagle’s Medium (DMEM) supplemented with 10% FBS, 200 IU/mL penicillin, and 100 µg/mL streptomycin. Both cell

lines were sub-cultured in tissue culture-treated 25 cm^3 flasks at 90% confluence before next-sub-cultures and media were changed every other day.

Cell-encapsulating DNA hydrogels

Cells were collected by centrifuged at 1000 rpm for 5 minutes. Then, the cell culture supernatant was replaced by trypsin-EDTA solution (Cellgro) to disaggregate cell clusters. Cells were suspended at specific densities in 5uL Optimem-I serum-free media from Invitrogen (Carlsbad, CA). The cell suspensions in Optimem-I media were homogeneously mixed and immediately added to 25 μL DNA hydrogel components. The cell-encapsulating DNA hydrogels were incubated for complete ligation at room temperature for 3 hours in a sterile condition. After formed, the cell-encapsulating DNA hydrogels were cultured in the full culture media (10% FBS containing F-12K media) in a humidified incubator at 37 °C and 5% CO_2 level.

3.7.4 In vitro characterization of cell-encapsulated DNAhydrogels

Cell toxicity

To determine biocompability of the DNA hydrogel formation, cells were plated at 12,000 cells per well in 96-well plate overnight before the experiment. Different conditions for the DNA hydrogel formation were mixed with 1x serum-free media final reaction volume. After incubated for 6 hours, cells were washed with PBS buffer and replenished with 10% FBS containing cell culture media and continued incubation for 48 hours. Next, cells were washed with serum-free media, replaced by 10% containing alamarBlue reagent, and incubated at 37 °C for 6 hours. The cell supernatant was transferred to a black 96-well plate for fluorescence reading at excitation and emission wavelength 560 and 590 nm, respectively, using a Synergy 4 microplate reader

(Winooski, VT). Serial dilution of cells was performed as a standard curve for each specific incubation time.

Cell proliferation

Total cell numbers were consequently counted after alamarBlue measurement at specific time points. Cell culture media was removed and the cell-encapsulating DNA hydrogels were disrupted by pipetting and trypsin-EDTA solution was incubated for 5-10 minutes to disaggregate the MCS. Total numbers of single cells were determined by the dye exclusion method.

Metabolic activities

At specific time points, cell culture media was removed and the cell-encapsulating DNA hydrogels were disrupted by pipetting and trypsin-EDTA solution was incubated with the MCS for 5-10 minutes. One equal volume of alamarBlue reagent was added and incubated for 1-4 hours at 37 °C depending on cell density conditions. After incubation, the cell suspension was centrifuged and the supernatant was transferred to a black 96-well plate for fluorescence reading at excitation and emission wavelength 560 and 590 nm, respectively, using a Synergy4 microplate reader (Winooski, VT). Serial dilution of cells was performed as a standard curve for each specific incubation times.

On-demand recovery of MCS from DNA hydrogels

After the MCS were cultured up to desired time points, cell culture media was replaced by 30 µl of DNase I buffer adapted for cell culture at 37 °C for 60 minutes. The buffer consists of 1 µl DNase I enzymes (2 units/µl) (Madison, WI) supplemented with 0.5 mM Ca^{2+} and 2.5 mM

Mg^{2+} in serum-free culture media. The released MCS were centrifuged at 200 rcf for 1 minute, separated from the supernatant and resuspended in cell culture media, and transferred to a 96-well plate. The reattachment of cell spheroids was observed after 6 hours by a confocal microscope.

3.7.5 Microscopic analysis

Scanning electron microscope (SEM)

All DNA hydrogel conditions were studied by SEM. First, the DNA hydrogels were formed and incubated at room temperature overnight. Then, the DNA hydrogels were washed with water to remove excess salt residue. Next, the DNA hydrogels were frozen by immersion in liquid nitrogen, and then freeze-dried by Labconco lyophilizer overnight. The lyophilized DNA hydrogels were immobilized on the stub and coated with gold nanoparticles. The samples were observed by LEO 1550 FESEM.

Fluorescence confocal microscope

The cells-encapsulating DNA hydrogels were washed with PBS buffer, fixed with 4% paraformaldehyde for 2 hours at room temperature, permeabilized with TBP solutions containing 1% Triton-X, 2% BSA in PBS solution for 1 hour, stained with phaloidin Alexa 488 conjugated proteins from Invitrogen (Carlsbad, CA), and then washed with PBS buffer. The cells-encapsulating DNA hydrogels in PBS buffer were sealed with cover glass slip on a chamber slide and 20 x or 40 x magnifications of oil immersion objective lens were used to capture 2D and 3D images using an upright Zeiss LSM 510 Meta confocal microscope.

Image analysis

To measure the size of MCS, images from a confocal microscope under 20x magnifications were used to determine the average sizes. The sizes of MCS were obtained by measurement of the pixel numbers of lines drawn crossing the spheroids followed by conversion to actual lengths using Image J (NIH). For irregular shapes of MCS, multiples crossing lines were drawn in directions to reflect the varied diameter of the spheroids, and the mean value of these measurements was used to characterize the spheroid size. The total MCS of 19 were used in the analysis.

3.7.6 Statistical analysis

Statistical analysis was performed using One-way *ANOVA*. Statistical significance was assigned for two-tailed 95% confidence. All experiments were conducted three times and results were reported as mean ± SD.

Table 3.1 Oligonucleotide sequences of regular and modified X-DNA building blocks for the DNA hydrogels

Strand		5' palindromic segment	Core segment	3'segment
X_1	Regular	5'-p-ACGT	CGACCGATGAATAGCGGTCAGATCCGTACCTAC	TCG-3'
X_2	Regular	5'-p-ACGT	CGAGTAGGTACGGATCTGCGTATTGCGAACGAC	TCG-3'
	NHS	5'-		
X_3	Regular	5'-p-ACGT	CGAGTCGTTCGCAATACGGCTGTACGTATGGTC	TCG-3'
X_4	Regular	5'-p-ACGT	CGAGACCATACGTACAGCACCGCTATTCATCGG	TCG-3'

Note that 1. p represents the phosphorylation on the 5' end of the oligonucleotide.

2. Regular represents the previously reported X-DNA sequences.

3. NHS represents the modified activated NHS ester oligonucleotide sequence.

4. Hybrid (12) and (20) represent the oligonucleotide sequence with extended (12 and/or 20) nucleotides for RNA/DNA hybridization

CHAPTER 4

Synthetic networked DNA structures for siRNA controlled release and 3D siRNA delivery

4.1 Introduction

RNA interference (RNAi) is an innate post-transcriptional mechanism that has rapidly developed as an alternative method for inhibiting a number of human disease mechanisms at a mRNA level and for investigating gene functions (114). The mechanism of the RNAi inhibition involves in short single-stranded RNA nucleotides called small interference RNA molecules (siRNA) that are specifically complementary to genes of interest. SiRNA typically consists of 19-22 RNA base pairs with 2 nucleotide overhangs at 3' end at both ends (114). In the process occurring in a cytoplsm, the siRNA induces the assembly of the RNA-induced silencing complex (RISC) in which the antisense siRNA strand is incorporated and bound to the complementary mRNA target (208). After binding, the RISC silences gene expression by degrading the mRNA and departs from the complex to find a new target. The process is recycled, thus repeatedly downregulating gene expression with only a small amount of siRNA. Unfortunately, the process is transient due to the fact that the siRNA does not integrate into genomic DNA. Hence, cell proliferation alleviates the efficiency of the silencing. As a consequence, multiple treatments are required to maintain effective therapeutic levels. Also, the siRNA cannot passively penetrate cell membranes resulting in a need in carriers to circumvent this issue. As a result, a number of synthetic carriers and delivering methods have been purposed to efficiently carry the siRNA into the targeted cells.

Early synthetic carriers for siRNA delivery are fundamentally transferred from DNA delivery. However, several obstacles have been presented from adopting DNA delivery to siRNA delivery

(209). In spite of being classified as nucleic acids, in fact, siRNA have several distinct characteristics to DNA. The shorter length of siRNA causing lower negative charge ratios forms weakly cationic complexes when mixed with the typical transfection reagents (209). In addition, the presence of oxy-ribose rings giving the RNA more prone to several enzymatic reactions. Furthermore, unlike circular DNA, the small size of siRNA molecules prevents them from physically being entrapped inside scaffolds for sustained and controlled release (210).

So far, many cationic siRNA transfection reagents have been reported and are one of the most widely used siRNA carriers. The cationic transfection reagents can be made of several materials, for example, liposomes, polyamines, and synthetic cationic polymers. However, the cationic tranfection reagents are reported to be highly toxic to cells and massive cell death. Neutral and anionic transfection reagents have also been purposed but reported to have lower tranfection efficiency. Alternatively, a transfection of circular DNA molecules expressing short hairpin RNA molecules (shRNA) which are processed to siRNA by Dicer was purposed to overcome the transient gene silencing issue (211, 212). Nevertheless, those direct siRNA delivery methods are simpler than indirect shRNA transcribed from the circular DNA transfection delivery as the direct delivered siRNA can promptly function in the cytoplasm after reaching the cell targets without the need of nuclear transportation.

Consequently, a lot of effort has put in order to improving the current direct siRNA delivery (114). First, several novel carriers have been generated to efficiently deliver siRNA into the targeted cells. Lipid platforms typically incorporate siRNA either by encapsulation within the hollow aqueous cores of lipid-based shells known as liposomes and/or by formation of electro-static complexes called lipoplexes. Lipoplexes have been widely used for its high transfection efficiency and ease of formation: nanocarriers can be generated simply upon a simple mixing of

lipids and siRNA at stoichiometric ratios. However, nonpermanent electrostatic interactions can make lipoplexes unstable. Thus, lipoplexes usually have a short shelf-life and often need to be prepared immediately prior to the transfection (213). In addition to lipids, synthetic polymers have been shown to effectively delivery siRNA due to their ability to readily complex with anionic siRNA molecules and also to induce endosomal escape into the cytosol. One of the most notable cationic synthetic polymers is polyethylenimine (PEI). PEI is a highly positively-charged polymer containing tertiary amines that has been established to facilitate endosomal escape via the proton sponge effect (214). Recently, Lee *et al.* has used PEI to form siRNA microsponge complexes and delivery them in vivo (108).

Second, the improvement of targeting delivery has been clearly increased the efficiency of the siRNA delivery (106, 215, 216). The cell-targeted siRNA delivery has proven tremendously beneficial to therapeutic applications such that the targeting delivery aiming only at silencing abnormal protein-transcribed mRNA surrounded by normally functional mRNA in the cells eliminating off-target effects to non-related or normal cells. As a consequence, several targeting molecules that specifically bind to specific cell-surface signals or receptors have been physically or chemically attached to the siRNA platforms. The targeting molecules are such as receptor-binding proteins, antibodies, cell- specific short peptides and nucleic acids (175, 183). Not only decreasing off-target effects, some of the targeting molecules can enhance the overall efficiency of the siRNA by increasing the cellular uptake of the siRNA into cells. (215-217). Moreover, some targeting molecules can directly conjugate to siRNA and simultaneously delivery the siRNA into the cells. These molecules are including cholesterols, short peptides, DNA and RNA aptamers (183, 216).

Third, the development of siRNA carriers that can control siRNA encapsulation and trigger a

controlled release of siRNA has been also gaining interests. Currently the release of siRNA is purely relying on diffusion based on a pore size, charge of materials, and material degradation (218-222). Thus, having the siRNA platforms in which the release of encapsulated siRNA can be controlled and timely triggered make the siRNA delivery more efficient and beneficial to *in vivo* studies. To encapsulate the siRNA for a controlled release study, a number of methods has been demonstrated such as physical entrapment, electrostatic interaction, and chemical conjugation (223-226). Most of the current siRNA controlled release platforms are only applicable to conventional 2D cell culture studies (222, 224-229). Also, most of these siRNA controlled release platforms are governed by diffusion-based method, not time-specific controlled. NIR-triggering siRNA nanoparticles are one of very rare platforms inducing the releases of siRNA upon request (224). Another triggered release of siRNA was performed by conjugating siRNA to the hydrogels employing disulfide linkages. The siRNA was released from the hydrogels in the reducing environment inside cells (226).

Even though, 3D cell culture systems have been greatly developed as ex vivo conditions, the siRNA delivery in 3D cell culture constructs do not improve fast enough to gain effective 3D siRNA delivery. The results from delivering siRNA to 3D cell constructs or MCS were always low at the siRNA delivery efficiency. This is due to the fact that the MCS consisting of tight adhesive junctions can block cells growing inside from exposing to siRNA. One way to solve the 3D gene delivery issue that was previously reported in DNA delivery of the MCS was to first transfect cells in monolayers and then reform the monolayer transfected cells into MCS (230). Even if the process was a success, two separate cell-handling procedures were required to achieve the 3D transfection which is only applicable for few samples. High throughput studies

are not possible with this current procedure. Thus, there are great challenges for achieving an effectively time-specific controlled release of siRNA delivery in 3D cell culture (175, 183).

Here, we proposed a novel platform for time-specific and controlled release of siRNA in which the siRNA simply tethered by hybridization to the DNA hydrogels without further modifications. The siRNA-hybridizing DNA hydrogels (siRNA hydrogels) acted as a siRNA reservoir that can control the release of siRNA with distinct releasing rates. The differences in siRNA releasing rates from the siRNA hydrogels were dependent on the amount of RNase H enzymes in the environments. In addition, we demonstrated a potential to combine the 3D cell culture and siRNA delivery as a two-in-one 3D siRNA delivery platform where only one step needed to simultaneously form 3D cell structures and tether siRNA inside the siRNA hydrogels.

4.2 Design and Concepts of siRNA-DNA and c1-siRNA-DNA chimera hydrogels

We tethered siRNA molecules inside the DNA hydrogels simply by hybridizing the siRNA to complementarily designed DNA sequences on X-DNA building blocks (X-siRNA) without any modifications. Specifically, one of four X-DNA's palindromic sticky ends was sacrificed and replaced with a 12-nucleotide non-palindromic overhang that was previously reported to stably hybridize between Y-DNA building blocks and form networked DNA structures under physiological conditions (64). As for the design of modified siRNA, the 3' end of sense siRNA strand was extended with the complementary sequences of that 12-nucleotide overhang and 5-nucleotide spacer (Figure 4.1a). Thus, the hybridization of siRNA to X-DNA building blocks generated RNA/DNA hybrids which were used to control the release of siRNA. The RNA/DNA hybrids were precisely controlled by the endonuclease RNase H-triggered enzymatic reaction as the endonuclease RNase H enzyme only degrades RNA oligonucleotides hybridizing to its

complementary DNA sequences (Figure 4.1b). By adding RNase H, the RNA nucleotides on RNA/DNA hybrid structure were degraded releasing the siRNA from the siRNA hydrogels (Figure 4.1d). The siRNA releasing system was accomplished without destructing the cultured MCS and DNA hydrogel structures. The time-specific controlled release of siRNA from the siRNA hydrogels was done by varying the amount of RNase H presented in the siRNA hydrogels' environment. We further demonstrated a potential in using our siRNA hydrogels for a two-in-one 3D siRNA delivery platform where only one step needed to simultaneously form 3D cell structures and tether ready-to-transfect siRNA inside the siRNA hydrogels. In our two-in-one siRNA hydrogel platform, we utilized c1 RNA aptamers that can enhance cellular uptake instead of transfection reagents as the whole process can be done in one step (97). The c1 RNA aptamer has been previously reported to enhance the cellular uptake in various cells such as human cervical (HeLa), mouse pancreas (Min 6B1), and mouse endothelial (Bend3) (97). The c1 aptamer was rationally designed to be on the 5' of the sense siRNA strand (Figure 4.1c). Also, we employed chemically 2' fluorine- modified cytidines (2'F-C) and 2' fluorine-modified uridines (2'F-U) for a nuclease resistance. In this case, we redesigned the RNA/DNA hybrid sequences to be a long 20-nucleotide adenine sequences (A_{20}) on the RNA strand and 20-nucleotide thymine sequences (T_{20}) on the sacrificed end of X-DNA building block, respectively (X-c1-siRNA). Like the previously controlled release, RNase H digests the (A-T_{20}) RNA/DNA hybrids, releasing c1-siRNA chimeras from c1-siRNA hydrogels into the environment. The newly formed MCS can thus uptake the c1-siRNA chimeras after the gels are triggered with RNase H. RNase H remarkably does not interrupt the MCS residing inside the hydrogels resulting in a continuous proliferation after the RNase H treatment.

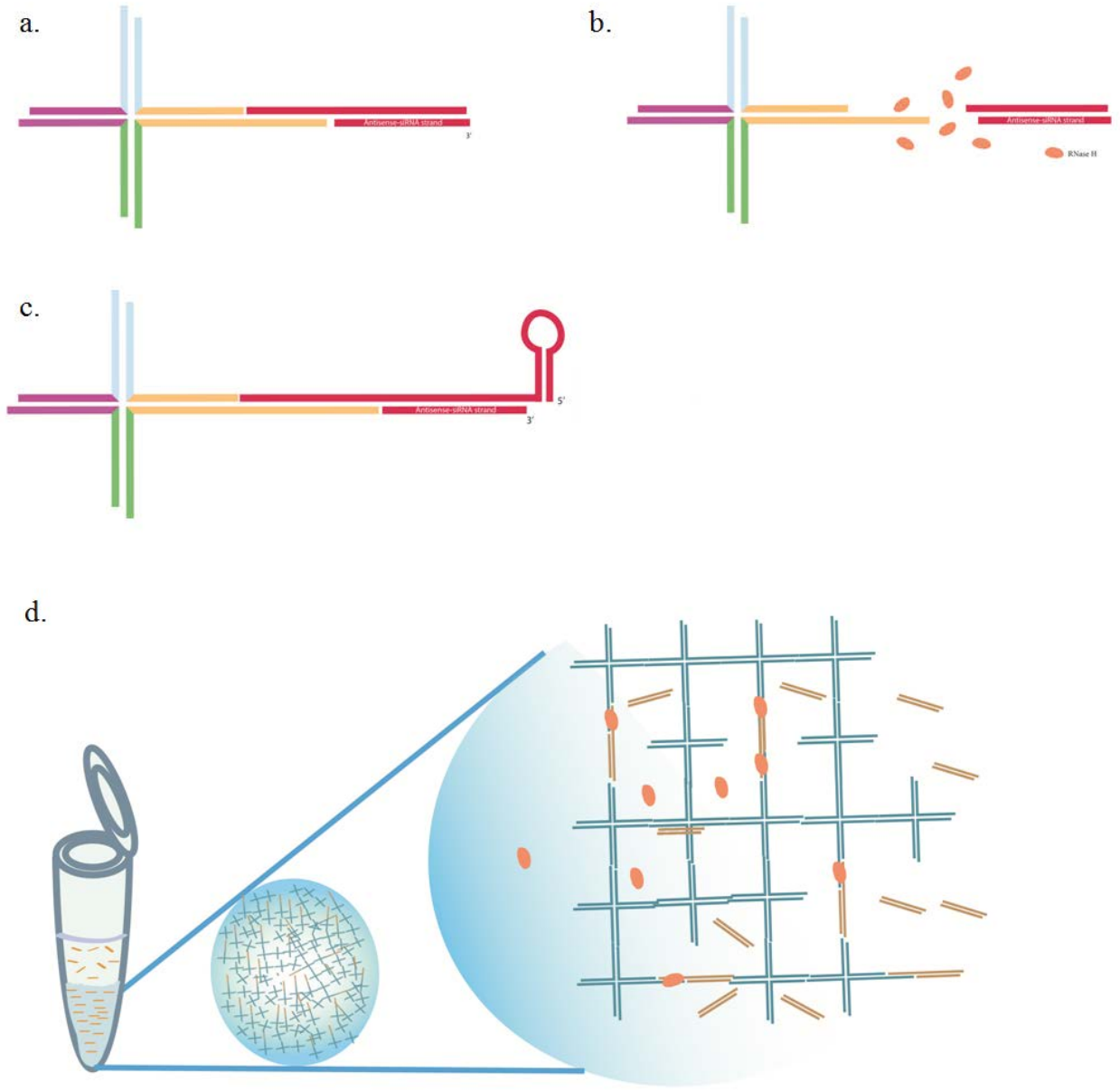

Figure 4.1. Schemes illustrating the siRNA-encapsulating DNA hydrogels. a. a X-siRNA building block consisted of four DNA oligonucleotides and two siRNA ribonucleotides. b. The X-siRNA digested by RNase H resulting in X-hybrid and released siRNA where the RNA hybrid were digested by RNase H. c. The X-c1-siRNA building block modified from X-siRNA with addition of c1 aptamer at the 5' end of the sense siRNA d. an experimental scheme of the siRNA hydrogels in the presence of RNase H enzymes representing RNase H-digesting siRNA hydrogels.

4.3 Fabrication and Characterization of X-siRNA, X-c1-siRNA building blocks and siRNA and c1-siRNA hydrogels

The X-siRNA building block was self-assembled with the same protocol of the X-DNA building block. The X-siRNA building block consists of four DNA oligonucleotides and two RNA oligonucleotides for X-DNA and siRNA, respectively. The self-assembly of X-siRNA was confirmed on 5% nusieve agarose gel electrophoresis (Figure 4.2a). From a titration experiment, the efficiency of self-assembled X-siRNA was 51.3% (±1.41%) calculated by band intensity from Image J. We have tested different molar ratios between X-DNA and siRNA by increasing the siRNA to 4 equivalents higher than the ratio of X-DNA. However, the efficiency of X-siRNA self-assembly did not give a better annealing result. This is very likely due to the short 5 nucletide spacers causing a steric hindrance and repulsive force between siRNA and X-DNA. As shown in figure 4.2a, the hybridization at 1:1 equivalent of sense and antisense siRNA strands, self-assembly of X-DNA, and X-DNA with extended sequences for hybrid hybridization (X-hybrid) on lane1,2, and 3, respectively gave only one major band meaning 100% successful annealing. On lane 4, the sense siRNA strand and X-hybrid annealed at 1:1 equivalent molar showed two major bands consisting of hybridized to the X-hybrid-sense-siRNA and X-hybrid representing a reduce in annealing efficiency of X-hybrid-sense-siRNA than X-hybrid alone. After the antisense siRNA strands were added (lane 5), two major products were obtained where the upper band showing the successful incorporation of antisense siRNA forming a X-siRNA building block and the lower band corresponded to the X-hybrid. Thus, we conclude that the limiting step of self-assembling X-siRNA was due to the hybridization of RNA and DNA hybrid. We further investigated the digestion of RNA/DNA hybrid on X-siRNA in the presence of

RNase H (Figure 4.2b). Within 30 minutes, the X-siRNA building blocks were completely digested resulting in X-hybrid (upper band) and digested siRNA (lower band).

To form the siRNA hydrogels, X-siRNA and X-DNA building blocks were mixed and ligated by adding T4 ligse enzymes. The efficiency of siRNA tethered inside the siRNA hydrogels was approximately at 1:50 mixing ratio of X-siRNA and X-DNA building blocks, respectively. The measurement was determined by fluorescence reading of fluorescein-conjugated antisense siRNA (FAM-antisense siRNA) of non-ligated X-siRNA building blocks after two days of washing with PBS buffer (Figure 4.3a). The encapsulation efficiency of siRNA was approximately 25% (±3.10%) at 1:50 mixing ratio of X-siRNA and X-DNA building blocks, respectively.

For the self-assembly of X-c1-siRNA building block, the modified c1-sense RNA strand was synthesized from in vitro transcription with 2'F-U and 2'F-C nucleotides incorporated to protect the RNA from nuclease degradation. The modified C1 RNA transcript hybridized to antisense siRNA forming c1-siRNA chimeras (Figure 4.3a). In order to preliminarily test the nuclease resistance of modified c1 RNA transcripts and c1-siRNA chimeras, both structures were incubated with 10% FBS containing media at 37 °C for 24 hours. Then, the samples were run on 9% native PAGE (Figure 4.3a). The modified c1-siRNA duplexes showed the integrity of siRNA representing one major band on the gel. As for non-modified c1 RNA transcripts, the RNA degraded within 24 hours after incubating with 10% FBS in media at 37 °C. For the X-c1-siRNA builing blocks, we started the self-assembly with 2.5 equivalents of modified c1-sense RNA transcripts to 1 equivalent of the X-hybrid and antisense-siRNA. The self-assembly of X-c1-siRNA building blocks were shown on 9% native PAGE (Figure 4.3b). Based on the gel image, only one product was obtained from the X-c1-siRNA self-assembly, representing 100% ligation

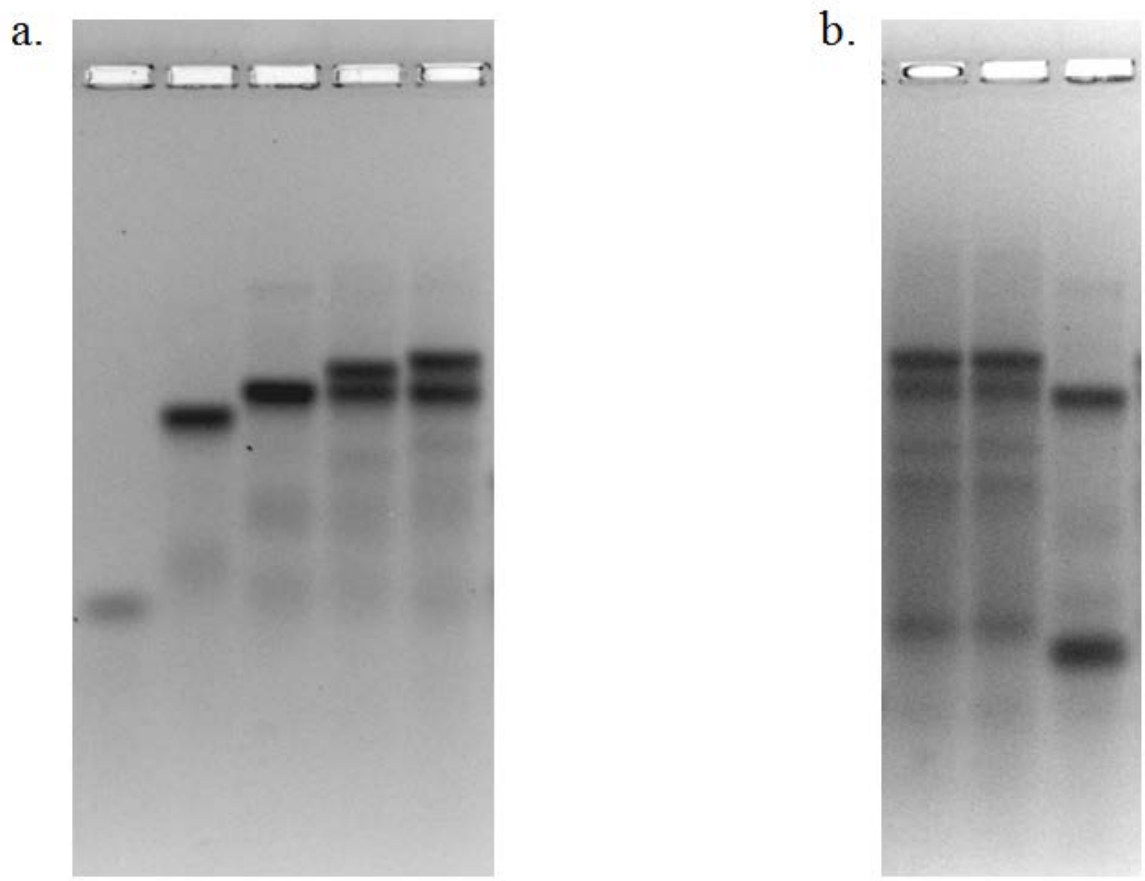

Figure 4.2. Characterization of X-siRNA on 5% nusieve agrose gel electrophoresis, ran at 4 °C with 0.5x TBE buffer, stained with gel red for 1 hour. a. Self-assembly of X-siRNA components. From left to right: siRNA duplexes with hybridization sequence on the sense siRNA strand, self-assembly of the X-DNA building block, self-assembly of the X-hybrid alone, self-assembly of X-hybrid and sense siRNA strand, and self-assembly of X-siRNA building block yielding two major products; X-DNA and X-siRNA. b. RNas H digestion of X-siRNA. From left to right: X-siRNA control at room temperature, X-siRNA control incubated at 37 °C for 30 minutes, and X-siRNA incubated with RNase H at 37 °C for 30 minutes.

efficiency of the X-c1-siRNA building block. The better annealing efficiency compared with the X-siRNA building block could be explained by the extension of hybridzation sequences which gave more flexibility and reduced the steric hindrance between the X-hybrid and c1-siRNA duplexes. Also, the X-c1-siRNA building blocks were tested for Rnas H digestion (Figure 4.3b, lane4). The RNase H-digesting X-c1-siRNA building blocks resulting in the X-hybrids and digested c1-siRNA chimeras. For nuclease degradation test, the X-c1-siRNA building blocks were incubated with 10% FBS containing media at 37 °C for 24 hours and the samples were run on the native PAGE to check the integrity of the structures (Figure 4.3c). The X-c1-siRNA building blocks were not degraded in the presence of 10% FBS over 24 hours. In addition, the RNase H digested the RNA/DNA hybrid sequences giving the complete c1-siRNA chimeras as the products. Once the X-c1-siRNA building blocks were incorporated into DNA hydrogels (c1-siRNA hydrogels), the incorporated siRNA efficiency was quantified by measuring FAM-conjugated antisense siRNA representing X-c1-siRNA in the supernatant. Unfortunately, the siRNA encapsulation efficiency greatly reduced as the amount of ligated X-c1-siRNA building blocks was only 10% (±3.04%).

4.4 Time-specific controlled release of siRNA from the siRNA hydrogels by RNase H

FAM-conjugated siRNA duplexes were released from the siRNA hydrogels after the gels were treated with an excess amount of RNase H. The siRNA-encapsulated DNA hydrogels before were shown in figure 4.4a. Two sets of siRNA hydrogels were treated with RNase H at 28 and 76 hours after incubation, respectively. We observed two sharp increases in siRNA cumulative release profiles within 30 minutes of the RNase H digestion (Figure 4.4b). This confirms the-

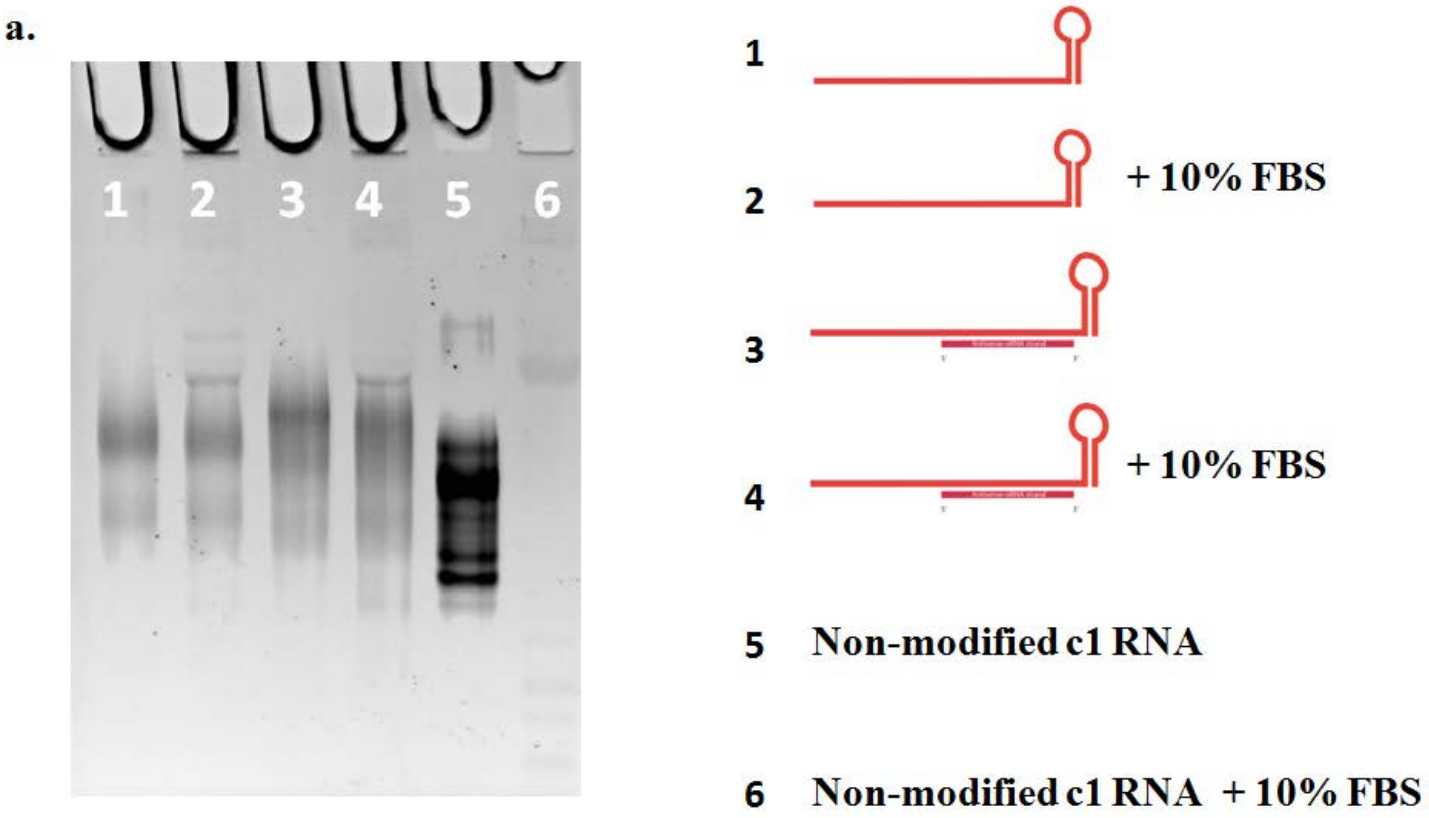

Figure 4.3. Characterization of X-siRNA and X-c1-siRNA building blocks by 9% native PAGE. a. Characterization of the modified c1 RNA transcript, hybridization test of the c1-siRNA chimeras, and 10% FBS degradation test. Lane 1, 3, and 5 are the modified c1 RNA transcripts, the c1-siRNA chimeras, and non-modifed c1 RNA transcripts, respectively. Lane 2,4, and 6 are the same samples according to lane 1,3, and 5 but were incubated with 10% FBS containing media at 37 °C for 24 hours.

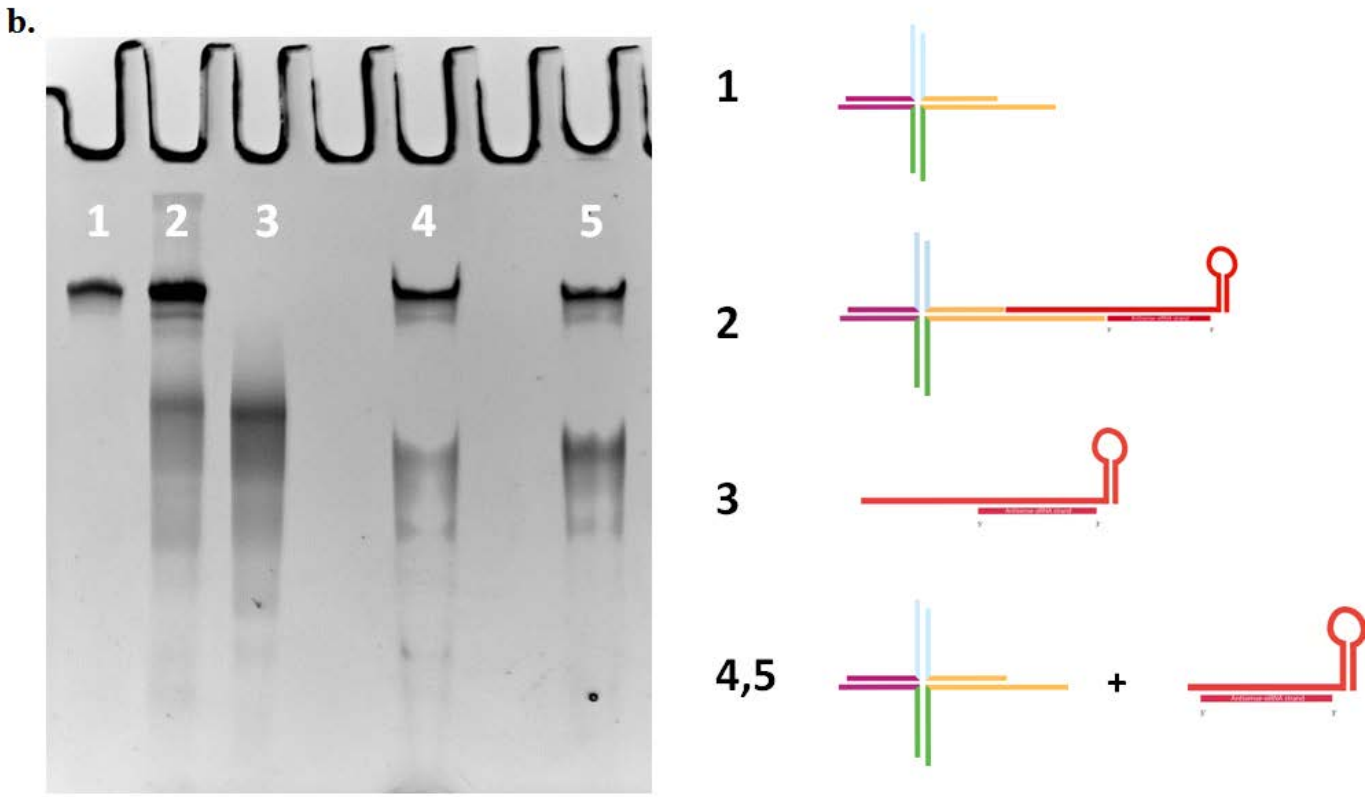

Figure 4.3 (continued) Characterization of X-siRNA and X-c1-siRNA building blocks by 9% native PAGE. b. RNase H digestion of X-c1-siRNA building blocks. From left to right, X-hybrid, X-c1-siRNA, c1-siRNA chimeras, and X-c1-siRNA in the presence of RNase H. The digested c1-siRNA chimeras were released from the X-c1-siRNA building blocks after treating with RNase H.

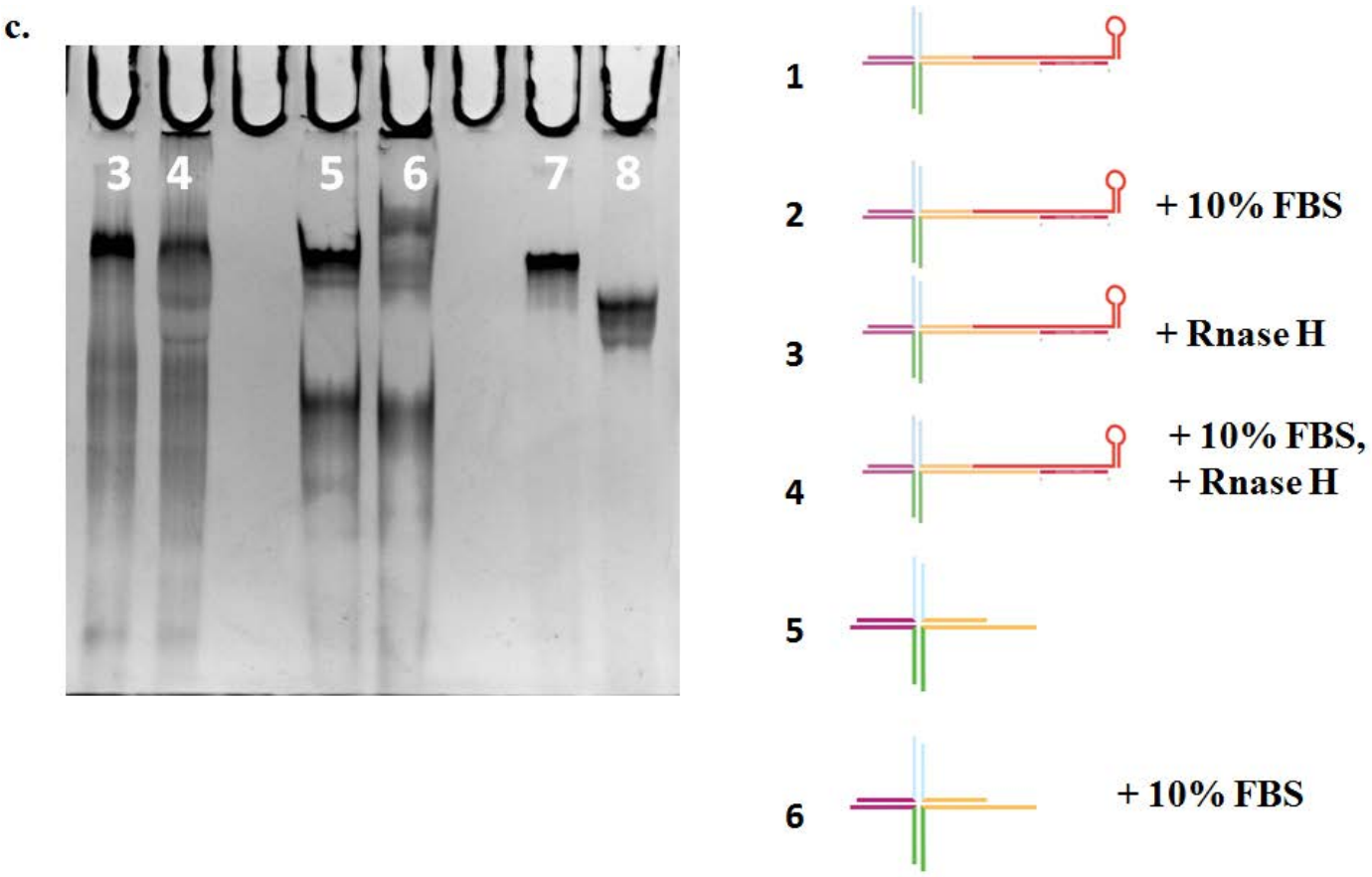

Figure 4.3 (continued) Characterization of X-siRNA and X-c1-siRNA building blocks by 9% native PAGE. c. Serum resistance of and RNase H activity in the presence of serum after 24 hours. Lane 1,3, and 5 are the X-c1-siRNA, X-c1-siRNA treated with Rnase H, and X-hybrid building blocks. Lane 2,4,and 6 are the same sample of lane 1,3, and 5 but were incubated with 10% FBS containing media. Note that the RNase H treatments were done after 24 hour incubation.

time-specific releases of siRNA from the siRNA hydrogels.

In addition to time-specific releases of the siRNA, we also performed series of siRNA controlled release profiles by controlling the amount of RNase H presented in the environment. The cumulative release of siRNA from three different RNase H amounts led to three distinct kinetic release profiles of siRNA (Figure 4.4c). Twenty units of RNase H resulted in 50% siRNA released within the first hour. Slower cumulative siRNA release profiles were obtained when less RNase H was presented in the environment. When the gels were treated with 0.5 and 0.125 unit of RNase H, 50% of the siRNA were released within 5 and 7 hours, respectively. Further optimization of the siRNA release rates is required for an optimal siRNA silencing.

The functional test of released siRNA was conducted by investigating a gene silencing of GAPDH mRNA in HeLa S3 cell lines. The GAPDH siRNA hydrogels were treated with 40 units of RNase H for one hour and the GAPDH siRNA-containing supernatant was collected. The RNase H-treated GAPDH siRNA formed complexes by mixing with commercial polyamine transfection reagents (siPORT Amine) and was transfected into pre-plated HeLa S3. The GAPDH silencing efficiency after 48 hour post-transfection was tested at 100, 150, and 200 nM siRNA concentrations after the siRNA hydrogels were treating with RNaseH (Figure 4.5). The remaining GAPDH proteins were tested for its functions and the results showed that approximately 45-55% of GAPDH proteins were silenced by the siRNA digested from siRNA hydrogels. Compared with commercial siRNA, our released siRNA showed comparable silencing effects. This enlightened us that the presence of RNase H and its digestion did not interfere with the functionality of the released siRNA.

a.

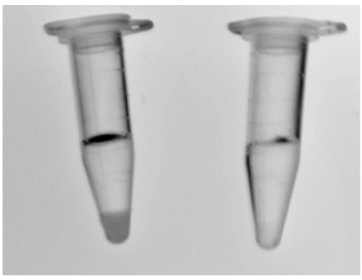

b.

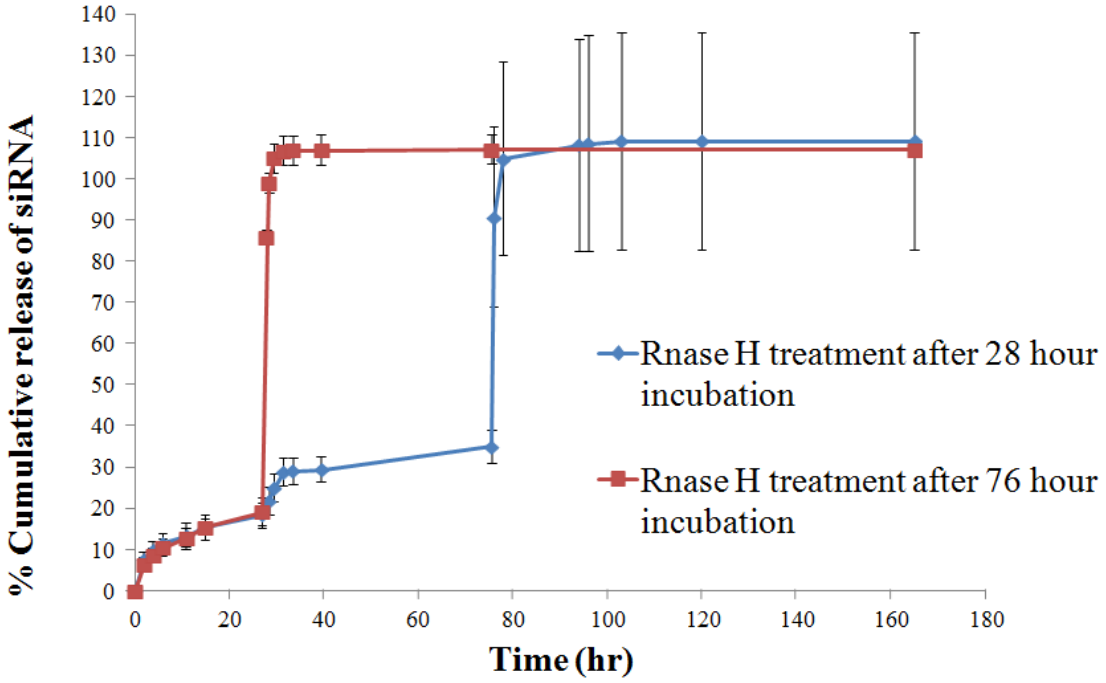

Figure 4.4. SiRNA-encapsulating DNA hydrogels, time-specific, and controlled siRNA release profiles a. The siRNA hydrogels (left tube) and the DNA hydrogels (right tube) after two days of washing imaging by Kodak imaging system. The siRNA hydrogels showed flurescence of FAM-conjugated siRNA tethered inside the DNA hydrogels. b. The time-specific controlled release profiles of the siRNA hydrogels after specifically adding RNAse H at 28 and 76 hours after incubation in PBS at 37 °, respectively.

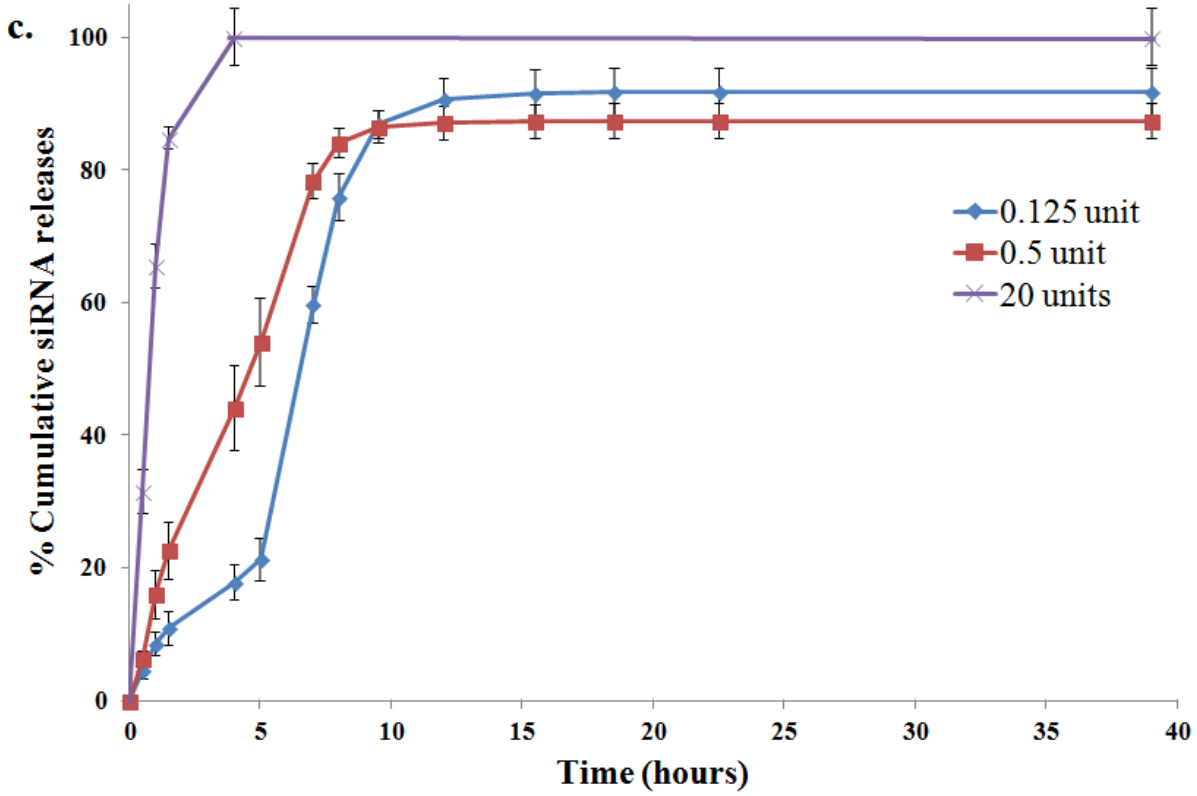

Figure 4.4 SiRNA-encapsulating DNA hydrogels, time-specific, and controlled siRNA release profiles (continued). c. The series of siRNA controlled release profiles of the siRNA hydrogels after adding various amounts of RNase H; 20, 0.5, and 0.125 units, respectively.

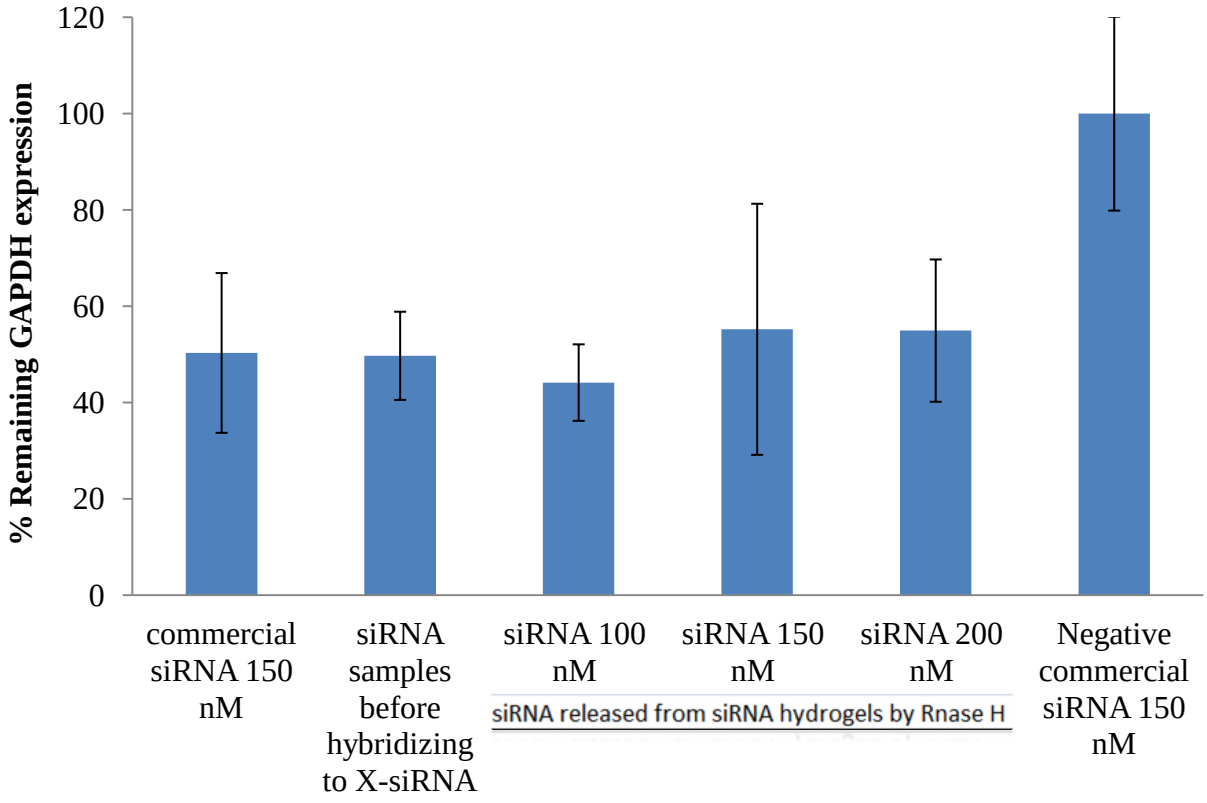

Figure 4.5. Remaining GAPDH protein activity 48 hour post-siRNA transfection. From left to right, 150 nM commercial GAPDH siRNA control, siRNA duplexes before hybridizing to X-siRNA building blocks, 100, 150, and 200 nM of the released siRNA from RNase H-digesting siRNA hydrogels, and 150 nM scramble negative siRNA control. All samples except released siRNA 150 nM are significantly different from the negative siRNA control at ($P < 0.05$).

4.5 A two-in-one c1-siRNA hydrogel platform for 3D siRNA delivery

In order to gain more advantages of our developed siRNA hydrogels, we created the two-in-one c1-siRNA hydrogel platform that simultaneously deliver siRNA to newly formed and/or forming MCS within one step. Also, our 3D siRNA delivery platform employs a cellular-enhancing uptake RNA aptamer instead of forming siRNA complexes with any external transfection reagents. As we demonstrated that the X-c1-siRNA and X-DNA building blocks are stable and not degraded in serum-containing media, we next perform the cell-encapsulating c1-siRNA hydrogels.

For 3D siRNA delivery, we began to investigate the cellular uptake of RNase H-treated siRNA released from X-c1-siRNA building blocks to a 2D conventional method. The Z-sliced images from a confocal microscope displayed c1-siRNA chimeras suggesting the c1 aptamers were still active in enhancing the cellular uptake after the RNase H treatment (Figure 4.6a-b). Next, HeLa cells were encapsulated inside the c1-siRNA hydrogels for 72 hours and an excess amount of RNase H was added to trigger the release of c1-siRNA chimeras. Based on Z-sliced images, HeLa MCS were formed inside the c1-siRNA hydrogels with heterogeneous uptakes of released siRNA chimeras in different location including outer and inner cells of the spheroids (Figure 4.6c). However, the MCS from non-treated RNase H siRNA hydrogels were also observed the siRNA. This might due to the non-ligated X-c1-siRNA inside the hydrogels. However, based on the preliminary results, we hope to be able to improve and establish the simple and efficient platform for the 3D siRNA delivery.

4.6 Summary

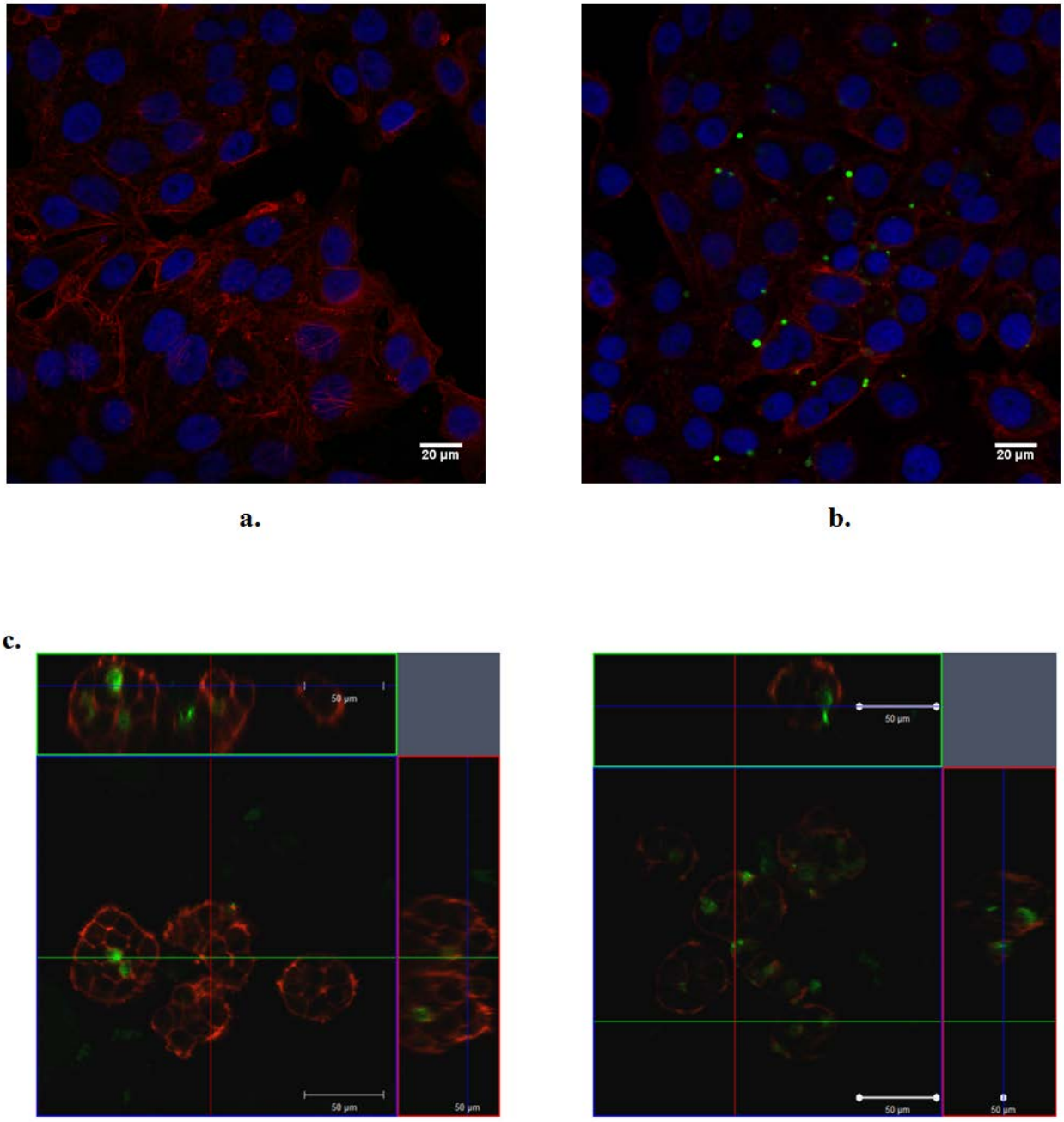

Figure 4.6. Z-stack confocal microscope images of FAM-labelled c1-siRNA chimeras transfecting HeLa cell lines. a. The 2D conventional uptake of cell only and b. released c1-siRNA chimeras. The cells were imaged by employing a 40x objective lens in oil. c. HeLa MCS grown inside the c1-siRNA hydrogels for 72 hours were treated with RNase H for 6 hours before imaging by compiling z-stack images. Nuclei were stained by DAPI (blue) and F-actin filaments were stained by rhodamine-labeled phalloidins (red).

In general, siRNA are very difficult to be encapsulated inside a scaffold without further modifications because of their small size and low negative charge per molecules. Here, we have successfully demonstrated the use of the DNA hydrogels to encapsulating the siRNA utilizing hybridization, the inherent property of nucleic acids. Thus, the DNA hydrogels tether the siRNA without further chemical conjugation. As a result, the siRNA were encapsulated inside the DNA hydrogel and the time-specific siRNA releases were occurred by adding RNase H. Also, we demonstrated the series of siRNA controlled release profiles by controlling the amount of RNase H in the environment. The siRNA encapsulating efficiency was approximately 30%. The released siRNA formed cationic complexes with transfection reagents and inhibited the protein function without loss of siRNA activity. Furthermore, we developed the two-in-one c1-siRNA hydrogel platform for 3D siRNA delivery application by combining the time-specific release of siRNA to the formation of MCS inside the DNA hydrogels. We were able to deliver siRNA to newly formed MCS and hoped to use the two-in-one c1-siRNA hydrogel platform to improve the siRNA delivery for MCS.

4.7 Materials and Methods

4.7.1 Materials

All DNA and RNA oligonucleotides were commercially synthesized from Integrated DNA Technologies, Inc (Coralville, Iowa) and used without further purification. All enzymes were purchased from New England Biolab, Inc. (Madison, WI). Nusieve agarose powder was purchased from Lonza Group Ltd. (Basel, Switzerland)**.** All cell lines were purchased from ATCC (Manessas, VA). All culture media and supplements were purchased from Mediatech, Inc. (Manessas, VA). The Optimem-I media was bought from Life Technologies (Grand Island, NY).

The DuraScribe® T7 transcription kits was purchased from Epicentre Biotechnologies (Madison, WI). Gel red was bought from Biotium Inc. (Hayward, CA). All chemicals were purchased from Sigma-Aldrich (St. Louis, MO) or otherwise indicated.

4.7.2 Synthesis, preparation of siRNA hydrogels and c1-siRNA hydrogels

Synthesis of X-siRNA and X-c1-siRNA building blocks

The DNA and RNA sequences in the experiments are reported in Table4.1. All DNA oligonucleotides were dissolved in TE buffer containing 10 mM Tris, 1 mM ethylenediaminetetraacetic acid (EDTA) solution (pH = 8.0). All RNA oligonucleotides were dissolved in nuclease-free (DEPC-treated) water at 1 mM concentration. For a X-siRNA building block annealing, four equivalent molars of the hybrid sense and antisense siRNA was mixed with one molar equivalent of all four X-DNA oligonucleotides (X_1, X_2, $X_{hybrid(12)}$, and X_4) at a final concentration of 50 µM X-DNA concentration. For a X-c1-siRNA building block, two and a half molar equivalents of c1-sense siRNA strands were mixed with one molar equivalent of all 4 X-DNA oligonucleotides (X_1, X_2, $X_{hybrid(20)}$, and X_4) and antisense siRNA strands at a final concentration of 50 µM X-DNA concentration.

In vitro transcription of modified c1 RNA aptamers

The modified c1-aptamer DNA templates were annealed in TE buufer containing 10 mM Tris (pH=8.0) in 1 mM ethylenediaminetetraacetic acid (EDTA) solution at 10 µM concentration with the same X-DNA building block protocol. One µg of modified c1-aptamer DNA template was used per one *in vitro* transcribtion. The reaction was done at 37 °C overnight and treated with DNAse I (NEB) to degrade the DNA templates. Then, the modified c1 RNA transcript products were purified by Microcon® centrifugal filters (Ultracel- 10 Membrane) (Billerica, MA) and used for the self-assembly of the X-c1-siRNA building blocks.

Formation of siRNA and cell-encapsulating c1-siRNA hydrogels

For the siRNA hydrogels, X-DNA and X-siRNA building blocks were mixed in 25:1 or 50:1 ratio, respectively. The hydrogel formation was followed the materials and methods in section 3.7. After forming, the siRNA hydrogels were incubated at room temperature for 5 hours and washed with PBS buffer overnight at 37 °C. For cells-encapsulating c1-siRNA hydrogels, X-DNA and X-c1-siRNA building blocks at 25:1 ratio (100:4 µM) were simultaneously mixed with HeLa cells suspended in Optimem-I media and formed the hydrogel according to the previously reported protocol in section 3.7. The cell-encapsulating c1-siRNA hydrogels (cell-siRNAgels) were incubated at room temperature for 5 hours for complete enzymatic reaction. After formed, the cell-siRNAgels were cultured in the full culture media (10% FBS containing F-12K media) in a humidified incubator at 37 °C and 5% CO_2 level.

4.7.3 Characterization of X-siRNA and X- c1-siRNA building blocks

Agarose gel electrophoresis

The nusieve agrose gel electrophoresis was used to confirm the successful self-assembly of X-siRNA building blocks. The 5% nusieve agarose gels were ran in the running buffer consisting of 89 mM tris-HCl (pH 8.0), 89 mM boric acid, and 2 mM EDTA (TBE), and post-stained with 1x gel red for 60 minutes. The samples were run in 1x sample orange loading dyes (NEB). The gels were run on a Bio-rad electrophoresis unit at 4 °C with constant voltage (5V/cm).

Native polyacrylamide gel electrophoresis (PAGE)

Acrylamide: Bisacrylamide (19:1) ratio was used to prepare native PAGE for characterizing X-c1-siRNA building blocks. The gels were composed of 9% (19:1) native PAGE and casted

with 1mm glass with the mini Bio-rad PAGE system. The gels were run in TBE buffer at 4 °C with constant voltage. The samples were run in 1x sample orange loading dyes (NEB). The gels were posted-stained with 1x gel red for 30 minutes and imaged by Kodak gel imaging system.

4.7.4 Characterization of siRNA hydrogel and c1-siRNA hydrogel formation

SiRNA and c1-siRNA encapsulation efficiency

The siRNA and c1-siRNA hydrogels were formed as described in section 4.7.1 with 3' FAM-conjugated antisense siRNA strands. After formed, the hydrogels were washed with PBS buffer twice at room temperature, 37 °C overnight and the supernatant was collected. The non-ligation X-siRNA and X-c1-siRNA in the supernatant was detected by measuring the fluorescence intensity using the synergy4 plate reader at 485/528 nm for excitation and emission wavelengths, respectively. The encapsulating efficiency was calculated as following.

$$\%\,\text{Encapsulation} = 100 - \frac{\text{Total fluorescence in the supernatant}}{\text{Total fluorescence of X-siRNA added}} \times 100\,\%$$

4.7.5 Chracterization of RNase H enzymatic reactions for siRNA time-specific and controlled release profiles

RNase H treatment of X-siRNA and X-c1-siRNA building blocks

The siRNA hydrogels were formed at 25:1 ratio (100:4 μM) and digested with 40 units of RNase H for time-specific profiles and 20, 0.5, and 0.125 unit of RNase H for different controlled release profiles. The reaction was incubated at 37 °C and all supernatant were collected at different time points. The collected supernatant was one hour and the RNAse H

digestion was characterized by 5% nusieve agarose gel electrophoresis following the section 4.8.3.

RNase H treatment of siRNA and aptamer-siRNA hydrogels

The siRNA and aptamer-siRNA hydrogels (with FAM-conjugated antisense siRNA) were formed as previously described by using FAM- conjugated antisense siRNA. The non-ligated siRNA was washed out from the gels with PBS buffer. For time-specific triggering siRNA, 40 units of RNase H enzymes were added in the siRNA hydrogels and incubate at 37 °C for 1 hour. Then, the supernatant was collected and the fluorescence intensity of FAM was determined. As for the siRNA controlled release study, the siRNA hydrogels were incubated with 0.125, 0.25, 0.5, and 40 units of RNAse H at 37 °C. At specific time points, the supernatant was transferred to new tubes and the fresh RNase H reaction mixtures were replaced. All the supernatant was measured by fluorescence using the synergy4 plate reader at 485/528 nm for excitation and emission wavelengths, respectively. The released FAM-conjugated siRNA were reported as cumulative release of siRNA relative to total encapsulated the siRNA in the hydrogels over releasing times.

4.7.6 Cell culture and cell encapsulation

Cell maintenance

Human cervical adenocarcinoma cells (HeLa) were cultured in Dulbecco's Modification of Eagle's Medium (DMEM) supplemented with 10% FBS, 200 IU/mL penicillin, and 100 µg/mL streptomycin. The cells were sub-cultured in tissue culture- treated 25 cm^3 flasks at 90% confluence and media were changed every other day.

Cell preparation for c1-siRNA hydrogel formation

HeLa Cells were trypsinized and centrifuged to pellet the cells at 1000 rpm for 5 minutes. The cells were re-suspended in 5uL Optimem-I serum-free media to desired density to get 200,000 cells/ mL at final cell density in the gels.

4.7.7 Fluorescence confocal microscopic analysis

Cell-encapsulating c1-siRNA hydrogels were washed twice with PBS buffer, fixed with 4% paraformaldehyde for 4 hours at room temperature, permeabilized with 1% Triton-X 100 containing 1% BSA in PBS solution for 1 hour, stained with Alexa 488-conjugated phaloidin proteins. In between each step, the samples were washed twice with PBS buffer. The cell-encapsulating hydrolgels were sealed with cover glass slip on a chamber slide and 20x or 40x oil immersion objective lens were used to capture 2d cell images using an upright Zeiss comfocal microscope.

Table 4.1 Oligonucleotide sequences of modified X-DNA building blocks and RNA for the siRNA-DNA hydrogels

Strand		5’ palindromic segment	Core segment	3’segment
X_1	Regular	5’-p-ACGT	CGACCGATGAATAGCGGTCAGATCCGTACCTAC	TCG-3’
X_2	Regular	5’-p-ACGT	CGAGTAGGTACGGATCTGCGTATTGCGAACGAC	TCG-3’
X_3	Regular	5’-p-ACGT	CGAGTCGTTCGCAATACGGCTGTACGTATGGTC	TCG-3’
	Hybrid (12)	5’-p-ACGT		TCGCGATTGACTCTC-3’
	Hybrid (20)	5’-p-ACGT		TCGTTTTTTTTTTTTTTTTTT-3’
X_4	Regular	5’-p-ACGT	CGAGACCATACGTACAGCACCGCTATTCATCGG	TCG-3’
C1-scramble siRNA antisense template strands		5’TAATACGACTCACTATAGGGTGCGAATCCTCTATCCGTTCTAAACGCTTTATGATTTCGCATTAGTACTGCT TACGATAC GGAAAAAAAAAAAAAAAAAAAA-3’		
C1-scramble siRNA sense template strands		5’-TTTTTTTTTTTTTTTTTTTTTCCGTATCGTAAGCAGTACTAATGCGAAATCATAAAGCGTTTAGAACGGA TAGAGGATTCGCACCCTATAGTGAGTCGTATTA-3’		
GAPDH antisense siRNA		5’-p-AAAGUUGUCAUGGAUGACCdTdT-3’		
GAPDH sense siRNA		5’-p-GGUCAUCCAUGACAACUUU-3’		
Scramble siRNA-FAM		5’-CCGUAUCGUAAGCAGUACUdTdT /36-FAM/-3’		

Note that 1. p represents the phosphorylation on the 5’ end of the oligonucleotide.

2. Regular represents the previously reported X-DNA sequences.
3. Hybrid (12) and (20) represent the oligonucleotide sequence with extended (12 and/or 20) nucleotides for RNA/DNA hybridization

CHAPTER 5

Conclusion and Future Outlook

It has been shown that emerging DNA nanotechnology has been playing important roles in biomedical fields in a number of ways. Due to the precisely controlled properties of DNA, DNA nanotechnology has been seen in constructing numerous unique DNA nanostructures that can later self-assembly to more complex and larger DNA structures. These DNA structures have been further employed in several biomedical applications. To give some examples, the highly accurate Watson-Crick base pairing rules of DNA have led them to be useful in target-specific detection systems where the DNA structures can complementarily hybridize to target genes even presenting in low copies. Moreover, the anisotropic property of DNA allows us to generate multifunctional DNA structures that can retain multi-functions in the only one DNA structure. Furthermore, the employment of molecular toolkits can add more advantages to DNA nanotechnology. A plethora of available recombinant enzymes can be used to modify, cut, extend, and decorate the DNA structures rendering a large room in tailoring the desire DNA structures to specific applications.

The works discussed in this dissertation have further expanded the use of DNA nanotechnology in three biomedical applications. First, Y-shaped DNA-lipid amphiphile building blocks were synthesized and utilized to create a liposome-like structure called DNAsomes. The DNAsomes facilitate the co-delivery of hydrophobic drugs and siRNA giving synergistic therapeutic effects, thereby reducing the requirement of therapeutic thresholds for both drugs and siRNA. Also, the multifunctional property of DNA that was employed in fluorescent dye conjugation allows DNAsome to be tracked and imaged under a fluorescence

microscope. Despite of success in demonstrating the proof-of-concept of utilizing DNAsomes for 2D *in vitro* systems, we, hence, aim at exploring the effects of the DNAsomes in *in vivo* models which will provide us more insights in developing the DNAsomes as a novel co-delivering platform for further clinical studies.

Second, we expanded the use of synthetic branched DNA building blocks that self-assembled into the DNA hydrogels for 3D cell culture application. Cells that encapsulated inside the DNA hydrogels formed loose or tight MCS morphology depending on types and characteristics of individual cell lines. Also, the DNA hydrogels underwent natural degradation over time without physical or chemical disruption. Additionally, on-demand DNA hydrogel degradation is achieved by adding DNase I enzymes. Even though we do not demonstrate the specific use of our novel 3D cell culture DNA hydrogel platform, we here propose the use of the DNA hydrogels for cancer biology study in which MCS are required to subsequently recover from the hydrogels. Importantly, we take an advantage of a unique DNA hydrogel property that can undergo both natural and on-demand degradation without strong physical and/or chemical disruption to cells. Specifically, avascular tumor spheroids, which are an *in vitro* model of various metastatic cancer cell lines, are formed and proliferate inside the degradable DNA hydrogels. The avascular tumor spheroids can be retrieved from the DNA hydrogels as desired for drug resistant study, high-throughput drug screening, and the responsive effects of different microenvironments to cancer cells. However, using the DNA hydrogels might raise a concern regarding the fast degradation of the DNA hydrogels *in vivo*. Therefore, further investigation is required to obtain the insights of the DNA hydrogel susceptibility to *in vivo* conditions.

Third, the concept of controlling siRNA releases has also proposed by taking advantages of innate siRNA-DNA hybridization and RNAse H-specific digestion of RNA/DNA hybrids.

Different controlled release siRNA profiles were obtained with prolonging siRNA from the DNA hydrogels. Last but not least, the two-in-one DNA hydrogels was purposed for 3D siRNA delivery. Although further characterization is required in this case, the success of the 3D siRNA delivery by the DNA hydrogels will be requiring less complexity and potentially sustaining the release of siRNA for a long period of times.

Nevertheless, there are challenges waiting to be resolve before the full use of DNA nanotechnology can be achieved in biomedical fields. The main challenge of using DNA nanostructures in biomedicines is the susceptibility of DNA *in vivo*. Natural linear DNA is degraded after being injected in to a blood circulation in few minutes. However, recent efforts have improved the DNA stability by employing different modification such as 2' fluoro-modified nucleotides and phosphorothioate-modified DNA back bones resulting in reduced affinity of the DNA to nuclease enzymes. In fact, the use of the DNA nanostructures has been proved to partially resistant to the nucleases as the building blocks of DNA nanostructures are made of branched structures delaying degradation. Thus, the combination of modified and branched DNA building blocks might potentially prolong the stability of the DNA structures *in vivo* giving enough time for the DNA structures to complete their functions.

BIBLIOGRAPHY

1. Watson JD, Crick FHC. Molecular structure of nucleic acids - a structure for deoxyribose nucleic acid. Nature. 1953;171(4356):737-8.

2. Watson JD, Crick FHC. Genetical implications of the structure of deoxyribonucleic acid. Nature. 1953;171(4361):964-7.

3. Hagerman PJ. Flexibility of DNA. Annual Review of Biophysics and Biophysical Chemistry. 1988;17:265-86.

4. Hartmann B, Lavery R. DNA structural forms. Q Rev Biophys. 1996;29(4):309-68.

5. Kennard O. Structural studies of DNA fragments - The G.T wobble base pair in A-DNA, B-DNA, and Z-DNA - The G.A base pair in B-DNA. J Biomol Struct Dyn. 1985;3(2):205-&.

6. Chalikian TV, Volker J, Srinivasan AR, Olson WK, Breslauer KJ. The hydration of nucleic acid duplexes as assessed by a combination of volumetric and structural techniques. Biopolymers. 1999;50(5):459-71.

7. Robinson H, Vandermarel GA, Vanboom JH, Wang AHJ. Unusual DNA conformation at low pH revealed by NMR-parallel-stranded DNA duplex with homo base-pairs. Biochemistry. 1992;31(43):10510-7.

8. Miyoshi D, Matsumura S, Li W, Sugimoto N. Structural polymorphism of telomeric DNA regulated by pH and divalent cation. Nucleosides Nucleotides Nucleic Acids. 2003;22(2):203-21.

9. Thomas TJ, Bloomfield VA. Collapse of DNA caused by trivalent cations - pH and ionic specificity effects. Biopolymers. 1983;22(4):1097-106.

10. Bloomfield VA. DNA condensation by multivalent cations. Biopolymers. 1997;44(3):269-82.

11. Yakovchuk P, Protozanova E, Frank-Kamenetskii MD. Base-stacking and base-pairing contributions into thermal stability of the DNA double helix. Nucleic Acids Research. 2006;34(2):564-74.

12. Gregory SG, Barlow KF, McLay KE, Kaul R, Swarbreck D, Dunham A, et al. The DNA sequence and biological annotation of human chromosome 1. Nature. 2006;441(7091):315-21.

13. Feldkamp U, Niemeyer CM. Rational design of DNA nanoarchitectures. Angew Chem-Int Edit. 2006;45(12):1856-76.

14. Chhabra R, Sharma J, Liu Y, Rinker S, Yan H. DNA Self-assembly for Nanomedicine. Adv Drug Deliv Rev. 2010;62(6):617-25.

15. Guo PX. The emerging field of RNA nanotechnology. Nat Nanotechnol. 2010;5(12):833-

42.

16. Abels JA, Moreno-Herrero F, van der Heijden T, Dekker C, Dekker NH. Single-molecule measurements of the persistence length of double- stranded RNA. Biophys J. 2005;88(4):2737-44.

17. Kebbekus P, Draper DE, Hagerman P. PERSISTENCE LENGTH OF RNA. Biochemistry. 1995;34(13):4354-7.

18. Seeman NC. Nanomaterials Based on DNA. In: Kornberg RD, Raetz CRH, Rothman JE, Thorner JW, editors. Annual Review of Biochemistry, Vol 79. Palo Alto: Annual Reviews; 2010. p. 65-87.

19. Lin C, Rinker S, Wang X, Liu Y, Seeman NC, Yan H. In vivo cloning of artificial DNA nanostructures. Proceedings of the National Academy of Sciences. 2008;105(46):17626-31.

20. Shih WM, Quispe JD, Joyce GF. A 1.7-kilobase single-stranded DNA that folds into a nanoscale octahedron. Nature. 2004;427(6975):618-21.

21. Cohen SN, Chang ACY, Boyer HW, Helling RB. Construction of Biologically Functional Bacterial Plasmids In Vitro. Proceedings of the National Academy of Sciences. 1973;70(11):3240-4.

22. Rothemund PWK. Folding DNA to create nanoscale shapes and patterns. Nature. 2006;440(7082):297-302.

23. Lin C, Xie M, Chen JJL, Liu Y, Yan H. Rolling-Circle Amplification of a DNA Nanojunction. Angewandte Chemie International Edition. 2006;45(45):7537-9.

24. Joyce GF. The antiquity of RNA-based evolution. Nature. 2002;418(6894):214-21.

25. Couzin J. Small RNAs Make Big Splash. Science. 2002;298(5602):2296-7.

26. Muller S, Wolf J, Ivanov SA. Current strategies for the synthesis of RNA. Curr Org Synth. 2004;1(3):293-307.

27. Verma S, Eckstein F. Modified oligonucleotides: Synthesis and strategy for users. Annu Rev Biochem. 1998;67:99-134.

28. Pogocki D, Schöneich C. Chemical stability of nucleic acid–derived drugs. Journal of Pharmaceutical Sciences. 2000;89(4):443-56.

29. Lindahl T. INSTABILITY AND DECAY OF THE PRIMARY STRUCTURE OF DNA. Nature. 1993;362(6422):709-15.

30. Ames BN, Shigenaga MK, Hagen TM. Oxidants, antioxidants, and the degenerative diseases of aging. Proceedings of the National Academy of Sciences of the United States of America. 1993;90(17):7915-22.

31. Armitage B. Photocleavage of nucleic acids. Chemical Reviews. 1998;98(3):1171-200.

32. Burrows CJ, Muller JG. Oxidative nucleobase modifications leading to strand scission. Chemical Reviews. 1998;98(3):1109-51.

33. Micklefield J. Backbone modification of nucleic acids: Synthesis, structure and therapeutic applications. Curr Med Chem. 2001;8(10):1157-79.

34. Clercq ED, Eckstein F, Merigan TC. Interferon Induction Increased through Chemical Modification of a Synthetic Polyribonucleotide. Science. 1969;165(3898):1137-9.

35. Akhtar S, Hughes MD, Khan A, Bibby M, Hussain M, Nawaz Q, et al. The delivery of antisense therapeutics. Adv Drug Deliv Rev. 2000;44(1):3-21.

36. Agrawal S. Importance of nucleotide sequence and chemical modifications of antisense oligonucleotides. Biochim Biophys Acta-Gene Struct Expression. 1999;1489(1):53-68.

37. Dias N, Stein CA. Antisense Oligonucleotides: Basic Concepts and Mechanisms. Molecular Cancer Therapeutics. 2002;1(5):347-55.

38. Sergueev D, Hasan A, Ramaswamy M, Shaw BR. Boranophosphate oligonucleotides: New synthetic approaches. Nucleosides Nucleotides. 1997;16(7-9):1533-8.

39. Summers JS, Shaw BR. Boranophosphates as mimics of natural phosphodiesters in DNA. Curr Med Chem. 2001;8(10):1147-55.

40. Beaucage SL, Iyer RP. The functionalization of oligonucleotides via phosphoramidite derivatives Tetrahedron. 1993;49(10):1925-63.

41. RAY A, NORDÉN B. Peptide nucleic acid (PNA): its medical and biotechnical applications and promise for the future. The FASEB Journal. 2000;14(9):1041-60.

42. Peffer NJ, Hanvey JC, Bisi JE, Thomson SA, Hassman CF, Noble SA, et al. Strand-invasion of duplex DNA by peptide nucleic acid oligomers. Proceedings of the National Academy of Sciences. 1993;90(22):10648-52.

43. Tomac S, Sarkar M, Ratilainen T, Wittung P, Nielsen PE, Nordén B, et al. Ionic Effects on the Stability and Conformation of Peptide Nucleic Acid Complexes. Journal of the American Chemical Society. 1996;118(24):5544-52.

44. Kuhn H, Demidov VV, Frank-Kamenetskii MD, Nielsen PE. Kinetic sequence discrimination of cationic bis-PNAs upon targeting of double-stranded DNA. Nucleic Acids Research. 1998;26(2):582-7.

45. Jensen KK, Ørum H, Nielsen PE, Nordén B. Kinetics for Hybridization of Peptide Nucleic Acids (PNA) with DNA and RNA Studied with the BIAcore Technique†. Biochemistry. 1997;36(16):5072-7.

46. Aurup H, Williams DM, Eckstein F. 2'-Fluoro and 2-amino-2'-deoxynucleoside 5'-triphosphates as substrates for T7 RNA polymerase. Biochemistry. 1992;31(40):9636-41.

47. Pieken WA, Olsen DB, Benseler F, Aurup H, Eckstein F. Kinetic Characterization of Ribonuclease-Resistant 2′-Modified Hammerhead Ribozymes. Science. 1991;253(5017):314-7.

48. Pyle AM, Cech TR. Ribozyme recognition of RNA by tertiary interactions with specific ribose 2' -OH groups. Nature. 1991;350(6319):628-31.

49. Aurup H, Williams DM, Eckstein F. 2'-fluoro-2'-deoxynucleoside and 2'-amino-2'-deoxynucleoside 5'-triphosphates as substrates for T7 RNA-polymerase. Biochemistry. 1992;31(40):9636-41.

50. Sousa R, Padilla R. Mutant T7 RNA-polymerase as a DNA-polymerase Embo J. 1995;14(18):4609-21.

51. Huang Y, Eckstein F, Padilla R, Sousa R. Mechanism of Ribose 2‘-Group Discrimination by an RNA Polymerase. Biochemistry. 1997;36(27):8231-42.

52. Shangguan D, Li Y, Tang Z, Cao ZC, Chen HW, Mallikaratchy P, et al. Aptamers evolved from live cells as effective molecular probes for cancer study. Proceedings of the National Academy of Sciences. 2006;103(32):11838-43.

53. Zhou JH, Li HT, Li S, Zaia J, Rossi JJ. Novel dual inhibitory function aptamer-siRNA delivery system for HIV-1 therapy. Mol Ther. 2008;16(8):1481-9.

54. Allerson CR, Sioufi N, Jarres R, Prakash TP, Naik N, Berdeja A, et al. Fully 2‘-Modified Oligonucleotide Duplexes with Improved in Vitro Potency and Stability Compared to Unmodified Small Interfering RNA. Journal of Medicinal Chemistry. 2005;48(4):901-4.

55. Szczelkun MD, Connolly BA. Sequence-specific binding of DNA by the EcoRV restriction and modification enzymes with nucleic-acid and cofactor analogs Biochemistry. 1995;34(34):10724-33.

56. Hess MT, Schwitter U, Petretta M, Giese B, Naegeli H. DNA synthesis arrest at C4'-modified deoxyribose residues. Biochemistry. 1997;36(8):2332-7.

57. Limauro S, Benseler F, McLaughlin LW. 1-Methylguanosine substitutions of the conserved guanosine residues inactivate the hammerhead ribozyme. Bioorg Med Chem Lett. 1994;4(18):2189-92.

58. Bevers S, Xiang GB, McLaughlin LW. Importance of specific adenosine N-3-nitrogens for efficient cleavage by a hammerhead ribozyme. Biochemistry. 1996;35(20):6483-90.

59. Kim MG, Zhurkin VB, Jernigan RL, Cameriniotero RD. Probing the structure of a putative intermediate in homologous recombination - The 3rd strand in the parallel DNA triplex is in contact with the major groove of the duplex. Journal of Molecular Biology. 1995;247(5):874-89.

60. Burgin AB, Gonzalez C, MatulicAdamic J, Karpeisky AM, Usman N, McSwiggen JA, et al. Chemically modified hammerhead ribozymes with improved catalytic rates. Biochemistry. 1996;35(45):14090-7.

61. Mendelman LV, Kuimelis RG, McLaughlin LW, Richardson CC. Effects of base analog substitutions in the noncoding DC of the 3'-D(CTG)-5' template recognition site of the bacteriophage-T7 primase Biochemistry. 1995;34(32):10187-93.

62. Murray JB, Adams CJ, Arnold JRP, Stockley PG. The roles of the conserved pyrimidine-bases in hammerhead ribozyme catalysis - Evidence for a magnesium ion-binding site. Biochem J. 1995;311:487-94.

63. Luo D. The road from biology to materials. Materials Today. 2003;6(11):38-43.

64. Xing YZ, Cheng EJ, Yang Y, Chen P, Zhang T, Sun YW, et al. Self-Assembled DNA Hydrogels with Designable Thermal and Enzymatic Responsiveness. Advanced Materials. 2011;23(9):1117-21.

65. Torchia C, Takagi Y, Ho CK. Archaeal RNA ligase is a homodimeric protein that catalyzes intramolecular ligation of single-stranded RNA and DNA. Nucleic Acids Research. 2008;36(19):6218-27.

66. Cai L, Hu C, Shen S, Wang W, Huang W. Characterization of Bacteriophage T3 DNA Ligase. Journal of Biochemistry. 2004;135(3):397-403.

67. England TE, Gumport RI, Uhlenbeck OC. Dinucleoside pyrophosphate are substrates for T4-induced RNA ligase. Proceedings of the National Academy of Sciences. 1977;74(11):4839-42.

68. Takahashi M, Yamaguchi E, Uchida T. Thermophilic DNA ligase. Purification and properties of the enzyme from Thermus thermophilus HB8. Journal of Biological Chemistry. 1984;259(16):10041-7.

69. Li YG, Tseng YD, Kwon SY, D'Espaux L, Bunch JS, McEuen PL, et al. Controlled assembly of dendrimer-like DNA. Nat Mater. 2004;3(1):38-42.

70. Um SH, Lee JB, Park N, Kwon SY, Umbach CC, Luo D. Enzyme-catalysed assembly of DNA hydrogel. Nat Mater. 2006;5(10):797-801.

71. Crooke ST, Lemonidis KM, Neilson L, Griffey R, Lesnik EA, Monia BP. Kinetic characteristics of Escherichia-coli RNase H1-Cleavage of various antisense oligonucleotide-RNA duplexs. Biochem J. 1995;312:599-608.

72. Park N, Um SH, Funabashi H, Xu J, Luo D. A cell-free protein-producing gel. Nat Mater. 2009;8(5):432-7.

73. Roh YH, Lee JB, Kiatwuthinon P, Hartman MR, Cha JJ, Um SH, et al. DNAsomes: Multifunctional DNA-Based Nanocarriers. Small. 2011;7(1):74-8.

74. Li YG, Cu YTH, Luo D. Multiplexed detection of pathogen DNA with DNA-based fluorescence nanobarcodes. Nature Biotechnology. 2005;23(7):885-9.

75. Hur J, Im K, Hwang S, Choi B, Kim S, Hwang S, et al. DNA hydrogel-based supercapacitors operating in physiological fluids. Scientific Reports. 2013;3.

76. Lu N, Pei H, Ge Z, Simmons CR, Yan H, Fan C. Charge Transport within a Three-Dimensional DNA Nanostructure Framework. Journal of the American Chemical Society. 2012;134(32):13148-51.

77. Dutta PK, Varghese R, Nangreave J, Lin S, Yan H, Liu Y. DNA-Directed Artificial Light-Harvesting Antenna. Journal of the American Chemical Society. 2011;133(31):11985-93.

78. Hu R, Zhang XB, Kong RM, Zhao XH, Jiang JH, Tan WH. Nucleic acid-functionalized nanomaterials for bioimaging applications. J Mater Chem. 2011;21(41):16323-34.

79. Yang D, Campolongo MJ, Nhi Tran TN, Ruiz RCH, Kahn JS, Luo D. Novel DNA materials and their applications. Wiley Interdisciplinary Reviews: Nanomedicine and Nanobiotechnology. 2010;2(6):648-69.

80. Guo PX. RNA nanotechnology: Engineering, assembly and applications in detection, gene delivery and therapy. J Nanosci Nanotechnol. 2005;5(12):1964-82.

81. Tan SJ, Campolongo MJ, Luo D, Cheng WL. Building plasmonic nanostructures with DNA. Nat Nanotechnol. 2011;6(5):268-76.

82. Cayrol B, Nogues C, Dawid A, Sagi I, Silberzan P, Isambert H. A Nanostructure Made of a Bacterial Noncoding RNA. Journal of the American Chemical Society. 2009;131(47):17270-6.

83. Jaeger L, Chworos A. The architectonics of programmable RNA and DNA nanostructures. Current Opinion in Structural Biology. 2006;16(4):531-43.

84. Ko SH, Su M, Zhang CA, Ribbe AE, Jiang W, Mao CD. Synergistic self-assembly of RNA and DNA molecules. Nat Chem. 2010;2(12):1050-5.

85. Nakashima Y, Abe H, Abe N, Aikawa K, Ito Y. Branched RNA nanostructures for RNA interference. Chem Commun. 2011;47(29):8367-9.

86. Shu D, Shu Y, Haque F, Abdelmawla S, Guo PX. Thermodynamically stable RNA three-way junction for constructing multifunctional nanoparticles for delivery of therapeutics. Nat Nanotechnol. 2011;6(10):658-67.

87. Seeman NC. Construction of 3-dimensional stick figures from branched DNA. DNA Cell Biol. 1991;10(7):475-86.

88. Shu Y, Cinier M, Fox SR, Ben-Johnathan N, Guo PX. Assembly of Therapeutic pRNA-siRNA Nanoparticles Using Bipartite Approach. Mol Ther. 2011;19(7):1304-11.

89. Chen C, Zhang C, Guo P. Sequence requirement for hand-in-hand interaction in formation of RNA dimers and hexamers to gear phi29 DNA translocation motor. RNA. 1999;5(6):805-18.

90. Garver K, Guo P. Boundary of pRNA functional domains and minimum pRNA sequence requirement for specific connector binding and DNA packaging of phage phi29. RNA. 1997;3(9):1068-79.

91. Bock LC, Griffin LC, Latham JA, Vermaas EH, Toole JJ. Selection of single-stranded DNA molecules that bind and inhibit human thrombin. Nature. 1992;355(6360):564-6.

92. Ellington AD, Szostak JW. Invitro selection of RNA molecules that bind specific ligands Nature. 1990;346(6287):818-22.

93. Sassanfar M, Szostak JW. An RNA motif that binds ATP. Nature. 1993;364(6437):550-3.

94. Lupold SE, Hicke BJ, Lin Y, Coffey DS. Identification and characterization of nuclease-stabilized RNA molecules that bind human prostate cancer cells via the prostate-specific membrane antigen. Cancer Res. 2002;62(14):4029-33.

95. Henderson BR, Menotti E, Bonnard C, Kuhn LC. Optimal sequence and structure of iron-responsive elements - Selection of RNA stem-loops with high-affinity for iron affinity factor. Journal of Biological Chemistry. 1994;269(26):17481-9.

96. Sefah K, Shangguan D, Xiong XL, O'Donoghue MB, Tan WH. Development of DNA aptamers using Cell-SELEX. Nat Protoc. 2010;5(6):1169-85.

97. Magalhaes MLB, Byrom M, Yan A, Kelly L, Li N, Furtado R, et al. A General RNA Motif for Cellular Transfection. Mol Ther. 2012;20(3):616-24.

98. Ke Y, Lindsay S, Chang Y, Liu Y, Yan H. Self-Assembled Water-Soluble Nucleic Acid Probe Tiles for Label-Free RNA Hybridization Assays. Science. 2008;319(5860):180-3.

99. Lin C, Katilius E, Liu Y, Zhang J, Yan H. Self-Assembled Signaling Aptamer DNA Arrays for Protein Detection. Angewandte Chemie International Edition. 2006;45(32):5296-301.

100. Lee JB, Campolongo MJ, Kahn JS, Roh YH, Hartman MR, Luo D. DNA-based nanostructures for molecular sensing. Nanoscale. 2010;2(2):188-97.

101. Kong WH, Bae KH, Hong CA, Lee Y, Hahn SK, Park TG. Multimerized siRNA Cross-linked by Gold Nanoparticles. Bioconjugate Chemistry. 2011;22(10):1962-9.

102. Grabow WW, Zakrevsky P, Afonin KA, Chworos A, Shapiro BA, Jaeger L. Self-Assembling RNA Nanorings Based on RNAI/II Inverse Kissing Complexes. Nano Lett. 2011;11(2):878-87.

103. Lee TJ, Schwartz C, Guo PX. Construction of Bacteriophage Phi29 DNA Packaging Motor and its Applications in Nanotechnology and Therapy. Ann Biomed Eng.

2009;37(10):2064-81.

104. Walsh AS, Yin HF, Erben CM, Wood MJA, Turberfield AJ. DNA Cage Delivery to Mammalian Cells. ACS Nano. 2011;5(7):5427-32.

105. Namgung R, Kim WJ. A Highly Entangled Polymeric Nanoconstruct Assembled by siRNA and its Reduction-Triggered siRNA Release for Gene Silencing. Small. 2012;8(20):3209-19.

106. Lee H, Lytton-Jean AKR, Chen Y, Love KT, Park AI, Karagiannis ED, et al. Molecularly self-assembled nucleic acid nanoparticles for targeted in vivo siRNA delivery. Nat Nanotechnol. 2012;7(6):389-93.

107. Chang M, Yang C-S, Huang D-M. Aptamer-Conjugated DNA Icosahedral Nanoparticles As a Carrier of Doxorubicin for Cancer Therapy. ACS Nano. 2011;5(8):6156-63.

108. Lee JB, Hong J, Bonner DK, Poon Z, Hammond PT. Self-assembled RNA interference microsponges for efficient siRNA delivery. Nat Mater. 2012;11(4):316-22.

109. Hong CA, Lee SH, Kim JS, Park JW, Bae KH, Mok H, et al. Gene Silencing by siRNA Microhydrogels via Polymeric Nanoscale Condensation. Journal of the American Chemical Society. 2011;133(35):13914-7.

110. Chang CI, Lee TY, Yoo JW, Shin D, Kim M, Kim S, et al. Branched, Tripartite-Interfering RNAs Silence Multiple Target Genes with Long Guide Strands. Nucl Acid Ther. 2012;22(1):30-9.

111. Chang CI, Lee TY, Kim S, Sun XG, Hong SW, Yoo JW, et al. Enhanced intracellular delivery and multi-target gene silencing triggered by tripodal RNA structures. J Gene Med. 2012;14(2):138-46.

112. Mathis G, Bourg S, Aci-Seche S, Truffert JC, Asseline U. Synthesis and properties of 2 '-O-neopentyl modified oligonucleotides. Org Biomol Chem. 2013;11(8):1345-57.

113. Bagmare S, Varada M, Banerjee A, Kumar VA. Synthesis of all four nucleoside-based beta-amino acids as protected precursors for the synthesis of polyamide-DNA with alternating alpha-amino acid and nucleoside-beta-amino acids. Tetrahedron. 2013;69(3):1210-6.

114. Tan SJ, Kiatwuthinon P, Roh YH, Kahn JS, Luo D. Engineering Nanocarriers for siRNA Delivery. Small. 2011;7(7):841-56.

115. Zhang Y, Chan HF, Leong KW. Advanced materials and processing for drug delivery: The past and the future. Adv Drug Deliv Rev. 2013;65(1):104-20.

116. Creixell M, Peppas NA. Co-delivery of siRNA and therapeutic agents using nanocarriers to overcome cancer resistance. Nano Today. 2012;7(4):367-79.

117. Iversen TG, Skotland T, Sandvig K. Endocytosis and intracellular transport of

nanoparticles: Present knowledge and need for future studies. Nano Today. 2011;6(2):176-85.

118. Grant CE, Valdimarsson G, Hipfner DR, Almquist KC, Cole SPC, Deeley RG. Overexpression of multidrug resistance-associated protein (MRP) increases resistance to natural product drugs Cancer Res. 1994;54(2):357-61.

119. Chen AM, Zhang M, Wei DG, Stueber D, Taratula O, Minko T, et al. Co-delivery of Doxorubicin and Bcl-2 siRNA by Mesoporous Silica Nanoparticles Enhances the Efficacy of Chemotherapy in Multidrug-Resistant Cancer Cells. Small. 2009;5(23):2673-7.

120. Davis ME, Chen Z, Shin DM. Nanoparticle therapeutics: an emerging treatment modality for cancer. Nat Rev Drug Discov. 2008;7(9):771-82.

121. Choudhury NN, He HX. Nanocarriers for the Simultaneous Co-Delivery of Therapeutic Genes and Anticancer Drugs. Curr Pharm Biotechnol. 2012;13(7):1317-31.

122. Hu CMJ, Zhang LF. Therapeutic Nanoparticles to Combat Cancer Drug Resistance. Curr Drug Metab. 2009;10(8):836-41.

123. Panyam J, Labhasetwar V. Biodegradable nanoparticles for drug and gene delivery to cells and tissue. Adv Drug Deliv Rev. 2012;64:61-71.

124. Chen XA, Wang XH, Wang YS, Yang L, Hu J, Xiao WJ, et al. Improved tumor-targeting drug delivery and therapeutic efficacy by cationic liposome modified with truncated bFGF peptide. J Control Release. 2010;145(1):17-25.

125. Kato T, Natsume A, Toda H, Iwamizu H, Sugita T, Hachisu R, et al. Efficient delivery of liposome-mediated MGMT-siRNA reinforces the cytotoxity of temozolomide in GBM-initiating cells. Gene Ther. 2010;17(11):1363-71.

126. Wang Y, Gao SJ, Ye WH, Yoon HS, Yang YY. Co-delivery of drugs and DNA from cationic core-shell nanoparticles self-assembled from a biodegradable copolymer. Nat Mater. 2006;5(10):791-6.

127. Zhang L, Radovic-Moreno AF, Alexis F, Gu FX, Basto PA, Bagalkot V, et al. Co-Delivery of Hydrophobic and Hydrophilic Drugs from Nanoparticle–Aptamer Bioconjugates. ChemMedChem. 2007;2(9):1268-71.

128. Pakunlu RI, Wang Y, Tsao W, Pozharov V, Cook TJ, Minko T. Enhancement of the Efficacy of Chemotherapy for Lung Cancer by Simultaneous Suppression of Multidrug Resistance and Antiapoptotic Cellular Defense: Novel Multicomponent Delivery System. Cancer Res. 2004;64(17):6214-24.

129. Nijhawan D, Fang M, Traer E, Zhong Q, Gao W, Du F, et al. Elimination of Mcl-1 is required for the initiation of apoptosis following ultraviolet irradiation. Genes & Development. 2003;17(12):1475-86.

130. Lee JB, Roh YH, Um SH, Funabashi H, Cheng WL, Cha JJ, et al. Multifunctional

nanoarchitectures from DNA-based ABC monomers. Nat Nanotechnol. 2009;4(7):430-6.

131. Kenny PA, Lee GY, Myers CA, Neve RM, Semeiks JR, Spellman PT, et al. The morphologies of breast cancer cell lines in three-dimensional assays correlate with their profiles of gene expression. Mol Oncol. 2007;1(1):84-96.

132. Ghosh S, Spagnoli GC, Martin I, Ploegert S, Demougin P, Heberer M, et al. Three-dimensional culture of melanoma cells profoundly affects gene expression profile: A high density oligonucleotide array study. Journal of Cellular Physiology. 2005;204(2):522-31.

133. Mishra DK, Sakamoto JH, Thrall MJ, Baird BN, Blackmon SH, Ferrari M, et al. Human Lung Cancer Cells Grown in an Ex Vivo 3D Lung Model Produce Matrix Metalloproteinases Not Produced in 2D Culture. PLoS One. 2012;7(9).

134. Bartosh TJ, Ylostalo JH, Mohammadipoor A, Bazhanov N, Coble K, Claypool K, et al. Aggregation of human mesenchymal stromal cells (MSCs) into 3D spheroids enhances their antiinflammatory properties. Proceedings of the National Academy of Sciences of the United States of America. 2010;107(31):13724-9.

135. Owen SC, Shoichet MS. Design of three-dimensional biomimetic scaffolds. J Biomed Mater Res Part A. 2010;94A(4):1321-31.

136. Hutmacher DW. Biomaterials offer cancer research the third dimension. Nat Mater. 2010;9(2):90-3.

137. Sivaraman A, Leach JK, Townsend S, Iida T, Hogan BJ, Stolz DB, et al. A microscale in vitro physiological model of the liver: Predictive screens for drug metabolism and enzyme induction. Curr Drug Metab. 2005;6(6):569-91.

138. Lutolf MP. Integration column: Artificial ECM: expanding the cell biology toolbox in 3D. Integr Biol. 2009;1(3):235-41.

139. Pampaloni F, Reynaud EG, Stelzer EHK. The third dimension bridges the gap between cell culture and live tissue. Nat Rev Mol Cell Biol. 2007;8(10):839-45.

140. Lee J, Cuddihy MJ, Kotov NA. Three-dimensional cell culture matrices: State of the art. Tissue Eng Part B-Rev. 2008;14(1):61-86.

141. Liu H, Lin J, Roy K. Effect of 3D scaffold and dynamic culture condition on the global gene expression profile of mouse embryonic stem cells. Biomaterials. 2006;27(36):5978-89.

142. Dhiman HK, Ray AR, Panda AK. Three-dimensional chitosan scaffold-based MCF-7 cell culture for the determination of the cytotoxicity of tamoxifen. Biomaterials. 2005;26(9):979-86.

143. Ivascu A, Kubbies M. Diversity of cell-mediated adhesions in breast cancer spheroids. Int J Oncol. 2007;31(6):1403-13.

144. Baharvand H, Hashemi SM, Ashtian SK, Farrokhi A. Differentiation of human

embryonic stem cells into hepatocytes in 2D and 3D culture systems in vitro. Int J Dev Biol. 2006;50(7):645-52.

145. Carpenedo RL, Sargent CY, McDevitt TC. Rotary suspension culture enhances the efficiency, yield, and homogeneity of embryoid body differentiation. Stem Cells. 2007;25(9):2224-34.

146. Kelm JM, Timmins NE, Brown CJ, Fussenegger M, Nielsen LK. Method for generation of homogeneous multicellular tumor spheroids applicable to a wide variety of cell types. Biotechnol Bioeng. 2003;83(2):173-80.

147. Enmon RM, O'Connor KC, Lacks DJ, Schwartz DK, Dotson RS. Dynamics of spheroid self-assembly in liquid-overlay culture of DU 145 human prostate cancer cells. Biotechnol Bioeng. 2001;72(6):579-91.

148. Nazarov R, Jin HJ, Kaplan DL. Porous 3-D scaffolds from regenerated silk fibroin. Biomacromolecules. 2004;5(3):718-26.

149. Lutolf MP, Hubbell JA. Synthetic biomaterials as instructive extracellular microenvironments for morphogenesis in tissue engineering. Nature Biotechnology. 2005;23(1):47-55.

150. Lutolf MP, Lauer-Fields JL, Schmoekel HG, Metters AT, Weber FE, Fields GB, et al. Synthetic matrix metalloproteinase-sensitive hydrogels for the conduction of tissue regeneration: Engineering cell-invasion characteristics. Proceedings of the National Academy of Sciences of the United States of America. 2003;100(9):5413-8.

151. Zhang SG. Fabrication of novel biomaterials through molecular self-assembly. Nature Biotechnology. 2003;21(10):1171-8.

152. Hoffman AS. Hydrogels for biomedical applications. Adv Drug Deliv Rev. 2002;54(1):3-12.

153. Tibbitt MW, Anseth KS. Hydrogels as extracellular matrix mimics for 3D cell culture. Biotechnol Bioeng. 2009;103(4):655-63.

154. Kleinman HK, Martin GR. Matrigel: Basement membrane matrix with biological activity. Seminars in Cancer Biology. 2005;15(5):378-86.

155. Smidsrød O, Skja˚k-Br↑k G. Alginate as immobilization matrix for cells. Trends in Biotechnology. 1990;8(0):71-8.

156. Azagarsamy MA, Anseth KS. Bioorthogonal Click Chemistry: An Indispensable Tool to Create Multifaceted Cell Culture Scaffolds. ACS Macro Letters. 2012;2(1):5-9.

157. Langer R, Tirrell DA. Designing materials for biology and medicine. Nature. 2004;428(6982):487-92.

158. Zaman MH, Trapani LM, Sieminski AL, MacKellar D, Gong H, Kamm RD, et al. Migration of tumor cells in 3D matrices is governed by matrix stiffness along with cell-matrix adhesion and proteolysis. Proceedings of the National Academy of Sciences. 2006;103(29):10889-94.

159. Lutolf MP, Raeber GP, Zisch AH, Tirelli N, Hubbell JA. Cell-Responsive Synthetic Hydrogels. Advanced Materials. 2003;15(11):888-92.

160. Zhu JM. Bioactive modification of poly(ethylene glycol) hydrogels for tissue engineering. Biomaterials. 2010;31(17):4639-56.

161. Kloxin AM, Kloxin CJ, Bowman CN, Anseth KS. Mechanical Properties of Cellularly Responsive Hydrogels and Their Experimental Determination. Advanced Materials. 2010;22(31):3484-94.

162. Lee JH, Lee HB, Andrade JD. Blood compatibility of polyethylene oxide surfaces. Prog Polym Sci. 1995;20(6):1043-79.

163. Alcantar NA, Aydil ES, Israelachvili JN. Polyethylene glycol-coated biocompatible surfaces. J Biomed Mater Res. 2000;51(3):343-51.

164. Lin C-C, Raza A, Shih H. PEG hydrogels formed by thiol-ene photo-click chemistry and their effect on the formation and recovery of insulin-secreting cell spheroids. Biomaterials. 2011;32(36):9685-95.

165. Lin CC, Anseth KS. PEG Hydrogels for the Controlled Release of Biomolecules in Regenerative Medicine. Pharm Res. 2009;26(3):631-43.

166. Sui ZJ, King WJ, Murphy WL. Protein-based hydrogels with tunable dynamic responses. Adv Funct Mater. 2008;18(12):1824-31.

167. Adelöw C, Segura T, Hubbell JA, Frey P. The effect of enzymatically degradable poly(ethylene glycol) hydrogels on smooth muscle cell phenotype. Biomaterials. 2008;29(3):314-26.

168. Cavallaro U, Christofori G. Cell adhesion and signalling by cadherins and Ig-CAMs in cancer. Nat Rev Cancer. 2004;4(2):118-32.

169. Nagata N, Iwanaga A, Inoue K, Tabata Y. Co-culture of extracellular matrix suppresses the cell death of rat pancreatic islets. Journal of Biomaterials Science, Polymer Edition. 2002;13(5):579-90.

170. Zhang S, Holmes TC, DiPersio CM, Hynes RO, Su X, Rich A. Self-complementary oligopeptide matrices support mammalian cell attachment. Biomaterials. 1995;16(18):1385-93.

171. Heilshorn SC, DiZio KA, Welsh ER, Tirrell DA. Endothelial cell adhesion to the fibronectin CS5 domain in artificial extracellular matrix proteins. Biomaterials. 2003;24(23):4245-52.

172. Almany L, Seliktar D. Biosynthetic hydrogel scaffolds made from fibrinogen and polyethylene glycol for 3D cell cultures. Biomaterials. 2005;26(15):2467-77.

173. Jin R, Moreira Teixeira LS, Krouwels A, Dijkstra PJ, van Blitterswijk CA, Karperien M, et al. Synthesis and characterization of hyaluronic acid–poly(ethylene glycol) hydrogels via Michael addition: An injectable biomaterial for cartilage repair. Acta Biomaterialia. 2010;6(6):1968-77.

174. Massia SP, Hubbell JA. An RGD spacing of 440 nm is sufficient for integrin alpha V beta 3-mediated fibroblast spreading and 140 nm for focal contact and stress fiber formation. The Journal of Cell Biology. 1991;114(5):1089-100.

175. Waite CL, Roth CM. PAMAM-RGD Conjugates Enhance siRNA Delivery Through a Multicellular Spheroid Model of Malignant Glioma. Bioconjugate Chemistry. 2009;20(10):1908-16.

176. Wang X, Yan C, Ye K, He Y, Li Z, Ding J. Effect of RGD nanospacing on differentiation of stem cells. Biomaterials. 2013;34(12):2865-74.

177. Tashiro K, Sephel GC, Weeks B, Sasaki M, Martin GR, Kleinman HK, et al. A synthetic peptide containing the IKVAV sequence from the A chain of laminin mediates cell attachment, migration, and neurite outgrowth. Journal of Biological Chemistry. 1989;264(27):16174-82.

178. Markó K, Ligeti M, Mezo″ G, Mihala N, Kutnyánszky E, Kiss E, et al. A Novel Synthetic Peptide Polymer with Cyclic RGD Motifs Supports Serum-Free Attachment of Anchorage-Dependent Cells. Bioconjugate Chemistry. 2008;19(9):1757-66.

179. Weber LM, Hayda KN, Haskins K, Anseth KS. The effects of cell–matrix interactions on encapsulated β-cell function within hydrogels functionalized with matrix-derived adhesive peptides. Biomaterials. 2007;28(19):3004-11.

180. Mann BK, Gobin AS, Tsai AT, Schmedlen RH, West JL. Smooth muscle cell growth in photopolymerized hydrogels with cell adhesive and proteolytically degradable domains: synthetic ECM analogs for tissue engineering. Biomaterials. 2001;22(22):3045-51.

181. Hersel U, Dahmen C, Kessler H. RGD modified polymers: biomaterials for stimulated cell adhesion and beyond. Biomaterials. 2003;24(24):4385-415.

182. Salinas CN, Anseth KS. The enhancement of chondrogenic differentiation of human mesenchymal stem cells by enzymatically regulated RGD functionalities. Biomaterials. 2008;29(15):2370-7.

183. Jiang L-Y, Lv B, Luo Y. The effects of an RGD-PAMAM dendrimer conjugate in 3D spheroid culture on cell proliferation, expression and aggregation. Biomaterials. 2013;34(11):2665-73.

184. Fairbanks BD, Schwartz MP, Halevi AE, Nuttelman CR, Bowman CN, Anseth KS. A Versatile Synthetic Extracellular Matrix Mimic via Thiol-Norbornene Photopolymerization.

Advanced Materials. 2009;21(48):5005.

185. Gelain F, Horii A, Zhang S. Designer Self-Assembling Peptide Scaffolds for 3-D Tissue Cell Cultures and Regenerative Medicine. Macromolecular Bioscience. 2007;7(5):544-51.

186. Chawla K, Yu TB, Liao SW, Guan ZB. Biodegradable and Biocompatible Synthetic Saccharide-Peptide Hydrogels for Three-Dimensional Stem Cell Culture. Biomacromolecules. 2011;12(3):560-7.

187. Petka WA, Harden JL, McGrath KP, Wirtz D, Tirrell DA. Reversible Hydrogels from Self-Assembling Artificial Proteins. Science. 1998;281(5375):389-92.

188. Holmes TC, de Lacalle S, Su X, Liu G, Rich A, Zhang S. Extensive neurite outgrowth and active synapse formation on self-assembling peptide scaffolds. Proceedings of the National Academy of Sciences. 2000;97(12):6728-33.

189. Kisiday J, Jin M, Kurz B, Hung H, Semino C, Zhang S, et al. Self-assembling peptide hydrogel fosters chondrocyte extracellular matrix production and cell division: Implications for cartilage tissue repair. Proceedings of the National Academy of Sciences. 2002;99(15):9996-10001.

190. Semino CE, Merok JR, Crane GG, Panagiotakos G, Zhang S. Functional differentiation of hepatocyte-like spheroid structures from putative liver progenitor cells in three-dimensional peptide scaffolds. Differentiation. 2003;71(4-5):262-70.

191. Pan Z, Ding JD. Poly(lactide-co-glycolide) porous scaffolds for tissue engineering and regenerative medicine. Interface Focus. 2012;2(3):366-77.

192. Makadia HK, Siegel SJ. Poly Lactic-co-Glycolic Acid (PLGA) as Biodegradable Controlled Drug Delivery Carrier. Polymers. 2011;3(3):1377-97.

193. Mikos AG, Lyman MD, Freed LE, Langer R. Wetting of poly(L-lactic acid) and poly(DL-lactic-co-glycotic acid) foams for tissue culture. Biomaterials. 1994;15(1):55-8.

194. Ignatius AA, Claes LE. In vitro biocompatibility of bioresorbable polymers: Poly(L,DL-lactide) and poly(L-lactide-co-glycolide). Biomaterials. 1996;17(8):831-9.

195. Allison SD. Effect of structural relaxation on the preparation and drug release behavior of poly(lactic-co-glycolic)acid microparticle drug delivery systems. Journal of Pharmaceutical Sciences. 2008;97(6):2022-35.

196. Melchels FPW, Barradas AMC, van Blitterswijk CA, de Boer J, Feijen J, Grijpma DW. Effects of the architecture of tissue engineering scaffolds on cell seeding and culturing. Acta Biomaterialia. 2010;6(11):4208-17.

197. Go Y-M, Jones DP. Redox compartmentalization in eukaryotic cells. Biochimica et Biophysica Acta (BBA) - General Subjects. 2008;1780(11):1273-90.

198. Tatu U, Braakman I, Helenius A. Membrane glycoprotein folding, oligomerization and intracellular- transport- effects of dithiothreitol in living cells. Embo J. 1993;12(5):2151-7.

199. Braakman I, Helenius J, Helenius A. Role of ATP and disulfide bonds during protein folding in the endoplasmic- reticulum. Nature. 1992;356(6366):260-2.

200. Nishikawa M, Mizuno Y, Mohri K, Matsuoka N, Rattanakiat S, Takahashi Y, et al. Biodegradable CpG DNA hydrogels for sustained delivery of doxorubicin and immunostimulatory signals in tumor-bearing mice. Biomaterials. 2011;32(2):488-94.

201. Klenow H, Hennings.I. Effect of monovalent cations on activity of DNA polymerase of Escherichia Coli B Eur J Biochem. 1969;9(1):133-&.

202. Hayashi K, Nakazawa M, Ishizaki Y, Obayashi A. Influence of mono-valent cations on the activity of T4 DNA-ligase in the presence of polyethylene-glycol Nucleic Acids Research. 1985;13(9):3261-71.

203. Feig M, Pettitt BM. Sodium and chlorine ions as part of the DNA solvation shell. Biophys J. 1999;77(4):1769-81.

204. Marquet R, Houssier C. Thermodynamics of cation-induced DNA condensation J Biomol Struct Dyn. 1991;9(1):159-67.

205. Chen CS, Mrksich M, Huang S, Whitesides GM, Ingber DE. Geometric Control of Cell Life and Death. Science. 1997;276(5317):1425-8.

206. Pierschbacher MD, Ruoslahti E. Cell attachment activity of fibronectin can be duplicated by small synthetic fragments of the molecule Nature. 1984;309(5963):30-3.

207. Craig WS, Cheng S, Mullen DG, Blevitt J, Pierschbacher MD. Concept and progress in the development of RGD-containing peptide pharmaceuticals Biopolymers. 1995;37(2):157-75.

208. Bernstein E, Caudy AA, Hammond SM, Hannon GJ. Role for a bidentate ribonuclease in the initiation step of RNA interference. Nature. 2001;409(6818):363-6.

209. Scholz C, Wagner E. Therapeutic plasmid DNA versus siRNA delivery: Common and different tasks for synthetic carriers. J Control Release. 2012;161(2):554-65.

210. des Rieux A, Shikanov A, Shea LD. Fibrin hydrogels for non-viral vector delivery in vitro. J Control Release. 2009;136(2):148-54.

211. McCaffrey AP, Meuse L, Pham TTT, Conklin DS, Hannon GJ, Kay MA. Gene expression - RNA interference in adult mice. Nature. 2002;418(6893):38-9.

212. Paul CP, Good PD, Winer I, Engelke DR. Effective expression of small interfering RNA in human cells. Nature Biotechnology. 2002;20(5):505-8.

213. Elouahabi A, Ruysschaert JM. Formation and intracellular trafficking of lipoplexes and

polyplexes. Mol Ther. 2005;11(3):336-47.

214. Boussif O, Lezoualch F, Zanta MA, Mergny MD, Scherman D, Demeneix B, et al. A versatile vector for gene and oligonucleotide transfer into cells in culture and in-vivo - polyethylenimine Proceedings of the National Academy of Sciences of the United States of America. 1995;92(16):7297-301.

215. Schiffelers RM, Ansari A, Xu J, Zhou Q, Tang QQ, Storm G, et al. Cancer siRNA therapy by tumor selective delivery with ligand-targeted sterically stabilized nanoparticle. Nucleic Acids Research. 2004;32(19).

216. McNamara JO, Andrechek ER, Wang Y, D Viles K, Rempel RE, Gilboa E, et al. Cell type-specific delivery of siRNAs with aptamer-siRNA chimeras. Nature Biotechnology. 2006;24(8):1005-15.

217. Davis ME, Zuckerman JE, Choi CHJ, Seligson D, Tolcher A, Alabi CA, et al. Evidence of RNAi in humans from systemically administered siRNA via targeted nanoparticles. Nature. 2010;464(7291):1067-U140.

218. Nelson CE, Gupta MK, Adolph EJ, Shannon JM, Guelcher SA, Duvall CL. Sustained local delivery of siRNA from an injectable scaffold. Biomaterials. 2012;33(4):1154-61.

219. Saito T, Tabata Y. Preparation of gelatin hydrogels incorporating small interfering RNA for the controlled release. J Drug Target. 2012;20(10):864-72.

220. Krebs MD, Jeon O, Alsberg E. Localized and Sustained Delivery of Silencing RNA from Macroscopic Biopolymer Hydrogels. Journal of the American Chemical Society. 2009;131(26):9204-6.

221. Kim Y-M, Park M-R, Song S-C. Injectable Polyplex Hydrogel for Localized and Long-Term Delivery of siRNA. ACS Nano. 2012;6(7):5757-66.

222. Raemdonck K, Van Thienen TG, Vandenbroucke RE, Sanders NN, Demeester J, De Smedt SC. Dextran Microgels for Time-Controlled Delivery of siRNA. Adv Funct Mater. 2008;18(7):993-1001.

223. Benoit DSW, Boutin ME. Controlling Mesenchymal Stem Cell Gene Expression Using Polymer-Mediated Delivery of siRNA. Biomacromolecules. 2012;13(11):3841-9.

224. Yang Y, Liu F, Liu X, Xing B. NIR light controlled photorelease of siRNA and its targeted intracellular delivery based on upconversion nanoparticles. Nanoscale. 2013;5(1):231-8.

225. Cao HQ, Jiang X, Chai C, Chew SY. RNA interference by nanofiber-based siRNA delivery system. J Control Release. 2010;144(2):203-12.

226. Dunn SS, Tian S, Blake S, Wang J, Galloway AL, Murphy A, et al. Reductively Responsive siRNA-Conjugated Hydrogel Nanoparticles for Gene Silencing. Journal of the American Chemical Society. 2012;134(17):7423-30.

227. Flessner RM, Jewell CM, Anderson DG, Lynn DM. Degradable Polyelectrolyte Multilayers that Promote the Release of siRNA. Langmuir. 2011;27(12):7868-76.

228. Wu SY, Chang HI, Burgess M, McMillan NAJ. Vaginal delivery of siRNA using a novel PEGylated lipoplex-entrapped alginate scaffold system. J Control Release. 2011;155(3):418-26.

229. Lee H, Mok H, Lee S, Oh YK, Park TG. Target-specific intracellular delivery of siRNA using degradable hyaluronic acid nanogels. J Control Release. 2007;119(2):245-52.

230. Hazama K, Asayama S, Kawakami H. Up-Regulation of Gene Expression by Transfection to Hepatocyte Spheroids. Molecular Pharmaceutics. 2012;9(12):3602-5.